ÇUKUROVA UNIVERSITY
INSTITUTE OF NATURAL AND APPLIED SCIENCES

MSc THESIS

Djaber MAOUCHE

MODELING AND CONTROL OF A TWIN ROTOR MIMO HELICOPTER SYSTEM USING VARIOUS CONTROL THEORIES

DEPARTMENT OF ELECTRICAL AND ELECTRONICS ENGINEERING

ADANA-2016

ÇUKUROVA UNIVERSITY
INSTITUTE OF NATURAL AND APPLIED SCIENCES

MODELING AND CONTROL OF A TWIN ROTOR MIMO HELICOPTER SYSTEM USING VARIOUS CONTROL THEORIES

Djaber MAOUCHE

MSc THESIS

DEPARTMENT OF ELECTRICAL AND ELECTRONICS ENGINEERING

We certify that the thesis titled above was reviewed and approved for the award of degree of the Master of Science by the board of jury on.

Prof. Dr. Ilyas EKER
SUPERVISOR

Assoc. Prof. Dr. Ramazan ÇOBAN
MEMBER

Asst. Prof. Dr. Lütfü SARIBULUT
MEMBER

This MSc Thesis is written at the Department of Institute of Natural And Applied Sciences of Çukurova University.
Registration Number:

Prof. Dr. Mustafa GÖK
Director
Institute of Natural and Applied Sciences

ABSTRACT

MSc THESIS

MODELING AND CONTROL OF A TWIN ROTOR MIMO HELICOPTER SYSTEM USING VARIOUS CONTROL THEORIES

Djaber MAOUCHE

ÇUKUROVA UNIVERSITY
INSTITUTE OF NATURAL AND APPLIED SCIENCES
DEPARTMENT OF ELECTRICAL AND ELECTRONICS ENGINEERING

Supervisor : Prof. Dr. Ilyas EKER
Year: 2016, Pages: 132
Jury : Prof. Dr. Ilyas EKER
: Assoc. Prof. Dr. Ramazan ÇOBAN
: Asst. Prof. Dr. Lütfü SARIBULUT

Helicopters are used widely in transportation sector and in emergency cases due to the capability of quick taking off and landing on from different kinds of limited terrains and areas. The helicopter's control performance is related directly to the regulation and control of its two angles of rotation (pitch and yaw). Any changes of the helicopter's motion in pitch angle (angle of attack) leads to undesired changes in yaw angle, and simultaneously another changes in yaw angle that effects the pitch angle. A flight helicopter simulator with Two-degrees-of-freedom (2-*dof*) so-called *TRMS* (Twin Rotor Multi Input Multi Output System) is largely used in control labs as test platforms due to its comportment similarities with real helicopters whether in its high nonlinearity, or the important cross-coupling between its axial motions, or even in its instability under both closed-loop and open-loop. Therefore TRMS allows us effectively to investigate and design the desired controllers those can handle safely the challenging dynamics encountered in helicopter's control, through a system more simplified, and with the aid of its hardware structure assistance that provide a rapid prototyping environment for testing the designed control approaches. The control of *TRMS* is doable through the adjustment of the rotation speed of the two electrical motors. The present thesis presents an introduction, including a Newtonian modeling approach, to the used *TRMS*, then a synthesis and application of various control strategies those are already demonstrated by utilizing this test developed model with detailed design procedures in order to stabilize the TRMS. The first applied control approach is the classical *PID* control. Second control scheme is fuzzy control which has a linguistic structure and finally fuzzy type-2 Control algorithm is applied to a TRMS process to check the performance. The results are compared with classical PID controller and fuzzy logic. Time domain analysis and tabletted results show that better performance specification are obtained using type2 fuzzy control.

Key Words: Helicopters, TRMS, Multivariable, Nonlinear, Newtonian Modeling, Fuzzy type-1 Control, Fuzzy type-2 Control, PID Control.

ÖZ

YÜKSEK LİSANS TEZİ

2 ROTURLU ÇOK GİRİŞLİ ÇOK ÇIKIŞLI HELİKOPTER SİSTEMİNİN DEĞİŞİK KONTROL TEORİLERİ KULLANARAK MODELLEMESİ VE KONTROLÜ

Djaber MAOUCHE

ÇUKUROVA ÜNİVERSİTESİ
FEN BİLİMLERİ ENSTİTÜSÜ
ELEKTRIK ELEKTRONIK NABİLİM DALI

Danışman : Prof. Dr. Ilyas EKER
Yıl: 2016, Sayfa: 132
Jüri : Prof. Dr. Ilyas EKER
: Doç. Dr. Ramazan ÇOBAN
: Yrd. Doç. Dr. Lütfü SARIBULUT

Helikopterler, farklı türlerdeki kısıtlanmış bölgeler ve arazilere hızlı iniş ve kalkış yapabilmeleri nedeniyle ulaştırma sektöründe ve acil durumlarda yaygın bir şekilde kullanılmaktadır. Helikopterin kontrol performansı, yükselme ve sapma açılarının ayar ve kontrolü ile doğrudan ilişkilidir. Helikopterin yükselme açısındaki (saldırı açısı) herhangi bir değişim, sapma açısında istenmeyen bir bozulmaya, benzer şekilde sapma açısındaki herhangi bir değişim ise yükselme açısında bir sapmaya neden olur. Genellikle TRMS (İkiz Rotor Çoklu Giriş Çoklu Çıkış Sistemi) olarak bilinen, iki dereceli serbestliğe (2-dof) sahip bir uçuş helikopter simülatörü, gerçek helikopterlerin yüksek doğrusalsızlık veya eksenel hareketler arasındaki önemli çapraz kavrama ve hatta hem kapalı devre hem de açık devre altında karasızlığına bağlı davranış benzerlikleri sebebiyle kontrol laboratuvarlarında test platformları olarak çoğunlukla kullanılırlar. Bu yüzden, TRMS, helikopter kontrolünde karşılaşılan zorlayıcı dinamikleri basitleştirilmiş bir sistem ve tasarlanmış kontrol yaklaşımlarının testi için hızlı bir prototiplendirme ortamı sağlayan donanım yapısı yardımı ile bizlere etkili idare sağlar. TRMS kontrolü, iki elektrik motorunun dönüş hızının ayarlanması ile yapılabilir. Bu tez çalışması, TRMS kullanımında Newton uyumlu bir modelleme yaklaşımı içeren bir giriş bölümünü ve sonrasında TRMS'nin kararlılaştırmak için detaylı tasarım prosedürleriyle geliştirilmiş modeli kullanan değişik kontrol stratejilerinin birleşimi ve uygulamasını sunmaktadır. İlk uygulanan kontrol yaklaşımı klasik PID kontroldür. İkinci kontrol şeması dilbilimsel bir yapıya sahip bulanık mantıktır ve son olarak da bulanık tip-2 kontrol algoritması performans kontrolü için TRMS prosesine uygulanmıştır. Elde edilen sonuçlar ise klasik PID kontrol ve bulanık mantık ile karşılaştırılmıştır. Zaman analığındaki analizler sonuç tabloları tip2 bulanık kontrol algoritması daha iyi performans özellikleri göstermiştir.

Anahtar Kelimeler: Helikopterler, TRMS, Çok Değişkenli, Doğrusalsız, Newton Uyumlu Modelleme, Bulanık Tip-1 Kontrol, Bulanık Tip-2 Kontrol, PID Kontrol

ACKNOWLEDGEMENTS

To start off I should acknowledge God for giving me reasons and guiding me throughout my experiment and thesis work. All praise be to Him; Allah, our self-sufficient. “Pay thanks to the man who has done a favor for you” said by His beloved prophet Mohammed (peace and blessings be upon him), I therefore have to thank firstly my supervisor Prof. Dr. Ilyas EKER for his patience and unlimited efforts to draw guidelines for my thesis work so as to be done on time.

To my parents, siblings and other family members for their continuous encouragement, to my friends, classmates, lab-mates, lab technicians and other lab assistants, I owe you all my kind respect and thanks.

I also would like to express my sincere gratitude towards the committee members.

I also would like to thanks to Turkish Government for the scholarship.

الي الجزائر الحبيبة ...

CONTENTS **PAGE**

LIST OF TABLES **PAGE**

LIST OF FIGURES **PAGE**

LIST OF SYMBOLS

θ_h, θ_v ..... Angles of rotation

V_{main}, V_{tail} ..... DC motors voltage inputs

ω_m, ω_t ..... Angular velocities of the DC motors

$\tau_m, \tau_{m,p}, \tau_t, \tau_{t,p}$ ..... Aerodynamic torques

U_t, U_m ..... Voltage controls

i_m, i_t ..... Input currents

E_t, E_m ..... Electromotive forces

$k_{am/t}$ φ_{at}, φ_{am} ..... Positive torque constants

ω_t, ω_m ..... Rotational speeds

M_{et}, M_{em} ..... Electromagnetic torques

M_{Lt} M_{Lm} ..... Load torques

B_{tr}, B_{mr} ..... Viscous friction coefficients of the tail and main DC motors

K_{mr}, K_{tr} ..... Static gains

T_{mr}, T_{tr} ..... Constant of motor- propeller system

F_h, F_v ..... Petonormal forces

$M_{fs}, M_{p/v}$ $M_g, M_c, M_{frict}, M_{c,m}$ $M_{c,t}$ $M_{c,c}$ M_h M_v ..... Torques applied to the system

J_{tr} J_{mr} J_m J_t J_{ms} J_{ts} J_v J_h J_b J_{cb} ..... Moments of Inertia

l_m l_t l_b l_{cb} l ..... Lengths

m_m m_{mr} m_t m_{tr} m_{cb} m_b m_{ts} m_{ms} ..... System complements masses

v ..... Velocity

$F_{c,th}$, $F_{s,m}$, $F_{s,t}$, $F_{s,c}$, $F_{c,c}$, $F_{c,mv}$ ..... Centripetal forces

r_m ..... Moment arm

ω_h , ω_v .....Velocities of the rotors

k_v , $k_{tm/t}$ ..... Positive constants

r_{ms} r_{ts} .....Radius shield

S_v , S_{tail} , $S_{v,res}$, S_h , S_{main} , $S_{h,res}$ ..... Angular momentums

$u_{\max}$, $u_{\min}$ ..... Maximum and minimum control inputs

e ..... Control error

y_{sp} .....Set point

r ..... Reference variable

y .....Measured process variable

u ..... Control signal

Ti .....Integral time

T_d ..... Derivative time

E ..... Error signal

U .....Output control

K , K_p , K_i , K_d .....Gains

g .....Gravity

LIST OF ABBREVIATONS

TRMS	**:** Twin Rotor Multi Input Multi Output System
DOF	**:** Degree Of Freedom
DC	**:** Direct Current
D/A	**:** Digital/Analog
PID	**:** Integral Derivative Proportional
PD	**:** Proportional Derivative
PI	**:** Proportional Integral
P	**:** Proportional
FL	**:** Fuzzy Logic
GA	**:** Genetics Algorithms
DCS	**:** Distributed Control System
H∞	**:** Hybrid Control
FLC	**:** Fuzzy Logic Controller
T2FLC	**:** Type 2 Fuzzy Logic Controller
T1FLC	**:** Type 1 Fuzzy Logic Controller
IT2FLC	**:** Interval Fuzzy Type 2 Logic Controller
Eq	**:** Equation
MFs	**:** Membership Functions
LMF	**:** Upper Membership Function
UMF	**:** Lower Membership Function
FOU	**:** Footprint Of Uncertainties
PC	**:**Personal computer
COG	**:**Center of Gravity
Freq	**:**Frequency

1. INTRODUCTION

1.1. Motivations

A helicopter is classified among the aircraft sorts that are moving up and elevating through the propelling force of one or more horizontal rotors, each of these horizontals rotors is consisted of at least two and more rotor blades (Federal, 2009). Helicopters also can be considered as rotorcrafts or a rotary-wing aircraft to differentiate them from aircrafts with fixed-wing due to the source of rising which takes it from the horizontal rotor blades rotating around an axe in the helicopter. The term of (Helicopter) actually is taken from the French word Hélicoptère, coined in 1861 by Gustave de Ponton. That is related meaningfully to the Greek words Helix/Helikos (spiral or turning) and Pteron (wing) (Federal, 2009). Figure 1.1 represents the most known type of Helicopters.

Figure 1.1. Military Helicopter UH-ONE

Due to the significant capabilities of taking off and landing from terrains vertically those personalize the helicopter, which allow it to keep hovering in a steady aerial position off a single point on the ground, helicopters get a huge importance and allowed to be used for rescue, medical evacuation and as an observation platform, also in other operation that involve the use of helicopters

such military firefighting, news gathering, tours, personnel transport, as an aerial crane, logging, electronic law enforcement, and for pleasure as well, including the important usage in the middle of the crowded cities and rugged places in craggy terrains (Nghia, 2007). In reality, helicopters can land everywhere that only need the ground lager than 1.5 times the helicopter's blades. Helicopter like aircraft can fly due to aerodynamic force or Zhukovski force (Nghia, 2007). That is the different pressure between top surface and bottom surface of the blade when the air flows cover it as illustrated below in Figure 1.2.

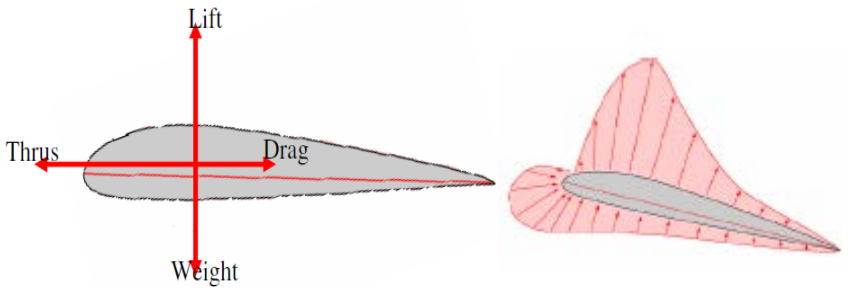

Figure 1.2. Propellers forces

The air flows around the blade that has to lift and simultaneously goes to drag. At the bottom side of the blade the produced pressure is higher than in the top's side, where here, this pressure creates a force starting from the bottom to the top and it is perpendicular with the blade. This difference in pressure depends the blade's type, attack-angle (pitch angle) of flowing and rotation of the blades. So the blades rotate with certain speed that is enough for helicopter to fly due to these aerodynamic forces, it means also that these created force are higher than helicopter's weight force (gravity). Later two factors are the angle of attack and the shape of the baled which will determine the value of the created lifting force and the level of helicopters flying through the. After the pilot can tilt the blades of the helicopter to the ground, this will make the helicopter tips forward or backward or sideward (Mahmoud and Yuanqing, 2012).

Nowadays the most popular kind among the huge varieties of helicopters is helicopter's model, the one that has a tail blade and lift blade. The blade here in this model of helicopters generally is airfoil. And the pilot can adjust through different means of control the angle of incidence. The lift rotor or (main rotor) of the helicopter may be consisted of two, three, four, five or six blades, depending upon the design. And to the rotor axe several main rotor blades are joined in such a way that they can be limited in moving up and down and they are able to change the pitch as well. Collective or Cyclic Controls is defining the controls for the main rotor (Mahmoud and Yuanqing, 2012).

The main rotor as shown in Figure 1.3 is responsible of generating a vertical thrust, this enable the helicopters to pitch, that can rotate in the vertical plane around the horizontal axe. It has two four or more big blades with different configurations, all are mounted on the head of the helicopter's main rotor.

Figure 1.3. Main rotor blade

The tail rotor's blades are smaller comparing to the main rotor's blades and may also include two or more blades. The tail rotor mounted vertically on the tail of the back side of the helicopter as shown in Figure 1.4, where can rotate in the vertical plane. rudder pedals are controlling the tail rotor, pitch can be changed as required to turn the helicopter in the direction desired (Mahmoud and Yuanqing Xia, 2012).

Figure 1.4 Tail rotor blades

When the blades lift, the body of helicopter also rotates around the blade at contrast direction. So avoiding this phenomena, it has a tail blade at vertical direction, blow the air in horizontal direction. Created moment of tail blade can eliminate with moment cross-action of the body. Besides that, it plays a role in changing the direction way of the helicopter into horizontal plane (Nghia, 2007).

These challenges make it a preferred control system setup for investigating, testing, and validating of the control theories those have challenges to keep the system stabilized (Dogan, 2015), by reaming its two angles yaw and pitch on to the desired positions area under any internal or external disturbances (Islam et al., 2003). The nonlinear, unstable and under actuated structure makes the control of TRMS a challenging problem. Control of such systems is an active subject in automatic control and robotic for both practical and theoretical interest. Various control design methodologies to solve tracking problem of TRMS have been investigated. Until recently, the control and system engineering framework offers several tools based on nonlinear control techniques, soft computing based adaptive and intelligent control techniques (Phillips and Sahin, 2014), and conventional linear control techniques (Ahmad et al., 2001). Fuzzy control is a versatile control technique that allows controlling through the descriptions of system behavior in items of linguistic variables constituting the rule base. The reason motivating us to experiment fuzzy control technique is mainly because of the appropriateness of the

behavior of the helicopter system. Furthermore, fuzzy controller can be used as an adaptive methodology as well it is combined with traditional control strategies to improve the stability, increase the robustness, and reduce the fuzzy rule base. As a general example, the combination between Fuzzy and PID controllers (Fuzzy-PID) is largely employed to control nonlinear systems by improving the control performance efficiency. While considering a feedback system with a fuzzy controller, there may be some uncertainties both in the controlled system and in the membership rules part of the fuzzy logic. However, the conventional fuzzy logic system or so-called fuzzy type-1 logic system cannot deal with such uncertainties (Rahideh and Shaheed, 2007; Patel et al., 2009). Recently, many researchers have been focused to increase fuzzy logic controller's performance and to overcome the uncertainty problems. In order to achieve robustness, an interval fuzzy type-2 strategy was introduced, as a new generation of fuzzy logic. The main structural difference between these two types of fuzzy logic controller is in the defuzzifier composited block, where a type reduction block is used during the defuzzification in type-2 fuzzy logic (Rahideh and Shaheed, 2007).

1.2. Objectives

This present thesis work is based on a helicopter simulator model of two degrees of freedom so-called Twin Rotor Multi-Input Multi-Output Systems (TRMS) which are widely used as control platforms (developed by Feedback Ltd) due to their high non-linearity and the coupling between axial motions. The system, which is driven vertically and horizontally through its two joined rotors placed at the end of the TRMS beam, is characterized with two degrees of freedom (DOF).

A new approach for the attitude stabilization for that kind of system TRMS is detailed presented. This approach is based on the type-2 fuzzy logic controller. The main strength of the proposed control algorithm is more robust than previous control algorithm (type-1FLC) with respect to parametric uncertainties and noise measurement. The proposed approach has been successfully applied, in simulation

and practical results, to the control of two degrees of freedom helicopter in the presence of parametric uncertainties and noise measurement.

1.3. Content Of Chapters

A brief introduction of structure, functional principle of the real helicopter and the objective of this project are given is chapter 1.

Chapter 2 consists of physical description of TRMS system and explanation of the mathematical modeling strategy that have been used to model the system.

Chapter 3 covers the literature review about the used control approaches and a synthesis and applications of various control strategies, namely, classical PID controller, Fuzzy type-1 PID controller and Fuzzy type-2 PID controller are demonstrated.

Chapter 4 is a discussion of the simulation results with a conclusion and the prospected work in future.

2. DYNAMICAL MODELLING OF THE TRMS

2.1. Description of the system

The TRMS is a laboratory setup which Feedback Instruments Ltd Company is providing it for the aim of testing and checking different new controllers. There also many other commercial products have been developed by several companies for some educational needs and especially for experiments of control theories in labs. Figure 2.1 shows a TRMS. The development and improvement design of TRMS have been taken firstly in the university labs like in Verzilli and Corradini (Dogan, 2015). Then to be produced after by National Instruments Company, which allows exchanging the data between the TRMS and the PC, and this setup of the TRMS is ensured by building an interface board to filter and to adapt sensor signals (Dogan, 2015).

Figure 2.1. Twin Rotor MIMO system (TRMS)

The Twin Rotor Multiple-Input Multiple-Output MIMO System so-called briefly a TRMS has functionality similarities with real helicopter's behavior in

different aspects like its high nonlinearity problem and the cross-coupling caused between two propellers and some other manners. which allow it to be a preferred tool in investigating, testing and validating of the control theories those have challenges to keep the system stabilized (Phillips and Sahin, 2014) by reaming its two angles yaw and pitch on to the desired positions area under any internal or external disturbances it is interesting also for control researchers to have in their laboratories such nonlinear problem. TRMS is characterized by a highly complex nonlinearity problem in dynamics and a cross-coupling between the two its axes with 2 two degrees of freedom (Dogan, 2015). The control objective for the researchers is to launch the two joined rotors to the beam of TRMS in a way to make it moving accurately as quick as possible to the wanted position and manner in terms of yaw angle and pitch angle under the decoupling effect caused due of the two axes simultaneous movements (2 degrees of freedom). In the system, pivot point allows the TRMS to move freely in vertical and horizontal planes (Islam et al., 2003) as it is shown above in Figure 2.1.

TRMS is provided for the purpose of testing new controllers (Phillips and Sahin, 2014) and comprises of tail rotor and main rotor. Where the first rotor can handle the system in horizontal plane and main rotor plane is for lift up the load in vertical. The TRMS is consisted of a rigid horizontal beam fixed through a 2 dimensional pivot to a vertical pillar on its base in a way that it can have a free rotation whether in the vertical planes or horizontal planes. The main rotor is attached laterally to one of the horizontal beam two extremes in a parallel position with the ground. The tail rotor is attached to the other extreme rear of the horizontal beam in a perpendicular position with the ground. A counterbalance weight is attached to second beam affixed vertically to the middle of the rotor's carried beam at the pivot to give the system a mobile equilibrium point. Both of the jointed rotors are controlled by two identical DC motors (Phillips and Sahin, 2014).

The angle of movement in horizontal plane θ_h and in vertical plane θ_v (Phillips and Sahin, 2014) can be measured by optical encoders and the calculated error between the desired positions that can be measured will become the input of our controller. If the TRMS is controlled for two degrees of freedom DOF, then in control structure two controllers are needed that will generate two outputs for each rotor. Each rotor has one propeller which generates a force directly proportional to the output of DC motor (Islam et al., 2003) as shown in Figure 2.2.

The objective of this literature review about the modeling part is to enable us to have a good idea about the system's physical functionality which leads to get the system stable and obtain a better system performance. The design a controller for the TRMS system is quite complicated due to the system's uncertainty, therefore, firstly having an idea about the physical behavior of the system should be known and transfer it after to a mathematical model that can be able to be controlled. In general the TRMS could be controlled by different control approach based on whether classical controllers, nonlinear controllers or soft computing as will be explained in next chapters (Islam et al., 2003).

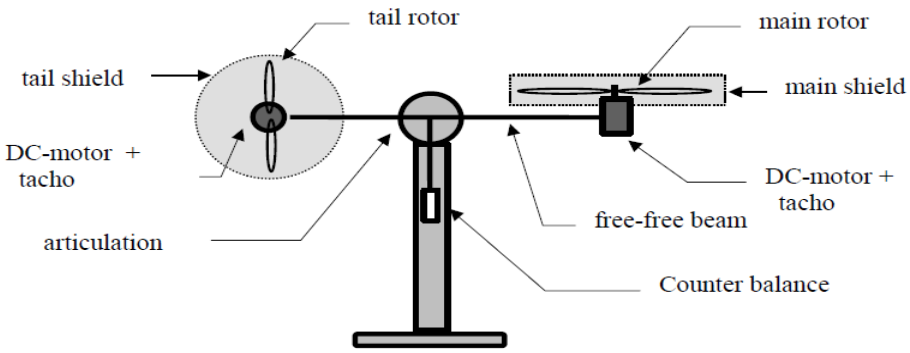

Figure 2.2. Structure model of TRMS

The position states of the beam are represented by four different variables, two of them are the vertical and the horizontal angles those are measured by the sensors placement fitted at the pivot.

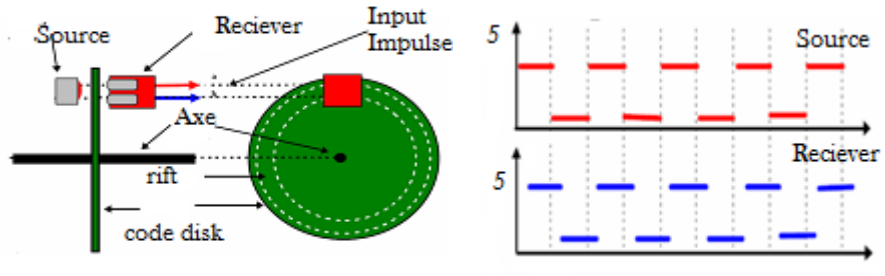

Figure 2.3. Position of the sensors

In order to calculate the angular velocity of each rotor, a Tacho-generator as shown in above Figure 2.3 is utilized. However varying the pitch angle or the (the angle of attack) in real-life helicopters allow us to control value of the aerodynamic forces, where in our used model these forces (aerodynamic) are controlled by changing the rotor's speed and acceleration. Furthermore that oppositely in real-life helicopters the angle of attack is fixed in the TRMS (Ahmad et al., 2001). Any effective changes in the input voltage value of the DC motors causes corresponding changes in the rotation speed of the propeller as well, which also causes changes of the corresponding altitude of the beam.

There are also optical encoders placed to the middle of the beam at the pivot to allow us to determinate the direction of rotor's rotation, through emitted lights from two light sources (Emitter1 and Emitter2) go via two canals of slits on the disc. The slits have a phase difference, so that the electric outputs of the receivers (Receiver1 and Receiver2) are rectangular waves with a phase difference. This last is employed to detect the rotor's rotation direction.

The TRMS control panel hardware is linked to a data acquisition board connected to the computer. Where the sensors and control signals flow from the computer via the D/A converter of the data acquisition. The outputs signals are directed to power amplifiers which drive the DC motor. All these components are enclosed in box located down of the TRMS (Phillips and Sahin, 2014) .

2.2. Review on the mathematical modeling of the TRMS

Before applying any of the control strategies, system identification is extremely important. Always a close model of TRMS can ensure a proper functionality and a similar response to the one in real. Although that the determination of an exact model of system dynamics is quite difficult and complex, many models have been developed mathematically based on different theories. There have been also some past research in the TRMS's dynamic modeling. Newtonian and Lagrangian approaches were employed in the physics-based methods and can be considered as the most popular approaches have been used. *Shih* had used Lagrangian approach (Gilardi and Sharf, 2002) to obtain a TRMS mathematical model and to check some of the characteristics of his proposed mathematical model such as gravity compensation, propeller thrust and the equilibrium position. (Rahideh and Shaheed, 2007) after together has brought two different dynamic models for the TRMS by using Lagrangian and Newtonian approaches and modeled the system's two DC motors , propulsive forces due to these motors, and the interface circuit as well (Rahideh et al., 2008). Artificial intelligence-based empirical approaches such as neural networks (Toha and Tokhi, 2009) , and genetic algorithms (Rahideha et al., 2012) were also utilized to improve the dynamic models of the TRMS. These previous presented approaches are generally developed by adding terms to the analytical model to reflect the effects that before were neglected when obtaining this analytical model. In (Rahideh and Shaheed, 2007), the Newtonian method utilized to improve the dynamic equations of the TRMS systems. In this analytical model some of the system's parameters were calculated and the rest of parameters those were neglected before, were estimated by using physical properties of the system. Later, GA optimization approach was utilized to improve the accuracy of the estimated parameters. (Rahideh et al., 2008) analytical approaches in conjunction with neural networks based empirical approaches were used to derive dynamic models for a one 2-DOF

TRMS. A black-box system identification technique is utilized to derive dynamic model of two DOF TRMS (Shih et al., 2008).

2.3. Modeling strategy

This section explains the chosen strategy for the modeling of the TRMS and the used simplifications to obtain the model.

2.3.1. Model simplifications

In order to simplify the modeling procedure, certain assumptions and simplifications are made concerning the system environment (Christensen, 2006).

- System isolation: The system is considered isolated. That is, it has a stationary (no accelerated) inertial frame with no external forces acting on the model.
- Inertia calculations: the calculations of the moments of inertia have been simplified by assuming the parts of the TRMS to be geometrically simple. Ex. the rotor blades are modeled as rectangular plates.
- Center of rotation: it is assumed that the beam with the rotors is attached to the center of the tower and hence the yaw motion is around this axis.
- Friction station: dry friction are not included in the models.

2.4. Sub-models of the TRMS

The strategy for modeling the TRMS is splitting the model into three sub-models for both the horizontal and vertical plane. All six sub-models are modeled separately.

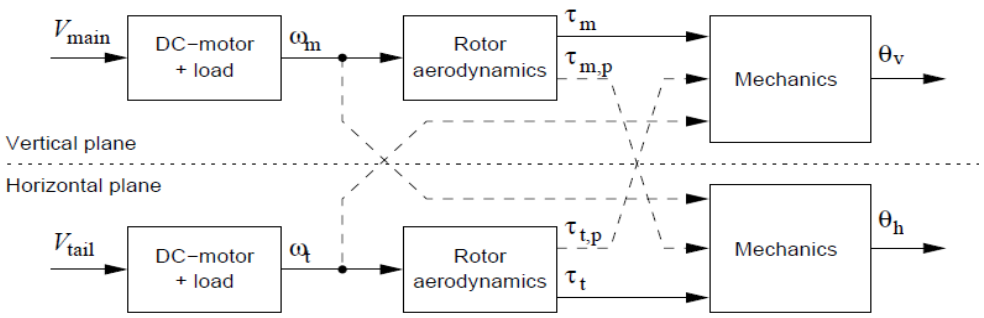

Figure 2.4. Schema diagram of TRMS modeling strategy

Figure 2.4 illustrates a schema diagram of the TRMS model and the couplings in the system. The system is divided into six sub-models which are each modeled independently (Phillips and Sahin, 2014). The sub-models are the DC-motors, the rotor aerodynamics and the mechanics for both the horizontal and the vertical plane. The DC-motor block has a main V_{main} and tail V_{tail} voltage input, and returns the angular velocities ω_m and ω_m respectively. The rotor aerodynamics has an angular velocity as input, and returns the aerodynamic torques τ_m , τ_t , $\tau_{m,p}$ and $\tau_{t,p}$. The mechanics of the system has inputs in the form of an aerodynamic force from the same plane, and the angular velocity is an aerodynamic force of the other plane. Example the horizontal plane has the input τ_m from the horizontal plane and $\tau_{t,p}$, τ_t from the vertical plane. The cross-couplings of the two planes are indicated by dashed lines. The output from the mechanics block is the azimuth (yaw) angle θ_h for the horizontal and the pitch angle for the vertical plane θ_v (Phillips and Sahin, 2014).

2.4.1. Dynamics of the DC motors

The purpose of this section is to develop a model for each of the two DC motors powering the rotors of the TRMS, thus identifying the relationship between the applied voltage to each motor and the resulting angular speed of their respective loads.

The non-linear model of the motor system is developed by combining models of the electrical and the mechanical characteristics of the DC motor with load.

2.4.1.1. Electrical properties of DC motor with load

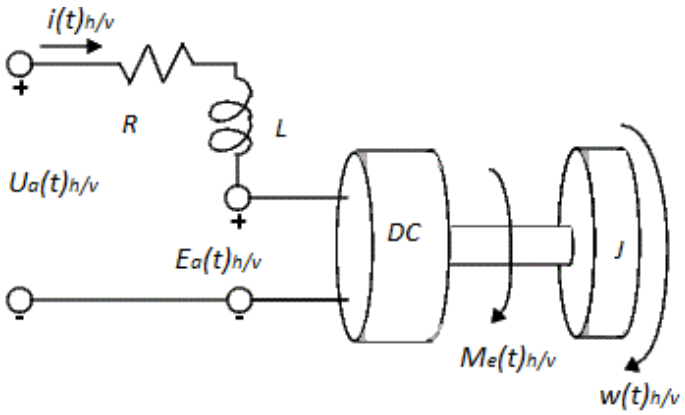

Figure 2.5. Circuit diagram of DC motor.

The DC motor with load equations is given as (Knudsen and Jensen, 1995):

$$U_{m/t}(t) = E_{m/t}(t) + R_{m/t} i_{m/t}(t) + L_{m/t} \frac{di_{m/t}(t)}{dt} \tag{2.1}$$

$$E_{m/t}(t) = k_{am/t} \varphi_{am/t} \omega_{m/t}(t) \tag{2.2}$$

where $U_m(t)$ and $U_t(t)$ are the horizontal and vertical voltage control inputs, $E_m(t)$ and $E_t(t)$ are the electromotive forces of the main and tail motor, $k_{am/t}\ \varphi_{am/t}$ are the

torque constants (positive constants), and $\omega_m(t)$ and $\omega_t(t)$ are the rotational speed of the main and tail rotors as shown in Figure 2.5.

from Eq. (2.1) and Eq. (2.2) we replace $E(t)_{av/h}$ to obtain:

$$U_{m/t}(t) = k_{am/t}\varphi_{am/t}\omega_{m/t}(t) + R_{m/t}i_{m/t}(t) + L_{m/t}\frac{di_{m/t}(t)}{dt} \tag{2.3}$$

Equation (2.3) relates the applied motor voltage $U_{v/h}(t)$ with the angular velocity of the motor, thereby bridging between the electric and mechanical part of the DC motor. Mechanical properties of DC motor.

2.4.1.2. Mechanical properties of DC motor with Load

The total moment $M_{em/t}$ applied to the DC motor with load is given as (Witczak, 2014):

$$M_{em/t}(t) = M_{Lm/t}(t) + J_{tr/mr}\frac{d\omega_{m/t}(t)}{dt} + B_{tr/mr}\omega_{m/t}(t) \tag{2.4}$$

where M_{em} and M_{et} are the electromagnetic moments of the main and tail motors, M_{Lm} and M_{Lt} are the load moments of the main and tail motors, J_{mr} and J_{tr} are the moments of inertia in the main and tail motors, B_{mr} and B_{tr} are the viscous friction coefficients of the main and tail motors, and $k_{tm/t}$ is a positive constant.

The load moment of the main and tail DC motors is given as (Rahideh and Shaheed, 2007):

$$M_{Lm/t}(t) = k_{tm/t}sign\left(\omega_{m/t}(t)\right)\omega^2{}_{m/t}(t) \tag{2.5}$$

The total moment $M_{em/t}(t)$ in relation of the current $i_{m/t}(t)$ it is given as (Witczak, 2014):

$$M_{em/t}(t) = k_{am/t}\varphi_{v/h} i_{m/t}(t) \tag{2.6}$$

Equation (2.6) and Eq. (2.5) are substituted into Eq. (2.4) to get:

$$k_{am/t}\varphi_{m/t} i_{m/t}(t) = k_{tm/t} sign\left(\omega_{m/t}(t)\right)\omega^2{}_{m/t}(t) + J_{tr/mr}\frac{d\omega_{m/t}(t)}{dt} + B_{tr/mr}\omega_{m/t}(t) \tag{2.7}$$

from the mechanical equivalent, the following differential equation of $i_{am/t}$ can be obtained:

$$i_{m/t}(t) = \frac{k_{tm/t} sign\left(\omega_{m/t}(t)\right)}{k_{am/t}\varphi_{m/t}(t)_{v/h}}\omega^2{}_{m/t}(t) + \frac{B_{tr/mr}}{k_{am/t}\varphi_{m/t}}\omega_{m/t}(t) + \frac{J_{tr/mr}}{k_{am/t}\varphi_{m/t}}\frac{d\omega_{m/t}(t)}{dt} \tag{2.8}$$

Equation (2.8) is substituted into Eq. (2.4) to get Eq. (2.9):

$$\begin{aligned} U_{m/t}(t) = {} & k_{am/t}\varphi_{m/t}\omega_{m/t}(t) + \frac{R_{m/t}k_{tm/t} sign\left(\omega_{m/t}(t)\right)}{k_{am/t}\varphi_{m/t}}\omega^2{}_{m/t}(t) + \frac{R_{m/t}B_{tr/mr}}{k_{am/t}\varphi_{m/t}}\omega_{m/t}(t) \\ & + \frac{R_{m/t}J_{tr/mr}}{k_{am/t}\varphi_{m/t}}\frac{d\omega_{m/t}(t)}{dt} + \frac{L_{m/t}k_{tm/t} sign\left(\omega_{m/t}(t)\right)}{k_{am/t}\varphi_{m/t}}\frac{d}{dt}\left(\omega^2{}_{m/t}(t)\right) + \\ & + \frac{L_{m/t}B_{tr/mr}}{k_{am/t}\varphi_{m/t}}\frac{d\omega_{m/t}(t)}{dt} + \frac{L_{m/t}J_{tr/mr}}{k_{am/t}\varphi_{m/t}}\frac{d^2\omega_{m/t}(t)}{dt^2} \end{aligned} \tag{2.9}$$

then:

$$\begin{aligned} U_{m/t}(t) = {} & \left(k_{m/t}\varphi_{m/t} + \frac{R_{m/t}B_{tr/mr}}{k_{am/t}\varphi_{m/t}}\right)\omega_{m/t}(t) + \frac{R_{m/t}k_{tm/t} sign\left(\omega_{m/t}(t)\right)}{k_{am/t}\varphi_{m/t}}\omega^2{}_{m/t}(t) \\ & + \left(\frac{R_{m/t}J_{tr/mr} + L_{m/t}B_{tr/mr}}{k_{am/t}\varphi_{m/t}}\right)\frac{d\omega_{m/t}(t)}{dt}\frac{L_{m/t}k_{tm/t} sign\left(\omega_{m/t}(t)\right)}{k_{am/t}\varphi_{m/t}}\frac{d\omega^2{}_{m/t}(t)}{dt^2} \\ & + \frac{L_{m/t}J_{tr/mr}}{k_{am/t}\varphi_{m/t}}\frac{d}{dt}\left(\omega^2{}_{m/t}(t)\right) \end{aligned} \tag{2.10}$$

and as a simplification Eq. (2.10) to be in order we will have Eq. (2.11):

$$U_{m/t}(t)=\frac{R_{m/t}k_{tm/t}sign\left(\omega_{m/t}(t)\right)}{k_{am/t}\varphi_{m/t}}\omega^{2}{}_{m/t}(t)+\left(k_{am/t}\varphi_{m/t}+\frac{R_{m/t}B_{tr/mr}}{k_{am/t}\varphi_{m/t}}\right)\omega_{m/t}(t)$$
$$+\left(\frac{R_{m/t}J_{tr/mr}+L_{m/t}B_{tr/mr}}{k_{am/t}\varphi_{m/t}}\right)\frac{d\omega_{m/t}(t)}{dt}+\frac{L_{m/t}J_{tr/mr}}{k_{am/t}\varphi_{m/t}}\frac{d^{2}\omega_{m/t}(t)}{dt^{2}} \quad (2.11)$$
$$+\frac{L_{m/t}k_{tm/t}sign\left(\omega_{m/t}(t)_{v/h}\right)}{k_{am/t}\varphi_{m/t}}\frac{d}{dt}\left(\omega^{2}{}_{m/t}(t)\right)$$

According to Eq. (2.11), describing the relationship between the inputs of the two motors $U_{v/h}(t)$ with the rotational speed $\omega_{av/h}(t)$ of the mechanical part of the model is reduced to the following non-linear differential equation:

$$U_{m/t}(t)=k_1\omega^{2}{}_{m/t}(t)+k_2\omega_{m/t}(t)+k_3\frac{d\omega_{m/t}(t)}{dt}+k_4\frac{d^{2}\omega_{m/t}(t)}{dt^{2}}+k_5\frac{d}{dt}\left(\omega^{2}{}_{m/t}(t)\right) \quad (2.12)$$

where k_1, k_2, k_3, k_4 and k_5 are constants :

$$k_1=\frac{R_{m/t}k_{tm/t}sign\left(\omega_{m/t}\right)}{k_{am/t}\varphi_{m/t}} \qquad k_3=\left(\frac{R_{av/h}J_{tr/mr}+L_{av/h}B_{tr/mr}}{k_{av/h}\varphi_{v/h}}\right) \qquad k_4=\frac{L_{m/t}J_{tr/mr}}{k_{am/t}\varphi_{m/t}}$$
$$k_5=\frac{L_{m/t}k_{tm/t}sign\left(\omega_{m/t}\right)}{k_{am/t}\varphi_{m/t}} \qquad k_2=\left(k_{am/t}\varphi_{m/t}+\frac{R_{m/t}B_{tr/mr}}{k_{am/t}\varphi_{m/t}}\right)$$

2.4.1.3. Modeling of DC Motor with Load

As a modeling strategy of the DC motor with load we can say that the nonlinear term is coming from the added joint of the mechanical part. And in fact the DC motor with load is sum of two blocks one is linear and the other is nonlinear.

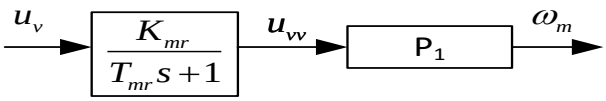

Figure 2.6. Block diagram of the main DC motors. And the relationship between the input voltage u_v and the angular speed ω_m

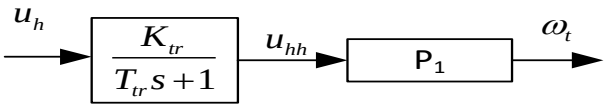

Figure 2.7. Block diagram of the tail DC motors. And the relationship between the input voltage u_h and the angular speed ω_t

The models given above in Figure 2.6 and Figure 2.7 of the motor's propeller dynamics are calculated by substituting the nonlinear system by a serial connection of a linear dynamic system and static non-linearity (Islam et al., 2003). where u_v and u_h are the DC motor voltage imputes, ω_m and ω_t are the velocities speed of the rotation, K_{mr} and K_{tr} is the static gain of the main/tail motor, T_{mr} and T_{tr} is propeller system's time constant of main and tail DC motor. The following non-linear function is necessary identified that can determine the relationship between the voltage input and the rational speed as a polynomial (Liu et al., 2011):

$$\omega_{m/t}\left(u_{v/h}(t)\right) = \sum_{i=1}^{6}\left\{P_1(i) * u_{v/h}(t)^i\right\} \tag{2.14}$$

where $P_1(i)$ is sixth degree polynomials can be approximated by measurements obtained experimentally.

2.5. Aerodynamics modeling

The actuators on the TRMS are two rotors which produce the thrust enabling the model to yaw and pitch. This chapter explains the theory behind rotor-generated thrust and develops a model for the moment created by the rotors about the TRMS's axes of rotation as shown in Figure 2.8.

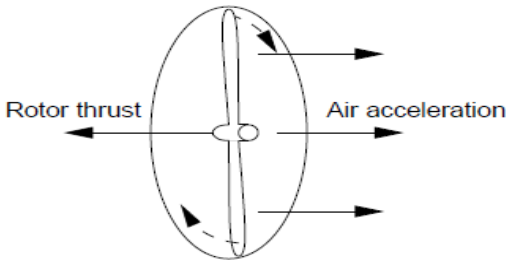

Figure 2.8. The acceleration of air through the rotor causes a thrust force in the opposite direction.

2.5.1. Main and tail rotor models

Modeling the aerodynamic torques using the method of first principle may yield a result that differs considerably from the actual behavior. Using a black-box test is much simpler and is more likely to produce more accurate results and because of gravity pulling the beam down, the main rotor is expected only to work with positive inputs. The tail rotor is expected to work in its entire range.

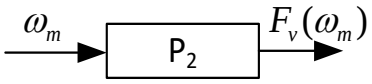

Figure 2.9. The relationship between the angular speed and the propulsive forces for the mail motor.

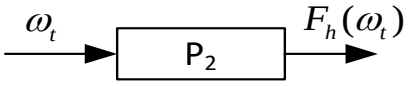

Figure 2.10. The relationship between the angular speed and the propulsive forces for the trail motor.

Figure 2.9 and Figure 2.10 insulated the relationship between the angular velocities ω_t and ω_m as inputs and the generated forces F_h and F_m. In addition to the thrust force, a force known as the petonormal force, perpendicular to the thrust force, was also identified. The relationship between the angular velocity of the rotors, and the

thrusts and petonormal forces of the main and tail rotors were found by experimentation. Thus, by knowing the transfer function of the DC-motors which includes the dynamics of the rotors, and knowing the aerodynamic forces generated by the rotors. The following non-linear function is necessary identified that can determine the relationship between the propeller thrust and the rational speed as a polynomial is given as (Liu et al., 2011):

$$F_v\left(\omega_m(t)\right)=\sum_{i=1}^{5}\left\{P(i)*\omega_m^i(t)\right\} \tag{2.15}$$

$$F_h\left(\omega_t(t)\right)=\sum_{i=1}^{5}\left\{P(i)*\omega_t^i(t)\right\} \tag{2.16}$$

where $P(i)$ is a sixth degree polynomials can be approximated experimentally.

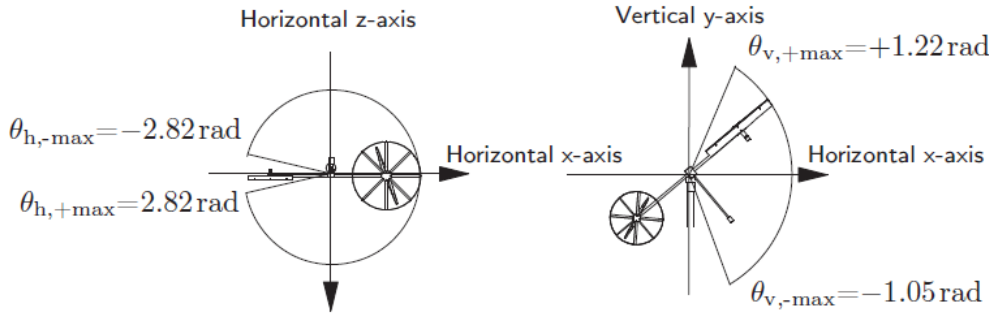

Figure 2.11. Working range of TRMS.

Figure 2.11 shows the working range of the TRMS system where $\omega_v(t)$ and $\omega_h(t)$ are the angular velocity of the main and tail rotor, respectively. From the working point, the model can turn from +2.82 rad to -2.82 in the horizontal plane and from -1.05 rad to 1.22 rad in the vertical plane.

In order to derive the physical model the torques and moments of inertia acting on the TRMS are found. To simplify the derivation the movement of the TRMS is divided into a vertical and a horizontal plane. With all the torques and

moments of inertia found, the laws of conservation of momentum leads to a transfer function in each plane (Ahmad et al., 2001).

2.6.Modeling of the mechanical part of the TRMS

As we mentioned before the Newtonian method is used to model the mechanical part of the TRMS which is based on determination of the moments of forces applied to the beam which making it rotates around the horizontal and vertical axis, consider the situation shown in Figure 2.11 below.

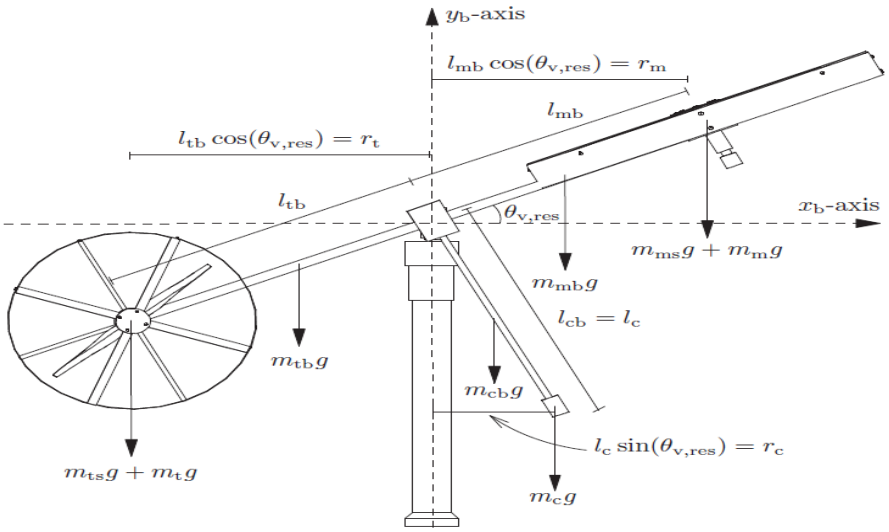

Figure 2.12. Propulsive force and gravity forces in the vertical plane

The mechanical system of TRMS is simplified using four points mass system as show in Figure 2.12 includes main rotor, tail rotor, balance weight and counter weight

2.6.1. Mathematical model of vertical plane

In the vertical plane, five distinct moments act on the TRMS:

- The moment M_{fs} generated by the thrust (propulsive force) from the main rotor.
- The moment $M_{p/v}$ generated by the petonormal force from the tail rotor.
- The moment M_g generated by the gravitational forces.
- The moment M_c generated by the centripetal forces.
- The moment M_{frict} generated by the friction force.

Moments of gravitational forces (M_g) is given as (Kim and Song, 2013):

$$M_g = gml \tag{2.16}$$

where g is the gravity, l is the length between the center of gravity and m_m is the mass.

In order to determine the moment from the gravitational force, it is divided into three parts, the tail part, the main part, and the counterweight part. The forces are depicted in Figure 2.12.

Moment generated from the tail part:

$$M_{g/t}(t) = gm_t \frac{l_t \cos\theta_v(t)}{2} + gm_{tr} l_t \cos\theta_v(t) + gm_{ts} l_t \cos\theta_v(t) \tag{2.17}$$

where m_t is the mass of the tail part of the beam, m_{tr} is the mass of the tail DC motor with the tail rotor, m_{ts} is the mass of the shield of the tail DC motor, l_l is the length between the of end point of the tail part and the pivot. The moment from the main part:

$$M_{g/m}(t) = -gm_m \frac{l_m \cos\theta_v(t)}{2} - gm_{mr} l_m \cos\theta_v(t) - gm_{ms} l_m \cos\theta_v(t) \tag{2.18}$$

where m_m is the mass of the main part of the beam, m_{mr} is the mass of the main DC motor with the main rotor, m_{ms} is the mass of the shield of the main DC motor and l_m is the length of the main part of the beam.

The moment from the counterweight and counterweight beam:

$$M_{g/b}(t) = -gm_b \frac{l_b \sin\theta_v(t)}{2} - gm_{cb} l_{cb} \sin\theta_v(t) \tag{2.19}$$

where m_b is the mass of the counter weight of the beam, m_{cb} is the mass of the counter weight, l_b is the length of the counter weight beam and l_{cb} is the length of the counter weight.

since:

$$l_b = l_{cb}$$

Equation (2.14.) Eq. (2.15.) and Eq. (2.16.) are used to obtain:

$$M_g(t) = gm_t \frac{l_t \cos\theta_v(t)}{2} + gm_{tr} l_t \cos\theta_v(t) + gm_{ts} l_t \cos\theta_v(t) - gm_m \frac{l_m \cos\theta_v(t)}{2} - \\ - gm_{mr} l_m \cos\theta_v(t) - gm_{ms} l_m \cos\theta_v - gm_b \frac{l_b \sin\theta_v(t)}{2} - gm_{cb} l_{cb} \sin\theta_v(t) \tag{2.20}$$

and it can be simplified as:

$$M_g(t) = g\left\{\left[\left(\frac{m_t}{2} + m_{tr} + m_{ts}\right) l_t - \left(\frac{m_m}{2} + m_{mr} + m_{ms}\right) l_m\right] \cos\theta_v(t) - \left(\frac{m_b}{2} l_b + m_{cb} l_{cb}\right) \sin\theta_v(t)\right\} \tag{2.21}$$

The moment of gravitational forces can be reduced to:

$$M_g(t) = \left\{\left[A - B\right] \cos\theta_v(t) - C \sin\theta_v(t)\right\} \tag{2.22}$$

Where the constants A, B,C are:

$$A = \left(\frac{m_t}{2} + m_{tr} + m_{ts}\right) l_t \qquad C = \left(\frac{m_b}{2} l_b + m_{cb} l_{cb}\right) \qquad B = \left(\frac{m_m}{2} + m_{mr} + m_{ms}\right) l_m$$

Moments of propulsive forces (M_{fp}) applied to the beam:

$$M_{fp}(t) = l_m F_v\left(\omega_v(t)\right) \tag{2.23}$$

Moment of the centrifugal forces (M_c). Corresponding to the motion of the beam around the vertical axis. The centripetal force is defined as (Raymond et al., 2004):

$$F_c = m\frac{v^2}{r} \tag{2.24}$$

where *v* is the velocity of the object with mass *m* moving in a circle with radius *r*. To determine the centripetal forces acting on the TRMS, this is divided into 3 parts.

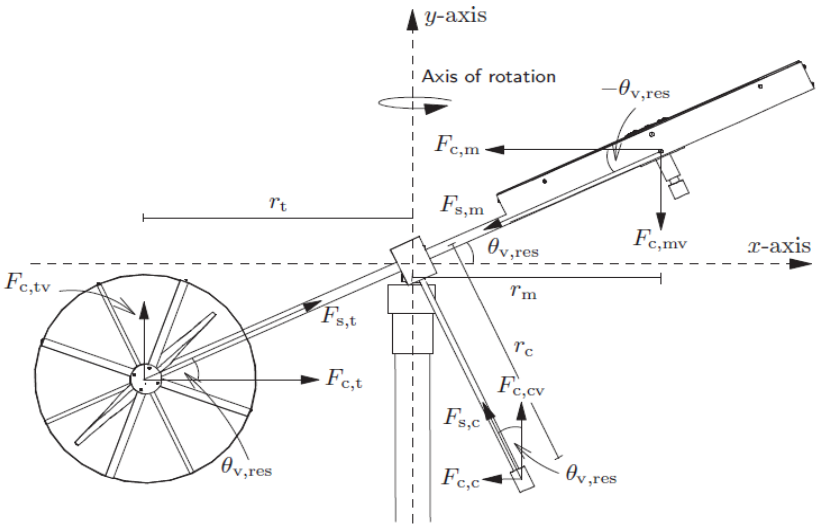

Figure 2.13. The centripetal force acting on the main rotor $F_{c,m}$ the tail rotor $F_{c,t}$ and the counter weight $F_{c,c}$ as the model spins around the *y* axis

The centripetal force from the main part is seen in Figure 2.13 can be described as:

$$F_{c,m}(t) = m\frac{v^2(t)}{r(t)} = \left(\frac{m_m}{2} + m_{mr} + m_{ms}\right)\frac{\omega_h^2(t) r_m^2}{r_m(t)} \tag{2.25}$$

where w_s is the velocity in the horizontal plane. $F_{c,m}$ Is the horizontal component of the string force $F_{s,m}$ exerted by the main beam.

$$F_{c,m}(t) = \left(\frac{m_m}{2} + m_{mr} + m_{ms} \right) \omega_h^2(t) r_m(t) \tag{2.26}$$

since

$$r_m(t) = l_m \cos\theta_v(t) \tag{2.27}$$

The vertical component $F_{c,mv}$ is given by multiplying by tangent to $-\theta_v(t)$:

$$F_{c,mv}(t) = \left(\frac{m_m}{2} + m_{mr} + m_{ms} \right) \omega_h^2(t) r_m \left(\tan - \theta_v(t) \right) \tag{2.28}$$

$$F_{c,mv}(t) = \left(\frac{m_m}{2} + m_{mr} + m_{ms} \right) \omega_h^2(t) l_m \cos\theta_v(t) \frac{\sin\left(-\theta_v(t)\right)}{\cos\left(-\theta_v(t)\right)} \tag{2.29}$$

$$F_{c,mv}(t) = -\left(\frac{m_m}{2} + m_{mr} + m_{ms} \right) \frac{\omega_h^2(t) l_m \cos\left(-\theta_v(t)\right) \sin\left(\theta_v(t)\right)}{\cos\left(-\theta_v(t)\right)} \tag{2.30}$$

Equation (2.30) can be represented as:

$$F_{c,mv}(t) = -\omega_h^2(t) \left(\frac{m_m}{2} + m_{mr} + m_{ms} \right) l_m \sin\left(\theta_v(t)\right)$$

The moment $M_{c,m}$ is obtained by multiplying the force by its moment arm r_m, which again is expressed in l_m:

$$M_{c,m}(t) = -\omega_h^2(t) \left(\frac{m_m}{2} + m_{mr} + m_{ms} \right) l_m \sin\left(\theta_v(t)\right) r_m(t) \tag{2.31}$$

$$M_{c,m}(t) = -\omega_h^2(t)\left(\frac{m_m}{2} + m_{mr} + m_{ms}\right) l_m \sin\left(\theta_v(t)\right) l_m \cos\theta_v(t) \tag{2.32}$$

as a simplification of the Eq. (2.32) it can be written :

$$M_{c,m}(t) = -\omega_h^2(t) B l_m \sin\left(\theta_v(t)\right) \cos\theta_v(t) \tag{2.33}$$

The centripetal force acting on the tail part is found in the same way:

$$F_{c,t}(t) = \frac{v^2(t)}{r_t(t)} = \left(\frac{m_t}{2} + m_{tr} + m_{ts}\right) \frac{\omega_h^2(t) r_t^2(t)}{r_t(t)} \tag{2.34}$$

where ω_h is the velocity in the horizontal plane. $F_{c,t}$ Is the horizontal component of the string force $F_{s,t}$ exerted by the tail beam.

$$F_{c,t}(t) = \left(\frac{m_t}{2} + m_{tr} + m_{ts}\right) \frac{\omega_h^2(t) r_t^2(t)}{r_t(t)}$$

since

$$r_t(t) = l_t \cos\theta_v(t) \tag{2.35}$$

Equation (2.35) became:

$$F_{c,t}(t) = \left(\frac{m_t}{2} + m_{tr} + m_{ts}\right) \omega_h^2(t) l_t \cos\theta_v(t) \tag{2.36}$$

This is the horizontal component which is multiplied with the tangent $\theta_v(t)$ to get the vertical component.

$$F_{c,tv}(t) = \left(\frac{m_t}{2} + m_{tr} + m_{ts}\right) \omega_h^2(t) l_t \cos\theta_v(t) \left(\tan\theta_v(t)\right) \tag{2.37}$$

$$F_{c,tv}(t) = \left(\frac{m_t}{2} + m_{tr} + m_{ts}\right) \omega_h^2(t) l_t \cos\theta_v(t) \frac{\sin\left(\theta_v(t)\right)}{\cos\left(\theta_v\right)(t)} \tag{2.38}$$

Equation (2.34.) can be represented as:

$$F_{c,tv}(t) = \omega_h^2(t)\left(\frac{m_t}{2} + m_{tr} + m_{ts}\right) l_t \sin\left(\theta_v(t)\right) \tag{2.39}$$

The moment $M_{c,t}$ is obtained by multiplying the force by its moment arm r_m, which again is expressed in l_t

$$M_{c,t}(t) = \omega_h^2(t)\left(\frac{m_t}{2} + m_{tr} + m_{ts}\right) l_t \sin\left(\theta_v(t)\right) r_m(t) \tag{2.40}$$

$$M_{c,t}(t) = \omega_h^2(t)\left(\frac{m_t}{2} + m_{tr} + m_{ts}\right) l_t \sin\left(\theta_v(t)\right) l_t \cos\theta_v(t) \tag{2.41}$$

as a simplification of the Eq. (2.41) it can be written:

$$M_{c,t}(t) = \omega_h^2(t)\left(\frac{m_t}{2} + m_{tr} + m_{ts}\right) l_t^{\,2} \sin\left(\theta_v(t)\right) \cos\theta_v(t) \tag{2.42}$$

and Equation (2.42) can be written as:

$$M_{c,t}(t) = \omega_h^2(t) A l_t \sin\left(\theta_v(t)\right) \cos\theta_v(t) \tag{2.43}$$

As this moment has to be referred to the main part of the TRMS the sign of $M_{c,t}$ must be altered:

$$M_{c,t}(t) = -\omega_h^2(t) A l_t \sin\left(\theta_v(t)\right) \cos\theta_v(t) \tag{2.44}$$

The centripetal force acting on the counterweight and counterweight beam is found in the same way:

$$F_{c,c}(t) = \frac{v^2(t)}{r_c(t)} = \left(\frac{m_{cb}}{2} + m_c\right) \frac{\omega_h^2(t) r_c^2(t)}{r_c(t)} \tag{2.45}$$

where ω_h is the velocity in the horizontal plane. $F_{c,c}$ Is the horizontal component of the string force $F_{s,c}$ exerted by the tail beam.

$$F_{c,c}(t) = \left(\frac{m_{cb}}{2} + m_c \right) \omega_h^2(t) r_c\ (t) \tag{2.46}$$

$$r_c\ (t) = l_c \sin \theta_v(t) \tag{2.47}$$

Equation (2.47) can be represented as:

$$F_{c,c}(t) = \left(\frac{m_{cb}}{2} + m_c \right) \omega_h^2(t) l_c \sin \theta_v(t) \tag{2.48}$$

To get the vertical component the expression is divided by tangent to θ_v

$$F_{c,c}(t) = \frac{\left(\frac{m_{cb}}{2} + m_c \right) \omega_h^2(t) l_c \sin \theta_v(t)}{\frac{\sin\left(\theta_v(t)\right)}{\cos\left(\theta_v(t)\right)}} \tag{2.49}$$

$$F_{c,c}(t) = \left(\frac{m_{cb}}{2} + m_c \right) \omega_h^2(t) l_c \cos \theta_v(t) \tag{2.50}$$

The moment from the centripetal force of the counterweight and counterweight beam is determined equivalently:

$$M_{c,c}(t) = \left(\frac{m_{cb}}{2} + m_c \right) \omega_h^2(t) l_c \cos \theta_v(t) l_c \sin \theta_v(t) \tag{2.51.}$$

Equation (2.51) can be written as:

$$M_{c,c}(t) = \omega_h^2(t) C l_c \cos \theta_v(t) \sin \theta_v(t) \tag{2.52}$$

Hence the total moment of the centripetal forces M_c is given by:

$$M_c = M_{c,m} + M_{c,t} + M_{c,c} \tag{2.53}$$

adding Eq. (2.32), Eq. (2.45) and Eq. (2.52) yields the total moment from the centripetal forces:

$$M_c(t) = -\omega_h^2(t)\left(\frac{m_m}{2} + m_{mr} + m_{ms}\right) l_m{}^2 \sin(\theta_v)\cos\theta_v(t) + \left(\frac{m_{cb}}{2} + m_c\right)\omega_h^2(t) l_c{}^2 \cos\theta_v(t)\sin\theta_v(t)$$
$$-\omega_h^2(t)\left(\frac{m_t}{2} + m_{tr} + m_{ts}\right) l_t{}^2 \sin\theta_v(t)\cos\theta_v(t) \tag{2.54}$$

Equation (2.49.) gives:

$$M_c(t) = -\omega_h^2(t)\left\{\left(\frac{m_t}{2} + m_{tr} + m_{ts}\right) l_t + \left(\frac{m_m}{2} + m_{mr} + m_{ms}\right) l_m + \left(\frac{m_b}{2} l_b + m_{cb} l_{cb}\right)\right\}\sin\theta_v(t)\cos\theta_v(t) \tag{2.55}$$

and Equation (2.55), it can be reduced to:

$$M_c(t) = -\omega_h^2(t)\left\{Al_m + Bl_t - Cl_c\right\}\sin\theta_v(t)\cos\theta_v(t) \tag{2.56}$$

Moment of friction (M_{frict}) depends on the angular velocity of the beam around the horizontal axis: The friction acting on the TRMS consists of two parts, the linear viscous friction and the non-linear static friction. Neglecting the static friction leaves a linear expression for the torque caused by the viscous friction (Raymond et al., 2004):

$$M_{frict}(t) = -k_v\omega_v(t) \tag{2.57}$$

where k_v is a positive given constant.

The moment $M_{p/v}$ generated by the petonormal force from the tail rotor (Raymond et al., 2004):

$$M_{p/v}(t) = -k_t \omega_t(t) \tag{2.58}$$

where k_t is a positive given constant.

Moments of inertia, to determine the total moment of inertia in the vertical plane the TRMS is separated into eight parts, each described individually.

The DC-motor is considered a solid cylinder with $J_m = \frac{1}{2} m_m r_m^2$. By the parallel-axis theorem the moment of inertia for the DC-motor placed at a distance of l_m from the rotation axis is (Raymond et al., 2004):

$$J_{mr} = \frac{1}{2} m_m r_m^2 + m_{mr} l_m^2$$

Since $r_{mr} << l_m$

So

$$J_{mr} = m_{mr} l_m^2$$

The moment of inertia for the main beam is given directly by:

$$J_m = m_m l \frac{l_m^2}{3}$$

Similarly the moment of inertia of the tail DC-motor with rotor and the tail beam is found,

$$J_{tr} = m_{tr} l_t^2 \text{ and } J_t = m_t \frac{l_t^2}{3}$$

And for the counterweight and counterweight beam:

$$J_{cb} = m_{cb} l_{cb}^2 \text{ and } J_b = m_b \frac{l_b^2}{3}$$

The main shield in the vertical plane can be approximated by a solid cylinder and using the parallel-axis theorem its moment of inertia can be expressed as:

$$J_{ms} = \frac{m_{ms}}{2} r_{ms}^2 + m_{ms} l_m^2$$

The tail rotor shield can be approximated by a cylindrical shell, yielding a moment of inertia given of:

$$J_{ts} = \frac{m_{ts}}{2} r_{ts}^2 + m_{ts} l_t^2$$

where J_{mr} is moment of inertia for main rotor with motor.

J_m is moment of inertia for main rotor beam .

J_{cb} is moment of inertia for the counter weight .

J_b is moment of inertia for the counter weight ‘s rod.

J_t is moment of inertia for tail rotor with motor.

J_t is moment of inertia for tail beam .

J_{ms} is moment of inertia for the main rotor’s shield.

J_{ts} is moment of inertia for the tail rotor’s shield.

r_{ms} is radius of main shield.

r_{ts} is radius of tail shield.

$$J_v(t) = \sum_{i=1}^{8} J_{vi}(t) \tag{2.59}$$

The total moments of inertia J_v in the vertical plane can be written as:

$$J_v = m_{mr} l_m^2 + m_m l \frac{l_m^2}{3} + m_{tr} l_t^2 + m_t \frac{l_t^2}{3} + m_{cb} l_{cb}^2 + m_b \frac{l_b^2}{3} + \frac{m_{ms}}{2} r_{ms}^2 + m_{ms} l_m^2 + \frac{m_{ts}}{2} r_{ts}^2 + m_{ts} l_t^2 \tag{2.60}$$

and the total moments of forces M_v applied in the vertical place are:

$$M_v(t) = \sum_{i=1}^{5} M_{vi}(t) \tag{2.61}$$

$$M_v(t) = \sum_{i=1}^{5} M_{vi}(t) = M_g(t) + M_c(t) + M_{fricti}(t) + M_{fp}(t) + M_{p/v}(t) \tag{2.62}$$

Summing the moments of forces applied to the vertical plane to each other we find:

$$M_v(t) = \left\{ \left[A - B \right] \cos\theta_v(t) - C \sin\theta_v(t) \right\} - \omega_h^2(t) \left\{ Al_m + Bl_t - Cl_c \right\} \sin\theta_v(t) \cos\theta_v(t) - \omega_v(t) k_v - \omega_t(t) k + l_m F_v(t) \left(\omega_m(t) \right)_t \tag{2.63}$$

where M_v is the total moment of forces applied in the vertical plane, J_v is the sum of the moments of inertia relative to the vertical axis.

From conservation of angular momentum of a rigid object, such as the TRMS, the following is stated (Raymond et al., 2004):

$$S_v(t) = J_v \omega_v(t) \tag{2.64}$$

Applying the theorem of angular momentum yields:

$$S_{v,res}(t) = S_v(t) + S_{tail}(t) \tag{2.65}$$

$$S_{tail}(t) = J_{tr} \omega_t(t) \tag{2.66}$$

where: S_v is angular momentum in the vertical plane arising from external torque affecting the TRMS, S_{tail} is the angular momentum from the tail rotor spinning and $S_{v,res}$ is the resulting angular momentum, J_{tr} the inertia is the inertia of the trail rotor blades.

$$S_{v,res}(t) = S_v(t) + J_{tr} \omega_t(t)$$

$$J_v \omega_{v,res}(t) = S_v(t) + J_{tr} \omega_t(t)$$

$$\omega_{v,res}(t) = \frac{S_v(t) + J_{tr}\omega_t(t)}{J_v} \tag{2.67}$$

in order to determine J_{tr} the rotors will be approximated as a rectangular plate which has inertia of (Raymond et al., 2004):

$$J = \frac{1}{12} M \left(a^2 + b^2\right) \tag{2.68}$$

From Eq. (2.68), J_{tr} can be written as:

$$J_{tr} = \frac{1}{12} m_{tr} \left(l_{wl}{}^2 + l_{tl}{}^2\right) \tag{2.69}$$

solving the system is considered the rotation of the beam in the vertical plane around the horizontal axis. Applying the Newton's second law of motion we obtain:

$$M_v(t) = J_v \frac{d^2\theta_v(t)}{dt^2} \tag{2.70}$$

$$\frac{d^2\theta_v(t)}{dt^2} = \frac{dS_v(t)}{dt} = \frac{M_v(t)}{J_v}$$

Eq. (2.70) can be written as:

$$\frac{dS_v(t)}{dt} = \frac{\sum_{i=1}^{5} M_{vi}(t)}{J_v} \tag{2.71}$$

the sun of the total moments of forces from Eq. (2.63) and put in Eq. (2.71) to obtain:

$$\frac{dS_v(t)}{dt} = \frac{\left\{\left[A-B\right]\cos\theta(t)_v - C\sin\theta_v(t)\right\} - \omega_h^2(t)\left\{A+B+C\right\}\sin\theta_v(t)\cos\theta_v(t)}{m_{mr}l_m^2 + m_m l\frac{l_m^2}{3} + m_{tr}l_t^2 + m_t\frac{l_t^2}{3} + m_{cb}l_{cb}^2 + m_b\frac{l_b^2}{3} + \frac{m_{ms}}{2}r_{ms}^2 + m_{ms}l_m^2 + \frac{m_{ts}}{2}r_{ts}^2 + m_{ts}l_t^2}$$
$$- \frac{\omega_v(t)k_v - \omega_t(t)k_t + l_m F_v(t)\left(\omega_m(t)\right)}{m_{mr}l_m^2 + m_m l\frac{l_m^2}{3} + m_{tr}l_t^2 + m_t\frac{l_t^2}{3} + m_{cb}l_{cb}^2 + m_b\frac{l_b^2}{3} + \frac{m_{ms}}{2}r_{ms}^2 + m_{ms}l_m^2 + \frac{m_{ts}}{2}r_{ts}^2 + m_{ts}l_t^2} \tag{2.72}$$

then:

$$\omega_v(t) = \frac{S_v(t) + J_{tr}\omega_t(t)}{J_v} \tag{2.73}$$

the $\theta_v(t)$ is given as (Raymond et al., 2004):

$$\frac{d\theta_v(t)}{dt} = \omega_v(t) \tag{2.74}$$

Where $\theta_v(t)$ is the pitch angle of the beam.

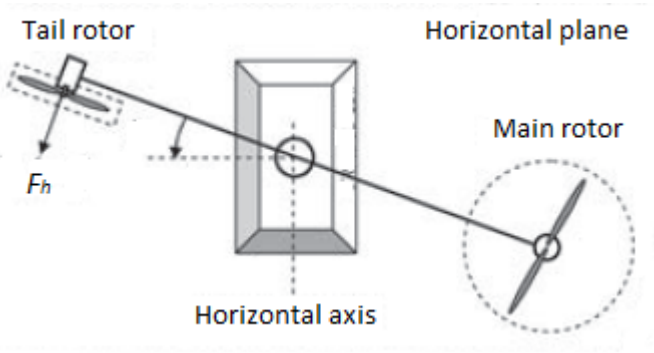

Figure 2.14. Propulsive force in the horizontal plane

2.6.2. Mathematical model of horizontal plane

It has four applied moments to the beam in the horizontal plane of the system as it is shown in Figure 2.14:

- The moment M_{fs} generated by the thrust (propulsive forces) from the tail rotor.
- The moment M_{frict} generated by the friction force.
- The moment M_{spri} generated by the spring force
- The moment $M_{p/h}$ generated by the petonormal force from the main rotor.
- The moments of inertia in the horizontal plane.

Moments of propulsive forces (M_{fp}) applied to the beam and making it rotate around vertical axis is given as (Rahideh and Shaheed, 2007):

$$M_{fp}(t) = F_h\left(\omega_t(t)\right) l_t \cos\theta_v(t) \tag{2.75}$$

Moment of friction (M_{frict}) depends on the angular velocity of the beam around the vertical axis (Rahideh and Shaheed, 2007):

$$M_{frict}(t) = -k_h \omega_h(t) \tag{2.76}$$

where k_h is a positive constant.

The spring moment M_{spri} originate from the flat cables connecting the computer with the TRMS. As the TRMS rotate these cables influence the TRMS. This influence is also assumed to be linear and will be described as (Raymond et al., 2004):

$$M_{spri}(t) = -\theta_h(t) k_{spri} \tag{2.77}$$

where k_{spri} is a positive constant.

The moment $M_{p/h}$ can be written as:

$$M_{p/h}(t) = -\omega_t(t) k_{p/h} \tag{2.78}$$

where $k_{p/h}$ is a positive constant.

The total moments M_h applied to the TRMS in the horizontal plane are:

$$M_h(t) = \sum_{i=1}^{4} M_{hi}(t) \tag{2.79}$$

$$M_h(t) = M_{fp}(t) + M_{frict}(t) + M_{spri}(t) + M_{p/h}(t)$$

Net torque in the horizontal plane:

$$M_h(t) = F_h(t)\left(\omega_h(t)\right) l_t \cos\theta_h(t) - \omega_h(t)k_h - \theta_h(t)k_{spri} - \omega_t(t)k_{p/h} \tag{2.80}$$

In the horizontal plane the moment of inertia is divided into eight parts. Using the parallel-axis theorem the moment of inertia of the DC-motor on the main beam can be expressed. The moment of inertia of the main beam is (Rahideh and Shaheed, 2007):

$$J_{h1}(t) = \frac{m_m}{3}\left(l_m \cos\theta_v(t)\right)^2 \text{ and } J_{h5}(t) = m_{mr}\left(l_m \cos\theta_v(t)\right)^2$$

The moment of inertia of the DC-motor and beam at the tail rotor is described in the same way:

$$J_{h2}(t) = \frac{m_t}{3}\left(l_t \cos\theta_v(t)\right)^2 \text{ and } J_{h4}(t) = m_{tr}\left(l_t \cos\theta_v(t)\right)^2$$

The moment of inertia of the counterweight and counterweight beam:

$$J_{h3}(t) = \frac{m_b}{3}\left(l_b \sin\theta_v(t)\right)^2 \text{ and } J_{h6}(t) = m_{cb}\left(l_{cb} \sin\theta_v(t)\right)^2$$

The tail shield in the horizontal plane is approximated as a cylindrical shell and using the parallel-axis theorem gives its moment of inertia:

$$J_{h7}(t) = \frac{m_{ts}}{2} r_{ts}^2 + m_{ts}\left(l_t \cos\theta_v(t)\right)^2$$

The main shield is approximated as a solid cylinder:

$$J_{h8}(t) = \frac{m_{ms}}{2} r_{ms}^2 + m_{ms} \left(l_m \cos \theta_v(t) \right)^2$$

Hence the total moment of inertia in the horizontal plane is:

$$J_h(t) = \sum_{i=1}^{8} J_{hi}(t) \tag{2.81}$$

Equation (2.78.) in compact:

$$J_h(t) = \frac{m_m}{3}\left(l_m \cos \theta_v \right)^2 + \frac{m_t}{3}\left(l_t \cos \theta_v \right)^2 + \frac{m_b}{3}\left(l_b \sin \theta_v(t) \right)^2 + m_{tr} \left(l_t \cos \theta_v(t) \right)^2 + m_{mr} \left(l_m \cos \theta_v(t) \right)^2$$
$$+ m_{cb} \left(l_{cb} \sin \theta_v(t) \right)^2 + \frac{m_{ts}}{2} r_{ts}^2 + m_{ts} \left(l_t \cos \theta_v(t) \right)^2 + \frac{m_{ms}}{2} r_{ms}^2 + m_{ms} \left(l_m \cos \theta_v(t) \right)^2 \tag{2.82}$$

Equation (2.82) can be re-written as:

$$J_h(t) = D \cos^2 \theta_v(t) + E \sin^2 \theta_v(t) + F \tag{2.83}$$

where

$$F = m_{ms} r_{ms}^2 + \frac{m_{ts}}{2} r_{ts}^2 \qquad D = \frac{m_b}{3} l_b^2 + m_{cb} l_{cb}^2$$

$$E = \left(\frac{m_m}{3} + m_{mr} + m_{ms} \right) l_m^2 + \left(\frac{m_t}{3} + m_{tr} + m_{ts} \right) l_t^2$$

from conservation of angular momentum of a rigid object, such as the TRMS, the following is stated (Raymond et al., 2004):

$$S_{h,res}(t) = S_h(t) + S_{main}(t) \cos\left(\theta_v(t) \right) \tag{2.84}$$

$$S_{main}(t) = J_{mr} \omega_m(t) \tag{2.85}$$

where S_h is the angular momentum arising from external torque affecting the TRMS. The S_{main} is the angular momentum arising from the spinning main rotor and $S_{h,res}$ is the resulting angular momentum.

Using Newton's Second Law and rearranging the equation the following is obtained:

$$J_h(t)\omega_{h,res}(t) = J_h(t)\omega_h(t) + J_{mr}\omega_m(t)\cos\left(\theta_v(t)\right) \tag{2.86}$$

by abstracting ω_h from Eq. (2.86) it will obtain:

$$\omega_{h,res}(t) = \frac{S_h(t) + J_{mr}\cos\left(\theta_v(t)\right)\omega_m(t)}{J_h(t)} \tag{2.87}$$

from other side J_{mr} is given as :

$$J_{mr} = \frac{1}{12} m_{mr}\left(l_{mw}{}^2 + l_{ml}{}^2\right) \tag{2.88}$$

where : J_{mr} is the inertia of the main rotor blades.

Solving the system is considered the rotation of the beam in the vertical plane around the horizontal axis. Applying the Newton's second law of motion we obtain (Rahideh and Shaheed, 2007):

$$M_h(t) = J_h(t)\frac{d^2\theta_h(t)}{dt^2} \tag{2.89}$$

where M_h is the total moment of forces applied in the horizontal plane and J_h is the sum of the moments of inertia relative to the horizontal axis.

using the above equation we find:

$$\frac{d^2\theta_h(t)}{dt^2} = \frac{dS_h(t)}{dt} = \frac{M_h(t)}{J_h(t)} \tag{2.90}$$

Equation (2.90) can be written as:

$$\frac{dS_h(t)}{dt} = \frac{\sum_{i=1}^{4} M_{hi}(t)}{J_h(t)} \tag{2.91}$$

that the sum of the total is gotten from Eq. (2.80) and put it in Eq. (2.91) to obtain :

$$\frac{dS_h(t)}{dt} = \frac{M_h(t)}{J_h} = \frac{l_t F_h(t)\left(\omega_h(t)\right)\cos\theta_v(t) - \omega_h(t)k_h - \theta_h(t)k_{spri} - \omega_t(t)k_{p/h}}{D\cos^2\theta_v(t) + E\sin^2\theta_v(t) + F}$$

then:

$$\frac{dS_h(t)}{dt} = \frac{l_t F_h(t)\left(\omega_h(t)\right)\cos\theta_v(t) - \omega_h(t)k_h - \theta_h(t)k_{spri} - \omega_t(t)k_{p/h}}{D\cos^2\theta_v(t) + E\sin^2\theta_v(t) + F} \tag{2.89}$$

The $\theta_h(t)$ is given as:

$$\frac{d\theta_h(t)}{dt} = \omega_h(t) \tag{2.90}$$

where ω_h is the angular velocity of the TRMS beam in horizontal plane (*rad/s*) and θ_h is the yaw angle of the beam.

$$\omega_h(t) = \frac{S_h(t) + J_{mr} l \cos\theta_v(t)\omega_m(t)}{J_h(t)} \tag{2.91}$$

Then regrouping all the equations together to get the systems mathematical model in order to move to the next step which is writing these obtained equations in Matlab/Simulink. Staring firstly by the vertical plane:

$$\begin{cases} \dfrac{dS_v(t)}{dt} = \dfrac{\left\{\left[A-B\right]\cos\theta_v(t) - C\sin\theta_v(t)\right\} + l_m F_v(t)\left(\omega_m(t)\right) - \omega_h^2(t)\left\{A+B+C\right\}\sin\theta_v(t)\cos\theta_v(t) - \omega_v(t)k_v}{m_{mr}l_m^2 + m_m l\dfrac{l_m^2}{3} + m_{tr}l_t^2 + m_t\dfrac{l_t^2}{3} + m_{cb}l_{cb}^2 + m_b\dfrac{l_b^2}{3} + \dfrac{m_{ms}}{2}r_{ms}^2 + m_{ms}l_m^2 + \dfrac{m_{ts}}{2}r_{ts}^2 + m_{ts}l_t^2} \\ \omega_v(t) = \dfrac{S_v(t) + J_{tr}\omega_m(t)}{m_{mr}l_m^2 + m_m l\dfrac{l_m^2}{3} + m_{tr}l_t^2 + m_t\dfrac{l_t^2}{3} + m_{cb}l_{cb}^2 + m_b\dfrac{l_b^2}{3} + \dfrac{m_{ms}}{2}r_{ms}^2 + m_{ms}l_m^2 + \dfrac{m_{ts}}{2}r_{ts}^2 + m_{ts}l_t^2} \\ \dfrac{d\theta_v(t)}{dt} = \omega_v(t) \end{cases}$$

$$\begin{cases} \dfrac{dS_h(t)}{dt} = \dfrac{l_t F_h(t)\left(\omega_h(t)\right)\cos\theta_v(t) - \omega_h(t)k_h}{\left(\dfrac{m_b}{3}l_b^2 + m_{cb}l_{cb}^2\right)\cos^2\theta_v(t) + \left(\left(\dfrac{m_m}{3} + m_{mr} + m_{ms}\right)l_m^2 + \left(\dfrac{m_t}{3} + m_{tr} + m_{ts}\right)l_t^2\right)\sin^2\theta_v(t) + \left(m_{ms}r_{ms}^2 + \dfrac{m_{ts}}{2}r_{ts}^2\right)} \\ \omega_h(t) = \dfrac{S_h(t) + J_{mr}l\cos\theta_v(t)\omega_m(t)}{\left(\dfrac{m_b}{3}l_b^2 + m_{cb}l_{cb}^2\right)\cos^2\theta_v(t) + \left(\left(\dfrac{m_m}{3} + m_{mr} + m_{ms}\right)l_m^2 + \left(\dfrac{m_t}{3} + m_{tr} + m_{ts}\right)l_t^2\right)\sin^2\theta_v(t) + \left(m_{ms}r_{ms}^2 + \dfrac{m_{ts}}{2}r_{ts}^2\right)} \\ \dfrac{d\theta_h(t)}{dt} = \omega_h(t) \end{cases}$$

3. LITERATURE REVIEW

The TRMS is a preferred common study case in the control engineering that allows the validation of novel control strategies. PID controllers can be often a conventional proposed solution strategy may employ to control the TRMS problem, due to its simplicity in structure and implementation, and be basically referenced to other controllers. However in complex and nonlinear systems, PID controllers cannot be able to deal with the uncertainty and sudden perturbation, therefore besides to PIDs, other control strategies have also been taken in researches including the usage and the application of machine learning systems in order to get the optimal parameters those to ensure a best efficiency and performance (Meon et al., 2012). Although that the control strategies those are based on machine learning algorithms can be effective, nevertheless do not guarantee a robust performance, which is largely required in several applications such as the aerospace and medical sciences. So to ensure a robust performance response of the system, various control methods such as optimal control (Phillips and Sahin, 2004; Wen and li, 2011), deadbeat control (Ahmad et al., 2003), H_∞ hybrid (Ahmad et al., 2013) and sliding mode control (Huang and Wu, 2013) , (Mondal and Mahanta, 2011) has been applied to the system as well.

3.1. Review on PID Controllers

PID controllers have successfully led to a lot of changes in technology. In the 1920's, it had began with pneumatic controllers, trough directional control to the Distributed Control System (DCS) (Aström and Wittenmark, 1973). Pneumatic controllers were based on the flapper-nozzle amplifier. Movement of the flapper arm towards or away from the nozzle causes a change of back pressure in the pneumatic circuits and this change in pressure results in a movement of a diaphragms bellows. This movement can be applied to a pilot valve which in turn

controls the opening and closing of the main control valve (Aström and Wittenmark, 1973).

Despite rapid evolution in control hardware over past 50 years, the PID controllers remain the workhouse in process industries. The proportional action (P mode) adjusts controller output according the size of the error. The integral action (I mode) can eliminate the steady state offset and future trend is anticipated via derivative action (D mode) (Aström and Wittenmark, 1973).

The first problem was quickly solved by *J.B. Ziegler* and *N.B. Nichols* of Engineering Sales and Engineering Research Department of Taylor Instrument Company in 1942. They published well known paper 'Optimum Setting for Automatic Controllers'. A second less well known paper, by Ziegler and Nichols appeared one year later in which they commented that too often in process plants when the plants is run it does not work as expected. The engineers release that some factor has been neglected but cannot identify what is missing. Another thing was also a big challenge the 'controllability' which is the ability of the process to achieve and maintain the desired stable and equilibrium value. Through those effort and by time the PIDs started to be developed and have a huge importance in the human use (Aström and Wittenmark 1973).

3.2. The Feedback Principles

The feedback idea is simple and powerful. It has had a profound influence on technology. Assume for simplicity that the process is such that the process variable increases when the manipulated variable is increased. The principle of feedback can then be expressed as follows: The manipulated variable is increased when the process variable is smaller than the set-point and is decreased when the process variable is larger than the set-point. This type of feedback is called negative feedback because the manipulated variable moves in opposite direction to the process variable (Chen and Moore, 2005) The feedback principle can be represented by the block diagram shown in Figure 3.1, where r and y denote the

set-point and measured output respectively, *e* is the error between set-point and the measured output and *u* is the control input.

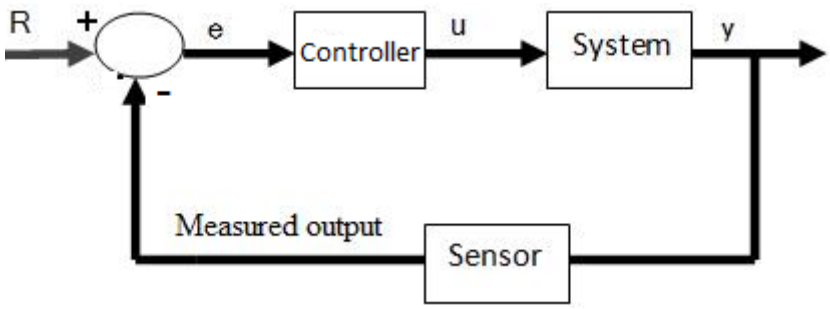

Figure 3.1. Block diagram of a simple feedback system.

Where *e* is the calculated input error, *u* is the control input , *y* is the output and *R* is the reference The reason why feedback systems are of interest is that feedback makes the process variable close to the set-point in spite of disturbances and variation of the plant characteristics (Chen and Moore, 2005).

3.2.1. On-Off Control

It is possible to arrange the feedback in many different ways. Starting by the simplest structure of its mechanism that can be described mathematically in on-off control as following:

$$u = \begin{cases} u_{\max} & \text{If} \quad e > 0 \\ u_{\min} & \quad\quad e < 0 \end{cases} \tag{3.1}$$

where $u_{\max}$ and $u_{\min}$ denote maximum and minimum control inputs, respectively. In this kind of control the maximum corrective action is ensured and always used. The manipulated physical variable has its largest value when the error is positive and its smallest value when the error is negative. This type of feedback is named by on-off control. It is not complicated and there are no tuning parameters to select. On-off control usually succeeds in ensuring a process variable close to the set-

point, but it will typically result in a system where the variables oscillate. Notice that in (3.1) the control variable is not denned when the error is zero. It is common to have some modifications either by introducing hysteresis or a dead zone as shown in Figure 3.2 (Aström and Wittenmark, 1973).

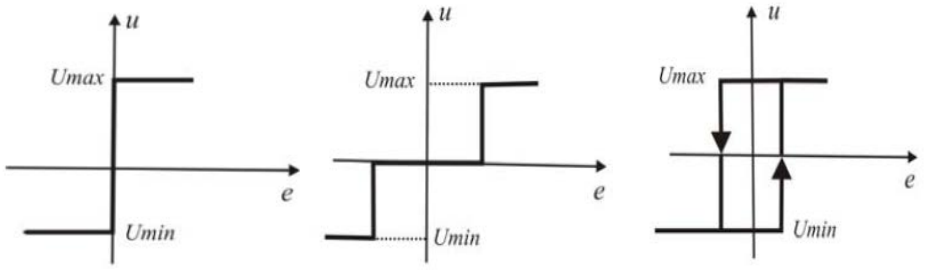

(a) (b) (c)

Figure 3.2. Controller characteristics for ideal on-off control (a) relay control, (b) dead-zone control, (c) hysteresis control.

3.2.2. Proportional (P) controller

In proportional control, the control input is produced as proportional to the error value as shown in Figure 3.3. In analog systems, the error signal is amplified to obtain the control input. In digital systems, the error value is multiplied by a constant which is the proportional control gain.

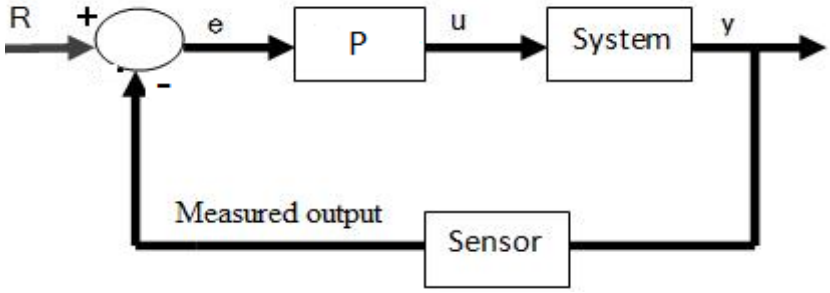

Figure 3.3. Basic scheme of P Controller

The P controller is defined as:

$$u(t) = K_p e(t) \tag{3.2}$$

Where K_p is the proportional gain that is often constant. Proportional control increases the speed of response, but as a disadvantage it causes larger transient overshoot. Thus, the gain constant K_p should be adjusted to an optimum value. Lower proportional gain results in a smaller control input and makes the system less sensitive to disturbances. When the error is small, the control input can be a very small value which results the system not to respond. Additionally, proportional control in this stage is not able sometimes to reject the constant disturbances and may have fixed steady state error (Bennett, 2001).

3.2.3. Proportional Integral (PI) controller

PI controller is generally utilized to eliminate the steady state error that caused by the proportional P controller. However, after using this term controller the system will be to speed up but overall the stability of the system (Bennett, 2001).

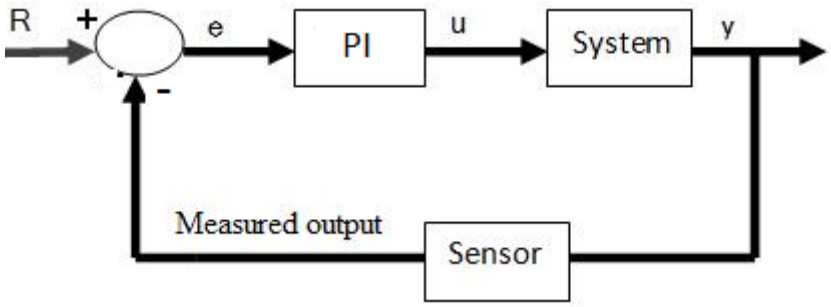

Figure 3.4. Basic scheme of PI Controller

It can be defined as:

$$u(t) = K_p e(t) + K_i \int_0^t e(\tau)\, d\tau \tag{3.3}$$

Where K_i is a constant gain. This controller is mainly utilized in fields where speed of the system is not an that much important. Since the ability of predicting future errors of the system's response is not existed where eliminating the caused oscillations is also less as well as the rise time. If applied, any amount of 'I' guarantees set point overshoot. Figure 3.4 represents a schema block of PI controller (Bennett, 2001).

3.2.4. Proportional Derivative (PD) controller

The purpose of using PD controller is to increase the time rise of the system's response as well to have a range of stability by improving control since it has an ability to predict the future error of the system response (Bennett, 2001). The schema block of this controller is represented in Figure 3.5.

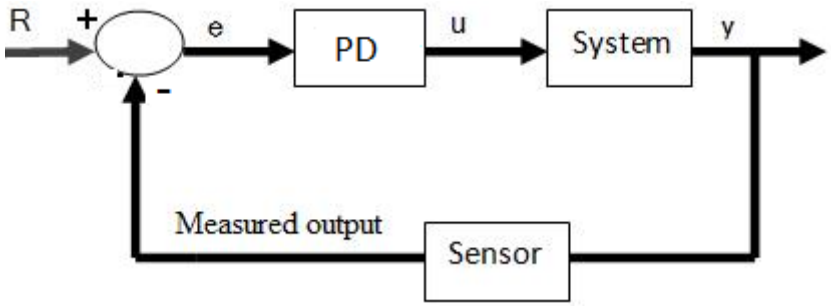

Figure 3.5. Basic scheme of PD Controller

PD controller is defined as:

$$u(t) = K_p e(t) + K_d \frac{de(\tau)}{dt} \tag{3.4}$$

Where K_d is a constant gain. Derivative term is proportional to the rate of change on error and has a role to speed up the system response. Derivative predicts the system behavior from the slope and improves the stability of the system. It usually reduces the settling time and improves the response of the system to sudden

changes. However, it may amplify the system noise at high frequencies. If the error signal is noisy or if the closed-loop system has a slow loop rate, the derivative response can make the system unstable. Additionally, it does nothing to reduce constant error, since the derivative of the error will be zero if there is no change on error.

3.2.5. Proportional Integral Derivative (PID) controller

PID controllers have included all the previous mentioned controllers, whether in speeding up the system's response by getting a short rise time or by eliminating the steady state error or even by pushing the suytem by the max energy, therefore he necessity of using a derivative gain component in addition to the PI controller is to eliminate the overshoot and the oscillations occurring in the output response of the system. PIDs have mainly a strong advantage that is suitable to be used in higher order processes (Bennett, 2001).

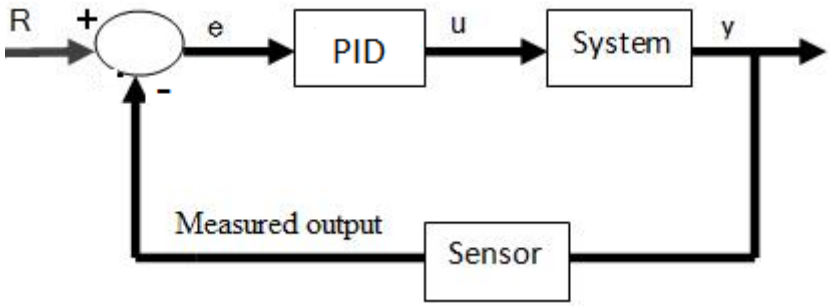

Figure 3.6. PID controller scheme using error feedback

The "time varying" version of the PID algorithm is described by (Bennett, 2001):

$$u(t) = K\left(e(t)+\frac{1}{Ti}\int_0^t e(\tau)\,d\tau + T_d\frac{de(\tau)}{dt}\right) \tag{3.5}$$

$$e(t) = r(t) - y(t) \tag{3.6}$$

where *u* is the control signal, *e* is the control error, *r* the reference variable, and *y* is the measured process variable,. There is often a reference variable is named by set point y_{sp}. A sum result of combining the three terms: the P, I and D all together results the control signal. However after there are some corresponding parameters of the controller to be adjusted up to needed , which are proportional gain *K*, integral time T_i, and derivative time T_d. The integral. as is illustrated in Figure 3.6. In general, a transfer function $C(s)$ of single loop PID controllers has the following form (Aström and Wittenmark, 1973):

$$C(s) = \frac{U(s)}{E(s)} = K_p + \frac{K_i}{s} + K_d s \tag{3.7}$$

where $E(s)$ is the error signal, which is the difference between the system input $U(s)$ and output, K_p, K_i and K_d are proportional, integral and derivative gains, respectively. The problem is to determine values of gins so that performance requirements are satisfied. However, for an MIMO system with complicated dynamics, it is difficult to design an appropriate PID controller by using the conventional control theory. The manner of obtaining the parameters of PID controllers for MIMO systems that satisfy a certain system performance requirement has been addressed in many studies (Aström and Wittenmark 1973).

3.2.6. PID's in TRMS systems

As a simplest way adjust the systems parameters generally is the hand tuned method, therefore this method is used with the TRMS as a complicated system too. However it will be a hard process to get the system's regulation by tuning three variable parameters which will cause a big effort where the PID controller is typically tuned via a machine learning process. In (Mohamed and Ishak, 2012) has proposed a method named by the PID Active Force Control in which a system itself is able to estimate the external torque disturbances and a

neural network and *fuzzy logic* were used to optimize the PID controller (Mohamed and Ishak, 2012) .

3.3. PID controllers tuning methods

To obtain the desired working behaviour of a system's response it is required to adjust the systems parameters through different tasks . Therefore many different ways it has been developed to obtain this adjustment. The first approach is to use the conventional calculation as explained above. But as long as the PID controller doesn't have too many parameters to be adjusted,. The first tuning rules were developed by *Ziegler and Nichols* (Hägglund and Åström, 2004). Their idea was to perform a simple experiment, extract some features of process dynamics from the experiment and determine the controller parameters from the features.

3.3.1. Manual Tuning Method

Manual tuning is realized by modifying the controller's parameters according to the response of the system. Until the wanted response is gotten K_p, K_d and K_i are varying by checking the behaviour of the system.

3.3.2. Ziegler-Nichols tuning method

Ziegler–Nichols method is very well know at control users that provides a systematic PID tuning approach. This method has experienced good load disturbance attenuation in many cases. however, it has some disadvantages, such as in the design criterion which is given closed loop systems with poor robustness, and in using insufficient process information and (Telbany, 2006). Ziegler and Nichols developed their tuning rules by simulating a large number of different processes, and correlating the controller parameters with features of the step response. The key design criterion was quarter amplitude damping. Process dynamics was characterized by two parameters obtained from the step response.

For improving a certain system performance, e.g., rise time, overshoot, and integral of the absolute error, many studies are attempting to incorporate features on the basis of the experiences of experts with regards to PID parameters selection (Telbany, 2006).

$$K_0 = \frac{X_0}{M_u}\frac{\tau}{\tau_{Dead}} \tag{3.8}$$

where it determines the transportation lag or dead time, τ_{Dead}, the time constant or time for the response to change τ , and the ultimate value that the response reaches at steady-state M_u, for a step change of X_0.

3.3.3. *Cohen-Coon* Tuning Method

Cohen-Coon tuning method has been developed approximately after a many years than the Ziegler-Nichols method. this tuning method requires to obtain three parameters from the reaction curve as .

$$gp = \frac{\Delta PV}{\Delta CO} \text{ in } (\%) \tag{3.9}$$

3.3.4. *Chien Hrones Reswich* Method .

Chien-Hrones-Reswich (*CHR*) method is the modified version of the *Ziegler-Nichols* method. This method was developed in 1952 by *Chien-Hrones-Reswich* provides a better way to select a compensator for process control applications (Telbany, 2006)..

3.4. Fuzzy Logic System

Professor *Lotfi Aliasker Zadeh*, the mathematician, electrical engineer and computer scientist at the University of California in Berkeley introduced the fuzzy

theory into the scientific literature in 1965. He published in the journal 'Information and Control' his study in an article was titled by "*Fuzzy Sets*" (Zadeh, 1965). In this study, his proposition was a fuzzy set theory that operated between the intervals zero to one includes the values between. The difference between Boolean logic and fuzzy logic is Boolean logic results can be '0' or '1', however, fuzzy logic results can take any value between '0' and '1'. In other words, the values between sharp results like true and false are defined by the fuzzy. Therefore, fuzzy sets can define some commonly used concept in daily life like "very wide", "wide", "narrow" and "very narrow". Fuzzy logic uses linguistic variables and it can define level and degrees of linguistic variables (Zadeh, 1965).

3.4.1. Fuzzy Logic System Sets

A Set in Boolean logic conventionally is characterized by a function that can hold a value of either 0 or 1 to each individual in the universal set, there by discriminating between members and nonmembers of the crisp set under consideration. The values assigned to. The elements of the universal set fall within a specified range and indicate the membership grade of these elements in the set. Larger values can denote a higher degree of set memberships such functions are named as membership functions and the set can be defined by, it is a fuzzy set.

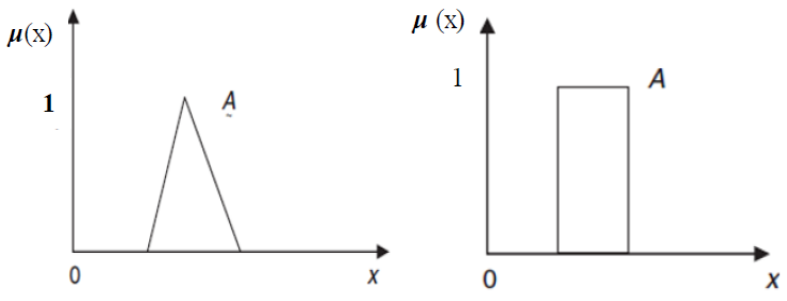

(a) (b)

Figure 3.7. (a) Membership function of fuzzy set and (b) crisp set

The basis of the fuzzy logic is the fuzzy sets as in (a) Figure 3.7. A fuzzy set is a set that can include elements with only a partial degree of membership. Therefore, a fuzzy set does not have a crisp boundary. When the universe, D_X , is infinite and continuous, a fuzzy set X in D_X will be defined as follows (Zadeh, 1965):

$$X = \{(x, \mu_X(x)) | D_X\} \tag{3.10}$$

In the equation given above, $\mu_X(x)$ is the Membership Functions MF of X in X , and it represents the degree of membership of the x belongs to X. The Membership function $\mu_X(x)$ maps and covers each component in D_X to an unit interval changes between continuously [0, 1]. If $\mu_X(x)$ value is close to zero, it means that belonging of the x to fuzzy set X is lower degree. If $\mu_X(x)$ value is close to one, it means that belonging of the x to fuzzy set X is higher degree.

3.4.1.1. Fuzzy Set Operations

In Table 3.1 below illustrate fuzzy set operations, between continuously [0, 1]. If $\mu_X(x)$ value is close to zero, it means that belonging of the x to fuzzy set X is lower degree. If $\mu_X(x)$ value is close to one, it means that belonging of the x to fuzzy set X is higher degree.

Table 3.1. Summarize of Fuzzy Set Operations

Operations	Fuzzy logic form
Complement	$\mu_{\bar{Y}}(y) = 1 - \mu_Y(y)$
Union	$\mu_{D\cup G}(y) = \max\left(\mu_G(y), \mu_D(y)\right) \quad u \in U$
Intersection	$\mu_{D\cap G}(y) = \min\left(\mu_G(y), \mu_D(y)\right) \quad u \in U$

3.4.1.2. Linguistic Variables

The same as in the algebraic, the variable holds numbers as value, and a linguistic variable can hold a word or a sentence as a value besides to numbers as well. Where namely by the 'Term Set' that represents these set of values. Fuzzy variable represents each value in the term set and the first can be defined through a base variable, where this last defines a discourse for all the fuzzy variables in the term set as well, briefly . linguistic variable (fuzzy variable) base variable.

3.4.1.3. Illustration

Let x for example be a linguistic variable with the label "Temperature", where the terms of this linguistic variable, which are fuzzy sets, could be "hot", "cold", "very cold" and " very hot" from the term set. So *T* can be, cold, very cold, less cold, hot, very hot, less hot…etc

Each term is a fuzzy variable defined on the base variable, which might be the scale from 0 to 100 degrees. A linguistic variable is represented by triplet (*x, T(x), U*).

x : is the label of the linguistic variable (position, angle error , speed …).

T(x) : is the set of the fuzzy sets, which is used to define x.

U: is the universe of discourse which related to linguistic variable x.

For example, if the angle is linguistic variable and defined in universe of discourse K= [-1, 1], the fuzzy labels of it can be: Positive Big (*PB*), Positive Small (*PS*), Negative Small (*NS*), Negative Big (*NB*), and Zero (*Z*) for example.

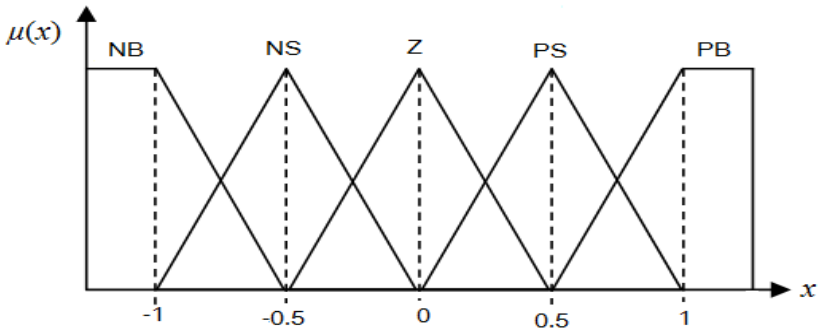

Figure 3.8. Depicts linguistics variable 'error' and its fuzzy sets

So the fuzzy sets are: *T* (*error*) = { Positive Big (*PB*), Positive Small (*PS*), Negative Small (*NS*), Negative Big (*NB*), and Zero (*Z*)}. The Figure 3.8 above depicts these conceptions.

3.4.1.4. Membership Functions

Many different Membership Functions (*MFs*) defined in literature. The most known and used MFs are triangular, trapezoidal and Gaussian MFs. (Liu et al., 2011).

A type-1 (ordinary) triangular membership functions MF is defined by three points :{ *a*, *b*, *c*}. Here, *a* indicates the left endpoint, *b* indicates the central point, and *c* indicates the right endpoint of the triangular. A type-1 triangular MF can be seen in Figure 3.9.

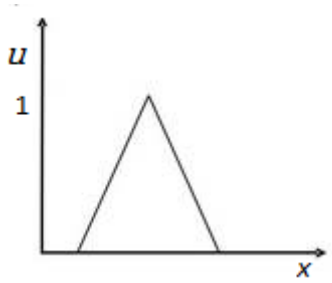

Figure 3.9. Triangular type-1 fuzzy MF.

A type-1 trapezoidal MF is defined by four parameters: $\{a, b, c, d\}$. The a, b, c, d (where $a<b<c<d$) parameters define the corner points of the trapezoidal MF as it can be seen in Figure 3.10.

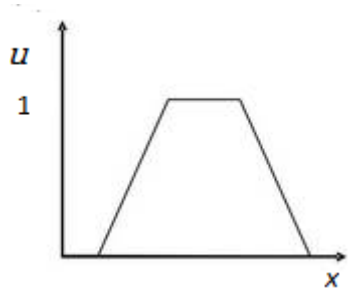

Figure 3.10. Trapezoidal type-1 fuzzy MF

A type-1 Gaussian MF is defined by two parameters: $\{c, \sigma\}$. Here, x represents the center of the MF and σ represents the width of the MF. A type-1 Gaussian MF can be seen in Figure 3.11.

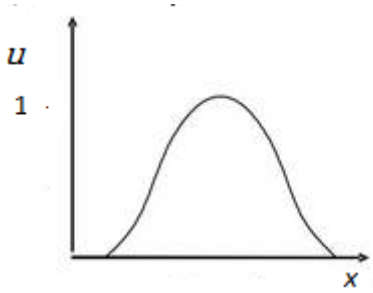

Figure 3.11. Gaussian type-1 fuzzy MF

3.4.2. Fuzzy Logic Control System

The fundamental structure of a FLC is depicted in Figure 3.12. As seen, a FLC comprises four principal components, which are rule base fuzzy, inference engine, fuzzifier, and defuzzifier. The operation of FLC is as following: The crisp inputs (u_1, u_2, ..., u_n) are converted to fuzzy sets in the "fuzzifier" block. Fuzzy rules which are under the form of the term "IF-THEN" are considered in the rule base block. Then the "inference engine" uses the fuzzy rules to generate fuzzy conclusions, and finally to generate crisp outputs (y_1, y_2,…, y_n). are obtained

through the “defuzzifier” block by convert the fuzzy outputs from the inference engine. In the next section, these principal components of fuzzy logic will be described detailly to explain how the fuzzy mathematical principles and logic are utilized in FLCs Identify ranges of the controller inputs.

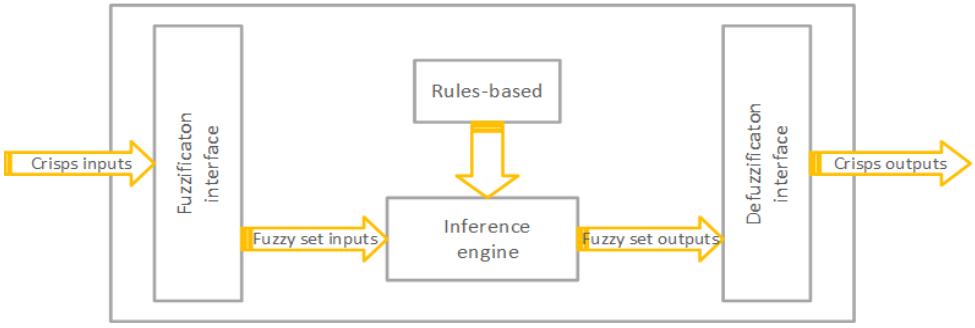

Figure 3.12. Basic structure of a type-1 fuzzy logic system.

3.4.2.1. Fuzzification

Fuzzification can be described as following: a process where allows to decompose the system input variable and output variable into one or different fuzzy sets. In order to realized this, curves with different shapes are used, but mainly trapezoidal and triangular types membership function are the common due to simplicity to be represented in embedded controllers. Each input from the fuzzy set is interpreted as well as each degree of memberships is interpreted. And to allow smooth mapping of the system, the membership functions should overlap. Furthermore in this part of fuzzification, it can be able to represent the input and outputs of the system to be expressed in linguistic terms so after applying the rules, it will be able to express a complex system in simple manner.

3.4.2.2. Rules base

Rules are used in Fuzzy logic based systems in order to represent the relationship between actions and observations. These rules are consisted of a precondition first part (IF) and a consequence second part (THEN). Where is

possible to the precondition to consist of multiple conditions with OR or AND conjunctions all linked together. The rule structure of T1FLS with one output $y \in Y$ and p inputs) $\left(x_1 \in X_1, \ldots, x_p \in X_p\right)$ and is as follows:

$Rule\ l^{th}$: $IF\ x_1\ is\ A_{1l}\ and\ \ldots\ and\ x_p\ is\ A_{pl}\ Then\ y\ is\ B$

3.4.2.3.Fuzzy inference engine

Moving to another component of the fuzzy logic which is the fuzzy inference engine that through it, the rules are combined and a mapping from fuzzy sets is given to the output universe of discourse based on the fuzzy logic principle from the fuzzy sets in the input universe of discourse. Multiple antecedents in the rules are connected in the inference engine by using AND operation, and the degree of membership in the input sets are combined using those in the output sets using sub-star composition, described in detail in (Jahed and Mohammad, 2013). Multiple rules are combined then by using a join operation as shown in Figure 3.13.

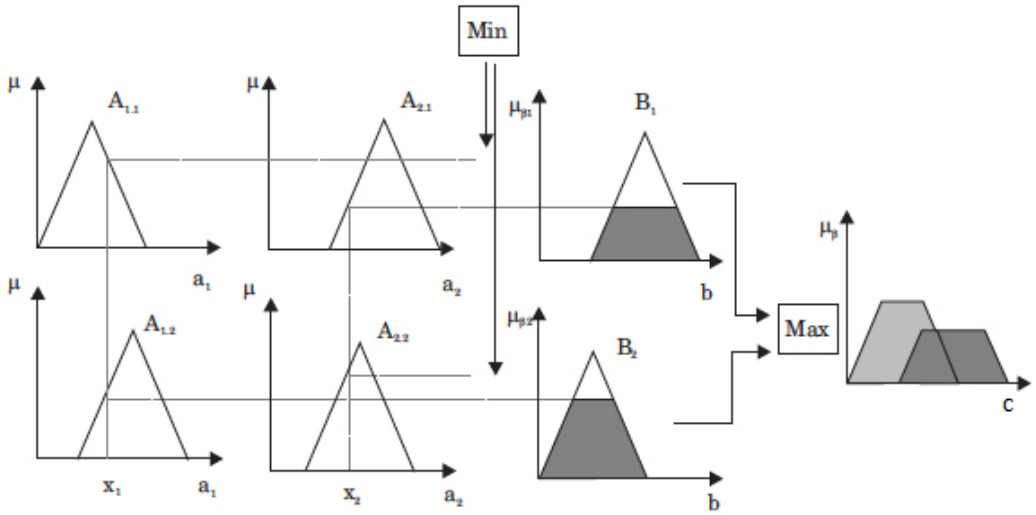

Figure 3.13. Inference engine calculation process

3.4.2.4. Defuzzification

Finally at the end of this process the defuzzification comes to ensure transferring fuzzy sets that obtained by the inference engine into a crisp value again. For engineering applications, there are many defuzzifier strategies in the literature. the criterion in choosing one of them of a defuzzifier is simplicity and computational, such as center of sets, modified height, center-of-sums, centroid , center average (Eker and Torin, 2006), and maximum.

3.4.3. Max-Membership Principle

Here one of these methods is described which is the max membership principle method that allows to find a Maximum at the membership corresponding the defuzzified value .

The defuzzified value can be determined from the following expression $\mu_A(Z*) \geq \mu_A(Z)$

Very accurate only for peaked output membership functions

Computes the defuzzified value at a very fast rate

In Figure 3.14 a graphical representation of maximum -membership defuzzification is shown.

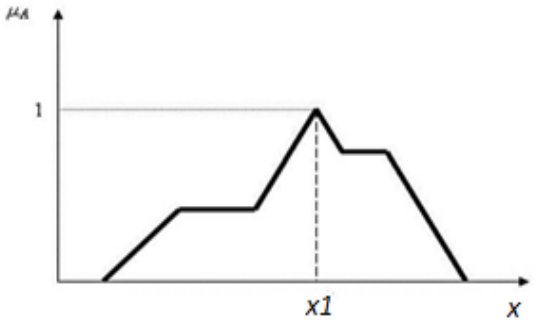

Figure 3.14. Max membership method

3.4.3.1. Centre of gravity (COG)

The most popular and the simplest among the defuzzification process methods is Centre of gravity method. One of the important advantages of the COG method is that all activated membership functions of the consequents (all active rules) take part in the defuzzification process. The *COG* method works based on the following equation for transferring fuzzy scheme into a crisp value (Zak Stanislaw, 2003):

$$COG = \frac{\sum_{i=1}^{n} x_i \mu_A(x_i)}{\sum_{i=1}^{n} \mu_A(x_i)} \tag{3.11}$$

where n is the number of the discrete elements in the universe of discourse, x and $\mu_A(x_i)$ are outputs of fuzzy of the membership functions as shown in Figure 3.15.

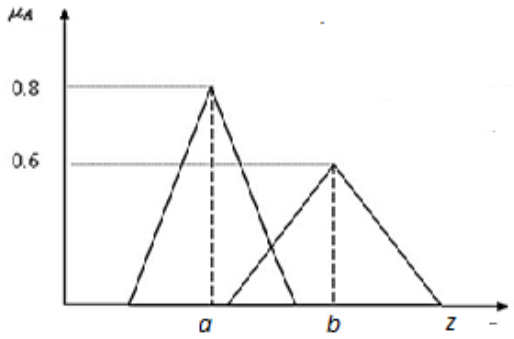

Figure 3.15. Weighted Average method

3.4.4. Types Of Fuzzy System

In fuzzy control there are two types of fuzzy systems those can be distinguished based on the form of the rules: Mamdani rules and Sugeno rules. Where the rules of Sugeno method are based on a many principle: they are also characterized by (linear) functions of the controller inputs.

3.4.4.1. Mamdani Type Fuzzy Systems

Principally in the first reported and published recourses of fuzzy control, the Mamdani type of fuzzy rule was utilized mainly (Simões and Friedhofer, 1997) and can be described as the following:

$$Rule\ l^{th}: IF\ x_1\ is\ A_1\ and \ldots and\ x_p\ is\ A_p\ Then\ y_1\ is\ B\ \ and\ \ \ldots\ and\ y_p\ is\ B_p$$

And the mamdani method type has some advantages that it is well suited to human input, it has widespread acceptance and It is intuitive.

3.4.4.2. Sugeno Type Fuzzy Systems

The other type of fuzzy system is named Sugeno rules, It was firstly introduced by *Takagi*, *Sugeno and Kang* (Simões and Friedhofer, 1997) which was further utilized by Sugeno and his co-workers. The general form of TSK rule is as follows:

$$Rule\ l^{th}\ :\ IF\ x_1\ is\ A_1\ and\ \ \ldots\ and\ x_p\ is\ A_p\ Then\ y = f_1\left(x_1,\ldots,x_2\right)$$

this shows that the consequents of these fuzzy rules are functions of the controller inputs. A simple expression is the linear functions as follows:

$$Rule\ l^{th}\ :\ IF\ x_1\ is\ A_1\ and\ \ \ldots\ and\ x_p\ is\ A_p\ Then\ y = a_1x_1 + \ldots + a_px_p + a_0$$

From Equation (2.16.), if $a_1 \ldots a_p = 0$, then the system is called zero-order TSK and if $a_1 \ldots a_p \neq 0$, then the system mapping is linear so it is called first-order TSK.

It should be pointed out that in the view of circuit implementation, realization of a *TSK* type *FLC* is easier and more efficient than Mamdani type Simões and Friedhofer, 1997). Hardware requirements of such controllers are less, as well as computational complexity and power consumption.

The computation efficiency is one of the sugeno's advantages. Its performance functionality is well with linear techniques like the PID. Also it works good with adaptive and optimization techniques.

3.4.5. Fuzzy type 1 logic controller in TRMS systems

Badar UI Islam, Nisar Ahmed, Daud Latif Bhatli and *Shahid Khan* had discussed about fuzzy logic controller for *TRMS*. They designed a controller for 2 *DOF* in such a way that change in one degree should have minimum effect on other and system remains stable. They designed a two controller using Sugeno inference. The simulation result indicates that system performance using fuzzy logic is give better performance rather than conventional PID or LQR controller Simões and Friedhofer, 1997).

3.4.6. Stabilizability of Fuzzy models

Lyapunov function is utilized mostly to investigate the stability analysis issue of perturbed or uncertain nonlinear systems, which an exponential stability of the nominal model is established for the uncertain system (Lendek et al., 2015) .
It is considered the autonomous nonlinear system for stability analysis,

$$\dot{x} = f\left(x\right) \tag{3.12}$$

which can be is approximated by the Takagi–Sugeno system

$$\dot{x} = \dot{f}\left(x\right) = \sum_{i=1}^{m} \omega_i\left(x\right) A_i x \tag{3.13}$$

where each local matrix A_i ,*(i = 1, 2, . . . , m)* is stable and $\overline{f} = f - \dot{f}$ the approximation error satisfies (Lendek et al., 2010):

$$\left\| \overline{f}\left(x\right) \right\| \leq \sigma_f + \delta_f \left\| x \right\| \quad \forall x \tag{3.14}$$

where δ_f and σ_f are non negative finite constants. The Lyapunov function $V = x^T Px$ is considered. if there exist $Q = Q^T > 0$, $P = P^T > 0$ so that the linear matrix inequality.

$$H\left(PA_i\right) < -2Q \quad , (\, i = 1, 2, \ldots, m) \tag{3.15}$$

Equation (3.15) is satisfied, then, to the original nonlinear system, the same Lyapunov function is applied (Lendek et al., 2010), Eq (3.16) is obtained:

$$\begin{aligned}
\dot{V} &= x^T H\left(P\left(\sum_{i=1}^{m}\omega(x)A_i x + \overline{f}(x)\right)\right) \\
&= x^T \sum_{i=1}^{m}\omega_i(x) H\left(PA_i\right)x + 2x^T\overline{f}(x) \\
&\le -2\lambda_{\min}Q\|x\|^2 + 2\lambda_{\max}(P)\delta_f\|x\|^2 + 2\lambda_{\max}(P)\delta_f\|x\| \\
&\le -2\left(\lambda_{\min}Q - \lambda_{\max}(P)\delta_f(1-\theta)\right)\|x\|^2 - 2\|x\|\left(\theta\left(\lambda_{\min}Q - \lambda_{\max}(P)\delta_f\right)\|x\| - \lambda_{\max}(P)\delta_f\right)
\end{aligned} \tag{3.16}$$

with θ (0, 1) arbitrarily chosen, and where $\lambda_{min}(\cdot)$ and $\lambda_{max}(\cdot)$ denote the Eigen values with the smallest and largest absolute magnitude. By analyzing the expression of $\dot{V}$, the following cases can be distinguished (Lendek et al., 2010):

1) $\left(\lambda_{\min}Q - \lambda_{\max}(P)\delta_f < 0\right)$ or $\left(\lambda_{\min}Q - \lambda_{\max}(P)\delta_f = 0\right)$ and $\sigma_f > 0$ there is not any conclusion can be drawn.

2) $\left(\lambda_{\min}Q - \lambda_{\max}(P)\delta_f = 0\right)$ and $\sigma_f = 0$, if $x = 0$ is the only equilibrium point, and the membership functions are sufficiently smooth, $x = 0$ is a globally asymptotically stable equilibrium point of the nonlinear system based on LaSalle's invariance principle and Barbalat's lemma (Lendek et al., 2010).

3) $\left(\lambda_{\min}Q - \lambda_{\max}(P)\delta_f > 0\right)$ and $\sigma_f = 0$ the nonlinear system has a globally exponentially stable equilibrium point in x = 0. This result is found only if the approximation error is Lipschitz continuous in the states (Lendek et al., 2010) .

4) $\left(\lambda_{\min} Q - \lambda_{\max}\left(P\right)\delta_f > 0\right)$ and $\sigma_f > 0$ the states of the nonlinear system (Lendek et al., 2010) are uniformly ultimately bounded by

$$\begin{cases} \gamma = \sqrt{\dfrac{\lambda_{\max}\left(P\right)}{\lambda_{\min}\left(P\right)}}\dfrac{\lambda_{\max}\left(P\right)}{\lambda_{\min}\left(P\right) - \lambda_{\max}\left(P\right)\delta_f}\sigma_f \\ or \\ \gamma = \sqrt{\dfrac{\lambda_{\max}\left(P\right)}{\lambda_{\min}\left(P\right)}}\dfrac{\lambda_{\max}\left(P\right)}{\lambda_{\min}\left(P\right) - \lambda_{\max}\left(P\right)\delta_f}\dfrac{\sigma_f}{\theta} \end{cases} \quad (3.17)$$

3.5. Type-2 Fuzzy Logic

in real-world applications, the uncertainty is an inherent part of intelligent systems have been used (Castillo, 2012). Therefore is extremely important for handling incomplete information, the use of new methods. And as long as the membership functions of fuzzy Type-1 controllers seta, as described above, are not directly able to handle such uncertainties (Castillo, 2012). A new method is described for creating intelligent controllers so-called “type-2 fuzzy logic controller” using type-2 fuzzy logic in which the antecedents or consequents membership functions are fuzzy type-2 sets. Such sets are fuzzy sets whose membership grades themselves are fuzzy type-1 sets; they are very useful in circumstances where it is difficult to determine an exact membership function for a fuzzy set (Castillo, 2012) . As well as Type-2 fuzzy sets that are used in type-2 fuzzy systems can handle such uncertainties in a better way because they provide us with more parameters (Castillo, 2012).

3.5.1. Introduction to Fuzzy Type-2 logic

Mainly there is no basic changes between the fuzzy logic type-1 and fuzzy logic type-2 in sets term, Also Zadeh had presented firstly the concept of a type-2

fuzzy set as an extension of the concept of an ordinary fuzzy set (henceforth called a “type-1 fuzzy set”) (Castillo, 2012). So the fuzzy type-2 set is characterized by a fuzzy membership function, i.e., the membership grade for each element of this set is a fuzzy set in [0,1], unlike a type-1 set where the membership grade is a crisp number in [0,1]. Such sets can be used in situations where there is uncertainty about the membership grades themselves, e.g., an uncertainty in the shape of the membership function or in some of its parameters. Consider the transition from ordinary sets to fuzzy sets. When we cannot determine the membership of an element in a set as 0 or 1, we use fuzzy sets of type-1. Similarly, when the situation is so fuzzy that we have trouble determining the membership grade even as a crisp number in [0, 1], we use fuzzy sets of fuzzy type-2. This does not mean that we need to have extremely fuzzy situations to use tfuzzy ype- 2 sets (Juang et al., 2008). There are many real-world problems where it is hard to determine the exact form of the membership functions, e.g., in time series prediction because of noise in the data. Another way of viewing this is to consider fuzzy type-1 sets as a first order approximation to the uncertainty in the real-world. Then fuzzy type-2 sets can be considered as a second order approximation. Of course, it is possible to consider fuzzy sets of higher types but the complexity of the fuzzy system increases very fastly (Castillo, 2012).

3.5.2. Type-2 Fuzzy logic sets

Mathematically , fuzzy Type-2 sets are generalized cases of these of fuzzy type-1sets., type-2 fuzzy sets are not easy to describe like type-1 fuzzy sets. A type-2 fuzzy set, denoted as $\tilde{X}$, is characterized by a type-2 membership function $\mu_{\tilde{X}}(x,u)$, and by two variables are $u \in J_x$ and $x \in D_X \subseteq [0,1]$ (Kumbasar, 2014). Figure 3.16 shows the differences between the two types.

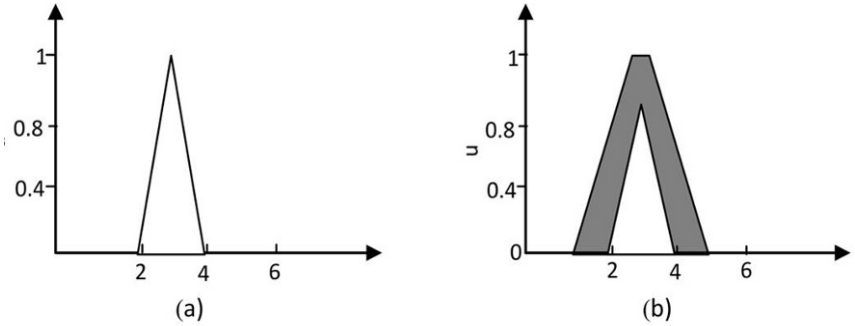

Figure 3.16. (a) Membership function of T1-FLC and (b) membership function of T2-FLC

where it can describe as following (Kumbasar, 2014):

$$\tilde{X} = \left\{ \left(x,u\right), \mu_{\tilde{X}}\left(x,u\right) \quad \forall\, x \in D_X \quad \forall\, u \in J_x \quad \subseteq [0,1] \right\} \tag{3.18}$$

Eq (3.12.) in which $0 \le \mu_{\tilde{X}}\left(x,u\right) \le 1$, can be expressed as:

$$\tilde{X} = \int_{x \in D_{\tilde{X}}} \int_{u \in J_x} \frac{\mu_{\tilde{X}}\left(x,u\right)}{\left(x,u\right)} \tag{3.19}$$

where $\int\int$ denote the union over all admissible *x* and *u*.

A type-2 fuzzy is consisted of two membership functions each is represented by a type-1 (Kumbasar, 2015), a secondary membership function and the domain of a secondary membership function which is called primary membership of x. Therefore, J_x is the primary membership of x. where $J_x \subseteq [0,1]$ for $\forall\ x \in D_X$. The uncertainty in the primary membership of a type-2 fuzzy set $\tilde{X}$ can be defined as a bounded region so-called Footprint of Uncertainty (FOU) (Kumbasar, 2014) as shown in Figure 3.17.

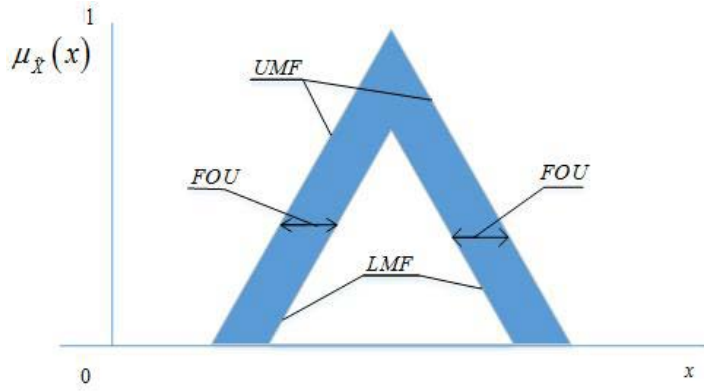

Figure 3.17. Footprint of uncertainties (FOU)

Between these type-1 fuzzy membership functions, one is an “upper membership function” (UMF) and the other is “lower membership functions” (LMF), mathematically FOU can be described as the union region between LMF and UMF.

Now the most common used of fuzzy type-2 sorts is the interval Type-2, where it can be taken as special case of the general type-2 wherein an interval type-2 fuzzy system (IT2FS) is one in which the membership grade of every domain point is a crisp set whose domain is some interval contained in the interval [0,1]. The membership grade of an IT2FS is an interval set with a unity value for each secondary grade in that set , mathematically $\tilde{X}$ is an interval type-2 fuzzy when all $\mu_{\tilde{X}}(x,u)=1$ (Kumbasar, 2014).

3.5.2.1. Operations in Type-2 Fuzzy Sets

Our goal now is describing the set theoretic operations of type-2 fuzzy sets. We are interested in the case of type-2 fuzzy sets, $\tilde{X}_i$ (i = 1 ,.., r), whose secondary membership functions are type-1 fuzzy sets. To compute the union, intersection, and complement of type-2 fuzzy sets, we need to extend the binary operations of minimum (or product) and maximum, and the unary operation of

negation, from crisp numbers to type-1 fuzzy sets, because at each x, $\mu_{\tilde{X}_i}(x,u)$ is a function (unlike the type-1 case, where $\mu_{\tilde{X}_i}(x)$ is a crisp number). The tool for computing the union, intersection, and complement of type-2 fuzzy sets is Zadeh's extension principle.

$$\tilde{X}_1 = \int_x \mu_{\tilde{X}_1}(x) \tag{3.20}$$

$$\tilde{X}_2 = \int_x \mu_{\tilde{X}_2}(x) \tag{3.21}$$

we focus our attention on set theoretic operations for such general type-2 fuzzy sets.

Table 3.2 Summarize of Type-2 Fuzzy Set Operations

Operations	Fuzzy type 2 logic form
Complement	$\tilde{X}' = \int_{x\in X} \mu_{\tilde{X}'1}(X)/X$
Intersection	$\tilde{X}_1 \cap \tilde{X}_2 = \int_{x\in X} \mu_{\tilde{X}_1\cap\tilde{X}_2}(X)/X$
Union	$\tilde{X}_1 \cup \tilde{X}_2 = \int_{x\in X} \mu_{\tilde{X}_1\cup\tilde{X}_2}(X)/X$

Similar to a T1-FIS, a T2-FIS includes Type-2 fuzzifier, Type-2 rule-base, Type-2 inference engine and substitutes the Type-1 defuzzifier by the output processor, Figure3.18 represents the schema structute of fuzzy type 2. The output processor includes a type-reducer (Hagras, 2004) and a Type-2 defuzzifier; it generates a T1-FS output (from the type-reducer), or a crisp number (from the Type-2 defuzzifier). A T2-FIS is again characterized by IF–THEN rules, but its

antecedent and consequents sets are now of the Type-2 form, that is (Hagras, 2004)

.

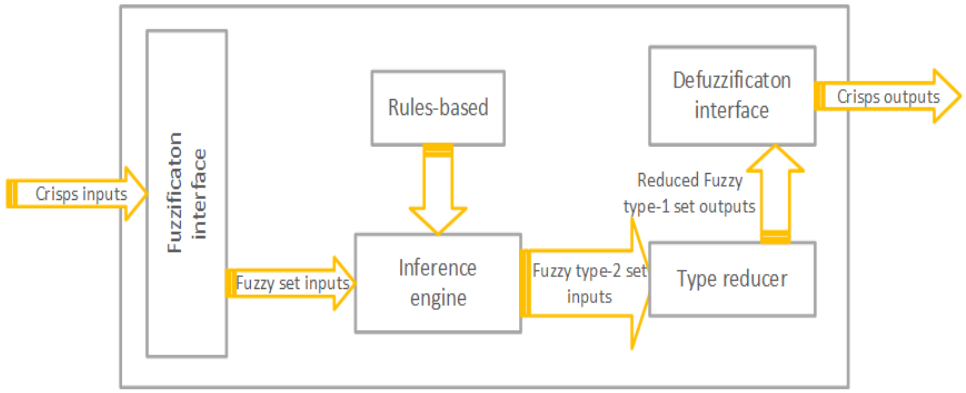

Figure 3.18. Schema of fuzzy type 2 structure.

3.5.3. Type-2 Fuzzy Control Systems

In fact, a type-2 fuzzy logic system or controller uses the same familiar notions as used in a type-1 fuzzy logic controller as membership functions, rules, t-norms operations, fuzzification, inference, defuzzification (Chaoui, 2013), but Since a higher type changes the nature of the membership functions, the operations that depend on the membership functions used in inference change; however, the basic principles of fuzzy logic are independent of the nature of membership functions and hence, do not change (Chaoui, 2013). A type-2 fuzzy logic system is very similar to type-1, where it follows the same methodology, but the only difference is in the third block where we no longer speak of only defuzzification but we speak about a type reducer and defuzzification parts that constitute both the output processing block. This difference is mainly associated with the nature of the membership functions, where type-reducer is needed due to the added degree in the kind of fuzzy sets. Figure 3.8 presents a type-2 fuzzy logic system (Cazarez-Castro et al., 2012).

Today, the two most popular fuzzy logic systems used by engineers in control are the Mamdani and TSK (Takagi–Sugeno) systems (Chaoui, 2013).

3.5.3.1. Fuzzifier

The fuzzifier maps a crisp point $x=(x_1,\ldots,x_p)$, $T \in X_1 \times X_2 \times \ldots \times X_p \equiv X$ into a type-2 fuzzy set $\tilde{A}_X$ in X, interval type-2 fuzzy sets in this case. We will use type-2 singleton fuzzifier, in a singleton fuzzification, the input fuzzy set has only a single point on nonzero membership. $\tilde{A}_X$ is a type-2 fuzzy singleton if $\mu_{\tilde{A}_X}(X) = 1/1$ for $x = x'$ and $\mu_{\tilde{A}_X}(X) = 1/0$ for all other $x \neq x'$.

3.5.3.2. Rules Based

A Type-2 Fuzzy System (T2FS) has the same IF-THEN rules as the conventional type-1 Fuzzy System (T1FS) except that the antecedent and consequent are in type-2 form as follows:

$$R^n : \text{if}\left(x_1\right)\text{is}\left(\tilde{X}_1^n\right)\text{and}\ldots\text{and}\left(x_p\right)\text{is}\left(\tilde{X}_p^n\right), \textit{then}\left(y\right)\text{is}\left(Y^n\right) \qquad n = 0,1,2,\ldots,N$$

where $\tilde{X}_p^n\left(i=1,\ldots,P\right)$ are interval type-2 fuzzy system and Y_n is the interval output, for an input vector $x=(x_1,x_2,\ldots,x_p)$ of the P^{th} inputs. n is the number of rules.

3.5.3.3. Inference Engine

This block expresses the relationship that exists between the input variables (expressed as linguistic variables) and the output variables (also expressed as linguistic variables) (Cazarez-Castro et al., 2012). It aggregates the if-then rules stored in the knowledge base with the fuzzy sets generated by the fuzzifier to form an overall output fuzzy set. Similarly, a type-2 fuzzy inference engine provides a mapping from the input type-2 fuzzy sets to the output ones. The intersection of multiple rule antecedents is computed using a t-norm operator while the union of multiple rules is computed through a t-conorm operation (Cazarez-Castro et al., 2012).

The firing strength of the i^{th} rule is as in Eq. (3.22). The result of the input and antecedent operations is an interval type-1 set (Fayek et al., 2014) is:

$$F^l\left(X^{'}\right)=\left[\underline{f}^l\left(X^{'}\right),\overline{f}^l\left(X^{'}\right)\right]=\left[\underline{f}^l,\overline{f}^l\right] \tag{3.22}$$

and

$$\left[\underline{f}^l,\overline{f}^l\right]=\left[\underline{\mu}^{'}_{\tilde{F}_1^l}\left(x_1^{'}\right)*...*\underline{\mu}^{'}_{\tilde{F}_p^l}\left(x_p^{'}\right),\overline{\mu}^{'}_{\tilde{F}_1^l}\left(x_1^{'}\right)*...*\overline{\mu}^{'}_{\tilde{F}_p^l}\left(x_p^{'}\right)\right] \tag{3.23}$$

where $\underline{\mu}^{'}_{\tilde{F}_p^l}\left(x_p^{'}\right)$ and $\overline{\mu}^{'}_{\tilde{F}_p^l}\left(x_p^{'}\right)$ designed respectively upper and lower membership grades of $\mu_{\tilde{F}}\left(x\right)$

$$\underline{f}^l\left(X^{'}\right)=\underline{\mu}^{'}_{\tilde{F}_1^l}\left(x_1^{'}\right)*...*\underline{\mu}^{'}_{\tilde{F}_p^l}\left(x_p^{'}\right) \tag{3.24}$$

And

$$\overline{f}^l\left(X^{'}\right)=\overline{\mu}^{'}_{\tilde{F}_1^l}\left(x_1^{'}\right)*...*\overline{\mu}^{'}_{\tilde{F}_p^l}\left(x_p^{'}\right) \tag{3.25}$$

The fired output consequent set of the l rule is a type-1 fuzzy set characterized by a membership function

$$\mu_{\tilde{B}^l}\left(y\right)=\int_{b\in\left[\underline{f}^1*\underline{\mu}_{\tilde{G}^1}(y),\overline{f}^l*\overline{\mu}_{\tilde{G}^l}(y)\right]}1/b^l \tag{3.26}$$

If N out of a total of L fuzzy rules in the FLS fire, where $N \le L$, then the overall aggregated output fuzzy set is defined by a type-1 membership function $\mu_{\tilde{B}^l}\left(y\right)$ obtained by combining the fired output consequent sets into one. In other words $\mu_{\tilde{B}}\left(y\right)=\cup_{l=1}^{N}\mu_{\tilde{B}^l}\left(y\right)$

with the *t*-norm operator denoted by "*", and t-conorm operator denoted by "*V*"

Since generally we use the meet operation under product or minimum t-norm. So, at each value of x the intersection and union operations are referred to as the meet and join operations, respectively (Fayek et al., 2014)

Example of firing strength of one rule with two antecedent and one consequent (two input and one output) using t-norm operator is depicted in Figure 3.19.

In fuzzy system interval type-2 using the minimum or product t-norms operations, the i^{th} activated rule $F_i(x_1,\ldots, x_n)$ gives us the interval that is determined by tow extreme $f_i(x_1,\ldots, x_n)$ and $f_i(x_1,\ldots, x_n)$.

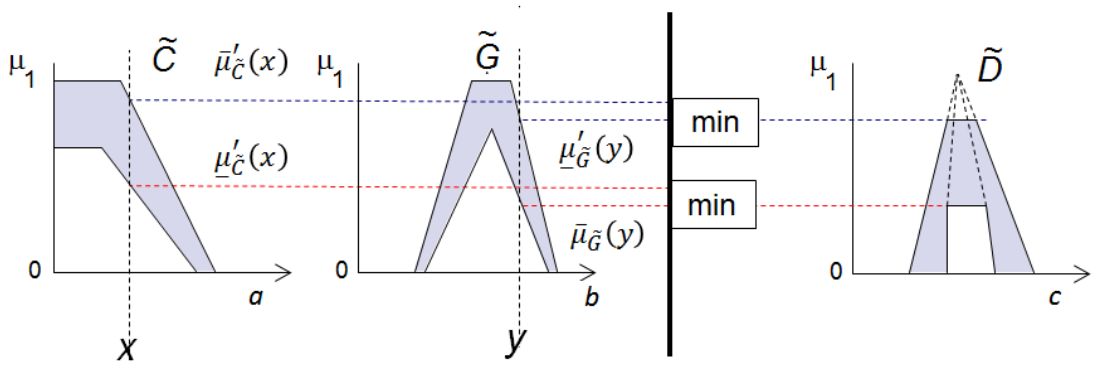

Figure 3.19. Inference engine calculation process

3.5.3.4. Type-reducer

The type-reducer generates a type-1 fuzzy set output, which is then converted in a crisp output through the defuzzifier. This type-1 fuzzy set is also an interval set, for the case of our FLS we used center of sets (*cos*) type reduction, Y_{cos} which is expressed as (Martinez et al., 2009):

$$Y_{\cos}(X) = [y_l, y_r]$$

$$[y_l, y_r] = \int y^1 \in \left[y_l^1, y_r^1\right] \ldots \int y^1 \in \left[y_l^M, y_r^M\right]$$
$$= \int f^1 \in \left[\underline{f}_l^1, \overline{f}_r^1\right] \ldots \int f^M \in \left[\underline{f}_l^M, \overline{f}_r^M\right] \cdot \frac{1}{\dfrac{\sum_{i=1}^{M} f^i y^i}{\sum_{i=1}^{M} f^i}} \tag{3.27}$$

This interval set is determined by its two end points, y_l and y_r, which corresponds to the centroid of the type-2 interval consequent set

$$C_{\tilde{G}^i} = \int \theta_1 \in J_{y_1} \ldots \int \theta_N \in J_{J_N} \frac{1}{\dfrac{\sum_{i=1}^{N} y_i \theta_i}{\sum_{i=1}^{N} \theta_i}} = \left[y_l^i, y_r^i\right] \tag{3.28}$$

Before the computation of $Y_{cos}\ (x)$, we must evaluate Eq. (3.27), and its two end points, y_l and y_r. If the values of *fi* and *yi* that are associated with *yl* are denoted f_l^i and y_l^i, respectively, and the values of f_i and y_i that are associated with y_r are denoted f_r^i and y_r^i, respectively, from Eq. (3.28), we have :

$$y_l^i = \frac{\sum_{i=1}^{M} f_l^i y_l^i}{\sum_{i=1}^{M} f_l^i} \tag{3.29}$$

$$y_r^i = \frac{\sum_{i=1}^{M} f_r^i y_r^i}{\sum_{i=1}^{M} f_r^i} \tag{3.30}$$

Type reducer converts the T2-FSs to T1-FSs before the defuzzifier. There are many Type Reduction (TR) method proposed in literature for IT2-FLSs. In this section, most widely used type reduction methods are explained. The most widely used common type reduction method is the iterative Karnik and Mendel algorithm

(Karnik and Mendel, 2009). In literature, there are some studies that aim to enhance the KM algorithm to improve the performance. Some of them are explained in detail in the next subsections. In addition, there are some studies that aim to reduce the type-2 sets to type-1 sets by using the approximations. These type of methods find approximations results and do not need any iteration. Therefore, they find the approximation results faster.

There are different methods for type reduction including *Karnik-Mendel* (KM) method, *Wu-Mendel* (WM) method, *Nie-Tan* (NT) method etc. Since the NT method has the precise computation and also benefits from simple and intuitive configuration, then it is preferred to another methods. It is based on taking average of the lower and upper MFs of the interval set as follows (Martinez et al., 2009).

3.5.3.5. Defuzzifier

The outputs of the type reduction block are applied to defuzzificaton block. The type reduced sets are determined by their left end point and right end point, and then the defuzzified value is calculated by the average of these points.

From the type-reducer we obtain an interval set Y_{cos}, to defuzzify it we use the average of y_l and y_r, so the defuzzified output of an interval singleton type-2 FLS is

$$y(X) = \frac{y_l + y_r}{r} \tag{3.31}$$

where *COG* is the defuzzified value, $\mu_A(x_i)$ is the activation degree of i^{th} rule, x_i is the weight of rule, and finally i and n represent the number of rules.

3.6. Stability Analysis Fuzzy Type-2

Generally in the real and hardware application the reliability of a controller is taken in consideration much more than the stability issued (Castilo, 2012),

furthermore the last is proved in the set-point oriented control such in the conventional controller where the fuzzy is classified as a task oriented controller. However, guaranteeing a robust interval fuzzy type-2 and proofing its stability is yet a big challenge objective for researchers because of its complicated structure, therefore the information taken from the (FOU) is used to develop some membership functions conditions which through them we can handle the stability analysis where the FOU here gives us the chance to generate different stages of nonlinear control curves to use while also providing a certain robustness which cannot found in type-1 (Kumbasar, 2015). Different approaches were used to realize the stability in fuzzy type-2, the well-known Lyapunov based approach (Kumbasar, 2015) and the other is the bounded input bounded output (BIBO) based approach (El-Nagar and Berdini, 2014) Consider the system shown in Figure 3.20. Let the subsystems H_1 and H_2 represent the type-2 controller and the plant under control. α_1 , α_1 the gain of H_1 H_2, . And β_1, β_2 are positive constants, $\alpha_1 \geq 0$, $\alpha_1 \geq 0$ so that

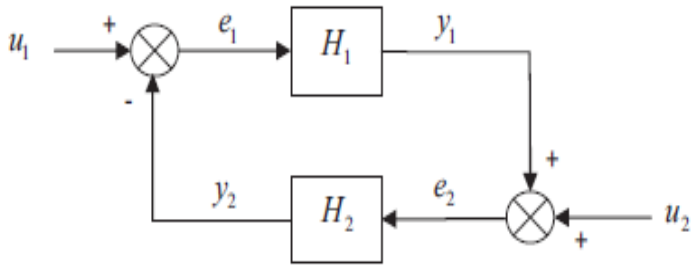

Figure 3.20. Feedback control (El-Nagar and Berdini, 2014)

$$\|y_1\| = \|H_1 e_1\| \leq \alpha_1 \|e_1\| + \beta_1 \tag{3.32}$$

$$\|y_2\| = \|H_2 e_2\| \leq \alpha_2 \|e_2\| + \beta_2 \tag{3.33}$$

Regarding to Eq (3.32) and Eq (3.33) as stability conditions and according to the small gain theorem, that any bounded input pair (u_1, u_2) generates a bounded output pair (y_1, y_2), the system is BIBO stable if $y_1 y_2 < 1$ (El-Nagar and Berdini, 2014).

3.7. Performance Criteria

Besides to the two fundamental performance criteria factors, time of response and the overshoot described as (O_s and T_s) those which have been employed, there are also other performance criteria factors normally utilized in the control engineering area for the evaluation of the response's behavior of systems. Generally are represented in integral functions. Regarding the type of integral of the error, one can give less or more weight to large errors, or consider the time of occurrence and duration of the error (Patel et al., 2009).

This type of performance has relatives changing with small errors. Ther integral square error (*ISE*). The formula of this integral is:

$$ISE = \int_0^\infty \left[e(t) \right]^2 dt \tag{3.34}$$

Caparing to the previous one the Integral absolute error (*IAE*). the small error has more influences, Also its analysis is a bt complicated and simple in implementation.w hile handling it. The formula is:

$$IAE = \int_0^\infty \left| e(t) \right|^2 dt \tag{3.35}$$

Initial error is not considered in integral time square error (*ITSE*).; more great error weighst are given to the errors that stay longer. The following formula:

$$ITSE = \int_0^\infty t \left[e(t) \right]^2 dt \tag{3.36}$$

Initial error is not considered in integral time square error (*ITSE*).; more great error weighst are given to the errors that remain longer time. It is obtained often when the higher overshoot and short settling times and are obtained. General formula as following:

$$ITAE = \int_0^\infty t\left|e(t)\right|^2 dt \tag{3.37}$$

This type of performance has relatives changing with small variation in the system's input energy:

Integral square control input (*ISCI*). Relatively related to the energy

$$ISCI = \int_0^\infty \left[u(t)\right]^2 dt \tag{3.38}$$

4. SIMULATION RESULTS AND DISCUSSION

The goal of this chapter is to synthesize some proposed theories of system's control in order to enslave the yaw and the pitch angles of the TRMS, basically with using the previous mentioned theories in the third chapter, we have taken the classical PID controller as a first application on the TRMS to compare its results later with FL controller's one, but before this we had to choose whether to take a centralized application with a PID controller for direct control the direct rotors and for the cross-coupling as well or to choose an independent PID controller for each rotor as an application strategy.

Secondly we get to control the TRMS through a FL controller application after, which it is not required a well knowing of the mathematical model of the systems, therefore before starting applying these theories we had to obtain the values of the model parameters. And it is necessary to get some measurements. First, geometrical dimensions and moving masses of TRMS should be measured.

In this chapter we are going to design the above mentioned controllers theatrically, and to apply them on the TRMS system.

- *PID controller*.
- *T1FLC-PID controller*
- *T2FLC-PID controller*

Here the desired target to be reached is to successfully implement on Matlab/Simulink the proposed controllers to make the system's angles (pitch and yaw) responses as same as the referred inputs and check each controller performance.

4.1. Static characteristics of the TRMS

The polynomials approximations is experimentally calculated and given as (Rahideha and Huijberts, 2008; Chalupa et al., 2015)

4.1.1. Main motor

$$\omega_v\left(u_{vv}\right) = 90.99u_{vv}^6 + 599.73u_{vv}^5 - 129.26u_{vv}^4 - 1238.64u_{vv}^3 + 63.45u_{vv}^2 + 1283.4u_{vv}$$

$$F_v\left(\omega_v\right) = -3.48.10^{-12}\omega_v^5 + 1.09.10^{-9}\omega_v^4 + 4.123.10^{-6}\omega_v^3 - 1.632.10^{-4}\omega_v^2 + 9.544.10^{-2}\omega_v$$

4.1.2. Tail motor

$$\omega_{hh}\left(u_{hh}\right) = 2020u_{hh}^5 - 194.69u_{hh}^4 - 4283.15u_{hh}^3 + 262.27u_{hh}^2 + 3796.83u_{hh}$$

$$F_h\left(\omega_h\right) = -3.10.10^{-14}\omega_h^5 + 1.595.10^{-11}\omega_h^4 + 2.511.10^{-7}\omega_h^3 - 1.808.10^{-4}\omega_h^2 + 0.8080\omega_h$$

After obtaining and calculating the required physical parameters and static characteristics of the system which allow us to know its general behavior mathematically, we move after that to the application of the control theories those are already discussed in the previous chapters. As it is shown on the Figure 4.1, the following is the block of TRMS on Matlab/Simulink is proposed.

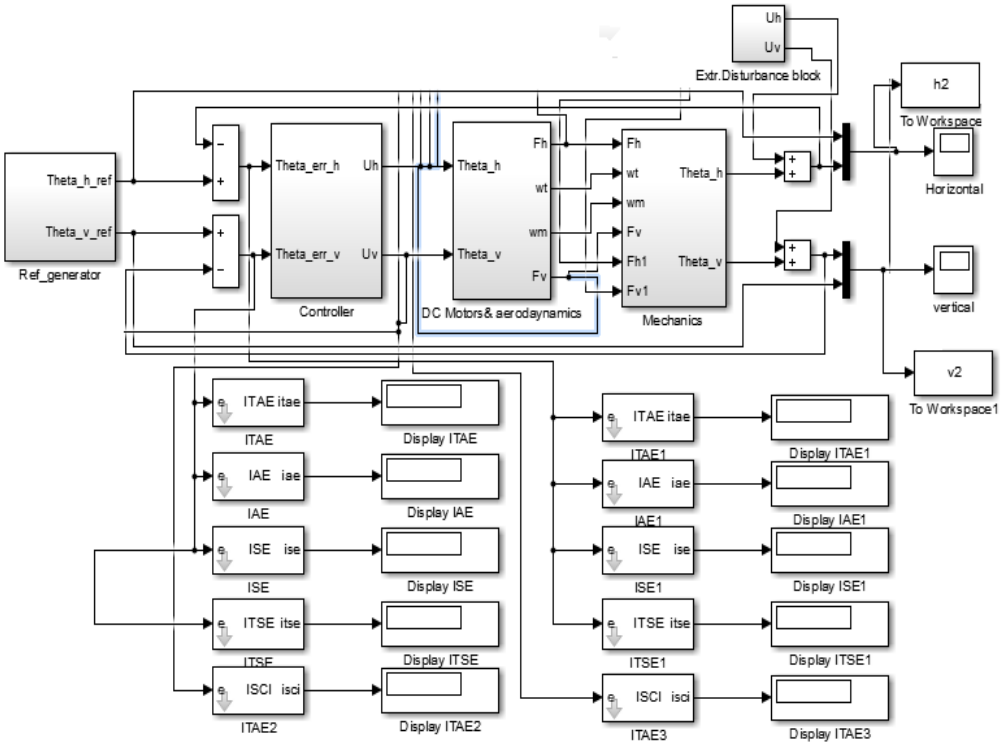

Figure 4.1. Schema block of the TRMS in Matlab/Simulink

Figure 4.1 shows sub systems are involved starting by the reference supply and the proposed controllers also the DC motors/ aerodynamics and the mechanical part of the TRMS as shown in Figure 4.2, besides to the performances indexes and the scopes which indicate and show the systems responses.

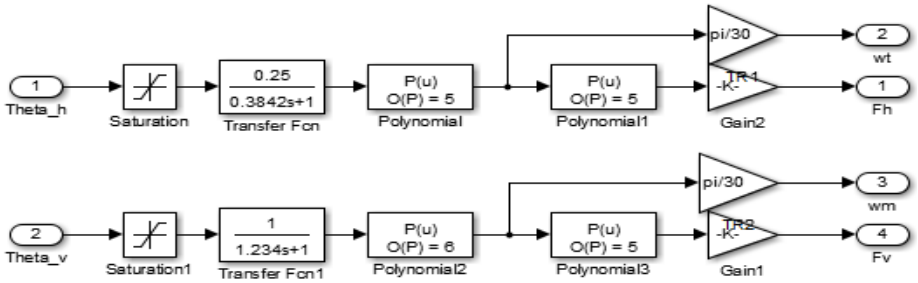

Figure 4.2. Schema block of the DC motors/Aerodynamics model in Matlab/Simulink

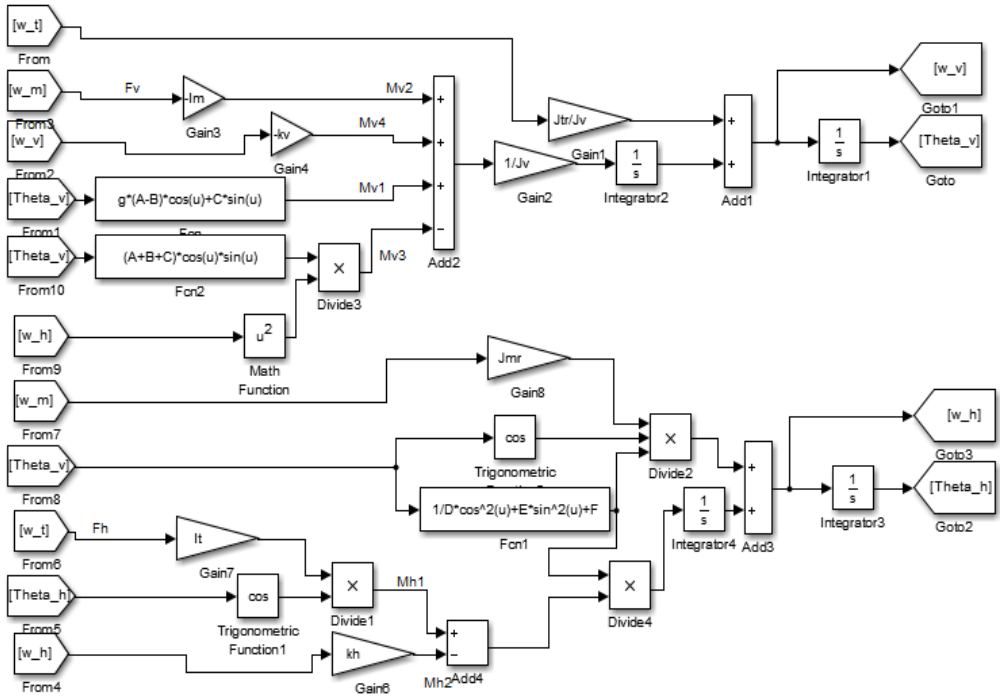

Figure 4.3. Mechanical model of TRMS in Matlab/Simulink

Figure 4.3 represents mechanical model of TRMS in Matlab/Simulink where the movements in two directions (horizontal and vertical) in our model can be known by plotting the graphs from scope block (horizontal and vertical signal outputs)..

4.2. Design of the PID controller

In the first proposed controller of the TRMS, two simple PID controllers are designed to control each of the vertical plane and the horizontal plane independently. The TRMS Simulink model consists two inputs are the control voltages and two output are the angular positions. The error is calculated by subtracting the feedback output of the angular position from the reference input which is represented the desired position. The error is entered later to the control block as it is shows in the following Figure 4.4.

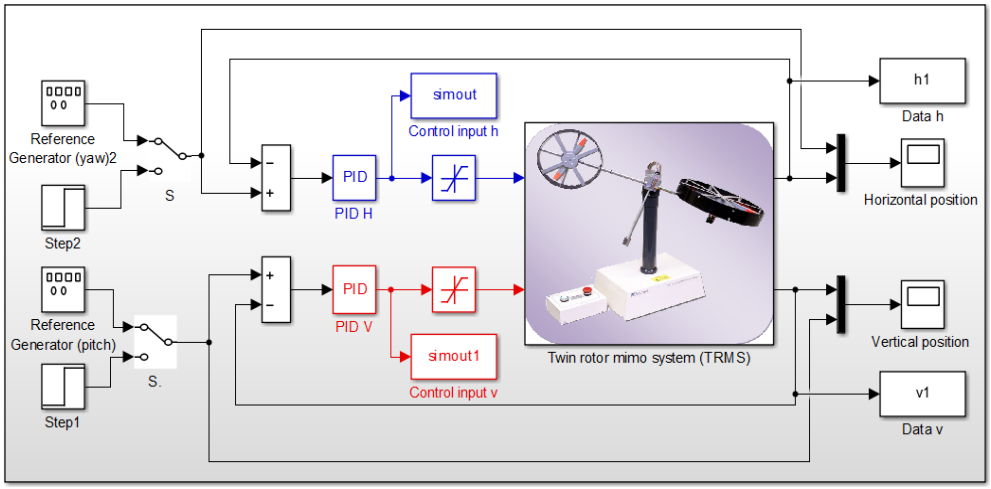

Figure 4.4. Scheme of the basic configuration of the MIMO PID Controller

In order to tune the PID controller parameters, Ziegler–Nichols oscillation approach closed loop tuning method is used and the controller parameters are given in Table 4.1.

4.2.1. Ziegler–Nichols approach

The well-known Ziegler–Nichols oscillation method provides a systematic PID tuning approach. In many cases Ziegler–Nichols method has experienced firstly good load disturbance attenuation. however, it have several disadvantages , they use insufficient process information and the design criterion gives closed loop systems with poor robustness, Ziegler and Nichols developed their tuning rules by simulating a large number of different processes, and correlating the controller parameters with features of the step response. The key design criterion was quarter amplitude damping. Process dynamics was characterized by two parameters obtained from the step response as tabled in Table 4.1. For improving a certain system performance, e.g., rise time, overshoot, and integral of the absolute error, many studies are attempting to incorporate features on the basis of the experiences of experts with regards to PID parameters selection.

Table 4.1. TRMS system performance indices using PID with Z-N

	Ziegler–Nichols				
Symbols	Kp	Ki	Kd	τ_d	T_d
Main rotor	9.7	1.21	6.76	4.9	1.54
Tail rotor	8.2	1.01	7.23	7.3	1.15

Later and in order to perform the system's response, an optimization algorithm have been used. However, there are many other algorithms used for the optimization, the Levenberg-marquardt training method is used as mentioned in the above section.

4.2.2. The PID parameters optimization

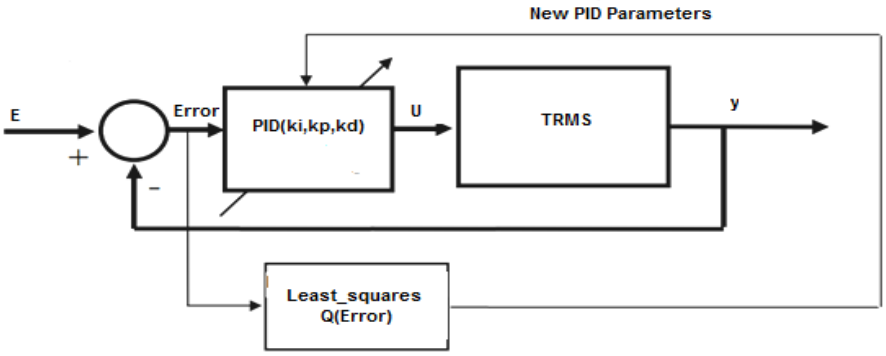

Figure 4.5. Optimization of the PID parameters

There are multiple algorithms of control popular due to their simplicity through the identification of the parameters easily (Allouani et al., 2012) the used one is based on the calculation nonlinear of the least square error levenburg marqurdt training method as shown in Figure 4.5. Matlab is already supported by this algorithm of calculation .

4.3. Design of Fuzzy logic controller

This control method has the advantage of not requiring knowing the mathematical model of the system for synthesizing it on systems on general and on the TRMS precisely. It is also characterized by the simplicity of using the control theories those are based on the human concluding and deciding.

As we had done before with the PID controller, we proposed a block of FL controller to each plane the horizontal and vertical one of the TRMS system as well, Figure 4.6 represents the structure of the controller.

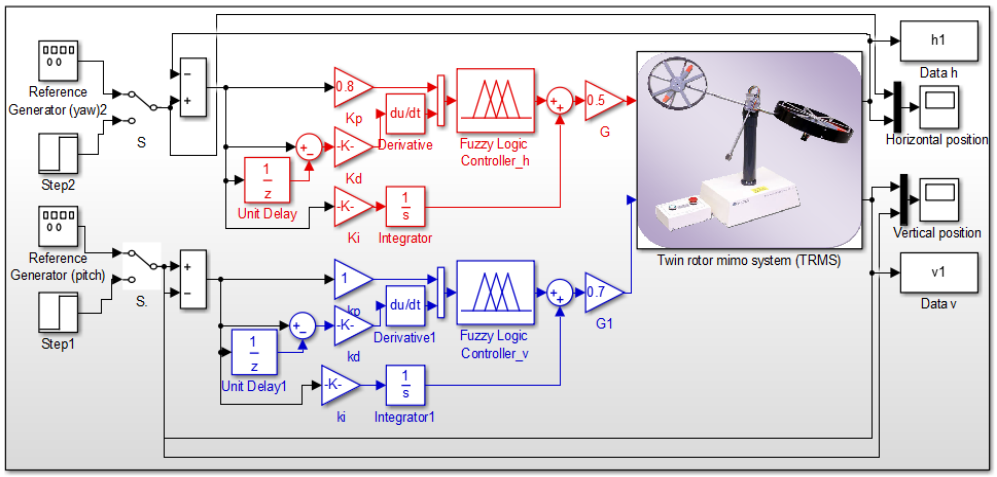

Figure 4.6. Block schema of the T1 FL-PID controller in Matlab/Simulink

The block schema contains the following block as shown graphically in Figure 4.7:

- An input block to calculate the error time varying and its variation.
- Normalization gains are associated to the error (k_p), to the variation (k_d) and to the control itself (G).
- Fuzzification block of the error and the error variation.
- Membership functions and control rules block.

- Defuzzification block based on the gravity center method its aim is to convert the control to significant numerical values.

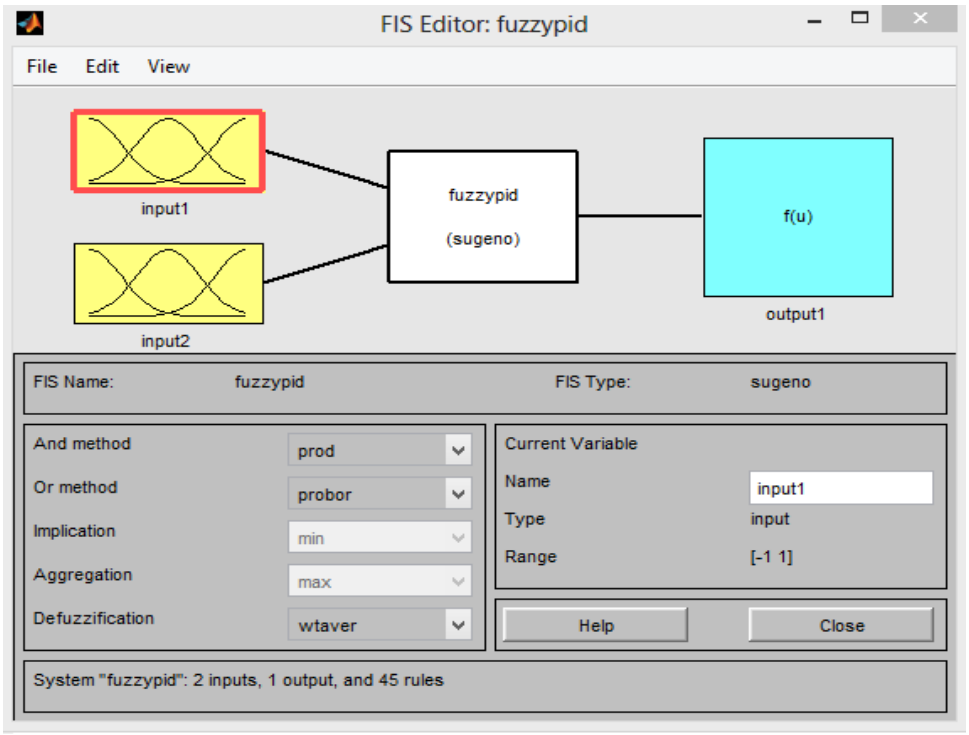

Figure 4.7. Fuzzy logic toolbox in Matlab/Simulink

The used control is a function of two chosen imputes for our controller and in an accuracy of the error and the error variation upon a sampling time T_e.

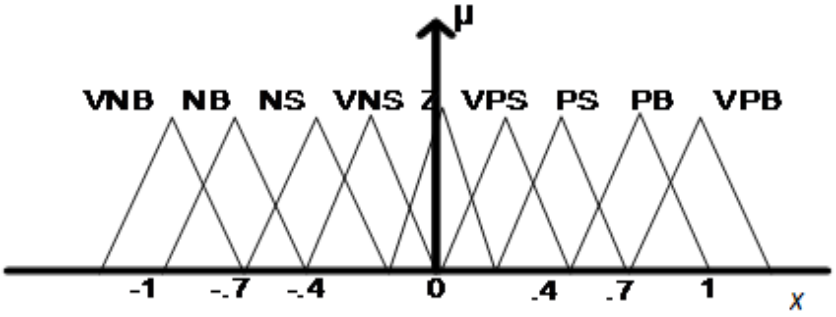

Figure 4.8. Error membership functions type-1 fuzzy logic controller ($\mu = 1$)

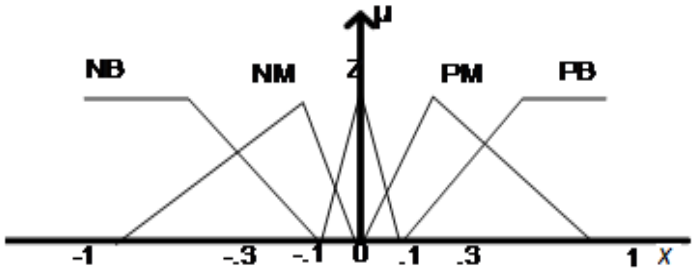

Figure 4.9. Error derivation membership functions type-1 fuzzy logic controller ($\mu = 1$)

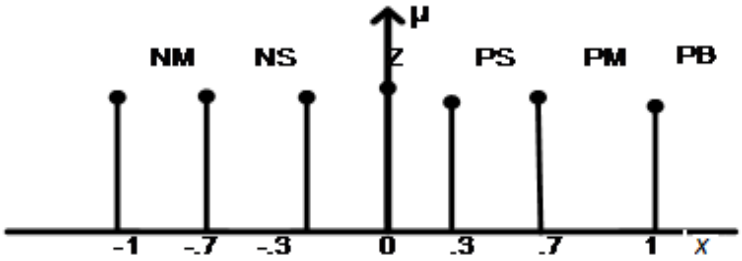

Figure 4.10. Output membership functions type-1 fuzzy logic controller ($\mu = 1$)

The chosen membership functions are respresented in Figure 4.8, Figure 4.9 and Figure 4.10 for the two inputs and the output respectively where the block abbreviations are shown in the following table 4.2:

Table 4.2. Fuzzy type-1 rules-base

Δe / e	NB	NM	ZE	PM	PB
VNB	N	N	NM	NM	NS
NB	N	NM	NM	NS	NS
NS	NM	NM	NS	NS	NS
VNS	NS	NS	Z	Z	Z
ZE	NS	Z	Z	Z	PS
VPS	Z	Z	Z	PS	PS
PS	PS	PS	PS	PM	PM
PB	PS	PS	PM	PM	P
VPB	PS	PM	PM	P	P

NS: negative small
VNS: very negative small
NM: negative medium
ZE: zero
VPS: very positive small
PS: positive small
PM: positive medium
PB: positive big
VPB: very positive big

$$U\left(kT_e\right) = f\left(e\left(kT_e\right), \Delta e\left(kT_e\right)\right) \tag{4.1}$$

where $e\left(kT_e\right)$ is the discretization of the input error and $\Delta e\left(kT_e\right)$ is its discrete variation. Consequently, the use of the ensemble of the associated decision rules gave the necessary control U which is built already at the output of our controller.

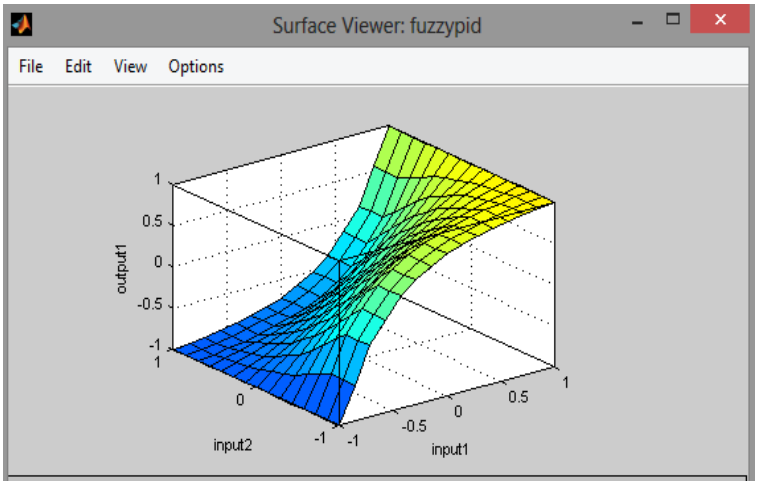

Figure 4.11. Surface of the fuzzy logic controller

This control U is obtained by interpreting of a predefined table of decision rules. Our control rule choice is taken the following form:

$$U\left(kT_e\right) = k_u u_n\left(kT_e\right) \tag{4.2}$$

where k_u is an associated gain to the commanded, and u_u is defuzzification output control.

One of the very important things in the FL controlling is to find the gains of the errors, the error variation and the associated gain of control or the normalization gains, adding to this, the gain of the integral actions, in fact this last is important to fix the performance of the control, there is not any systematical methods which can give its parameters therefore it must proceed by a groping using empirical rules and by the experience gained experimentally with time.

In order to eliminate the steady state static error we add in parallel of the FL controller an integrator action which allow our control to have finally a FLPID structure. Figure 4.11 shows the surface of fuzzy controller.

4.4. Design of Type-2 Fuzzy system controller

The design of fuzzy type-2 controller is similar in structure to the type-1 we considered two sub-controllers, the first to the vertical plane by controlling the main rotor, and another controller to the horizontal plane by controlling the tail rotor of the TRMS system, both of those two sub-controllers have fuzzy-PID structure. where was necessary to determinate the two fuzzy inputs the error and the error deviation, tuning gains K_p and K_d of those last inputs already provides a fuzzy-PD controllers, besides to a summed third gain K_{i} in order to improve tracking and transient response and to eliminate the steady state error as well. A developed software called Type-2 Fuzzy Logic Toolbox is used a collection of MATLAB based M-files (Celikyilmaz and Türksen, 2009).

The design of fuzzy type-2 controller is similar in structure to the type-1 which we designed by two sub-controllers. The first controller is corresponding to the pitch motion to the vertical plane by controlling the main rotor, and the other controller is corresponding to the yaw motion of the horizontal plane by controlling the tail rotor of the TRMS system. Both of the two sub-controllers are designed by fuzzy-PID strategies. A developed software is called Type-2 Fuzzy Logic Toolbox is used a collection of MATLAB based M-files algorithms (Kumbasar, 2014). In the type-2 fuzzy rule two inputs were chosen by representing the error and the error variation under the linguistic representations as rule base; N, NM, ZE, PM, P denotes negative, negative medium, zero, positive medium and positive, respectively as shown in Table 4.2 For both of the error the FOU is chosen between 1 and 0.5 for all the membership functions, also for the error derivation which is the second input the FOU is chosen between 1 and 0.72 for all the membership functions but for the zero ZLMF and ZUMF that it is chosen between 1 and 0.5. Triangular membership functions are chosen as introduced previously, then fuzzy inference engine infers the input variables to a suitable fuzzy set, as it can be seen in Figure 4.8 the first input and Figure 4.9 shows the second input. And an output signal is obtained by defuzzification. Takagi-Sugeno (TS), is chosen

as method of fuzzy inference with an output range of -1/+1 for the negative and positive respectively and -0.8/0.8 for the positive medium and negative medium respectively as shown in Figure 4.10.

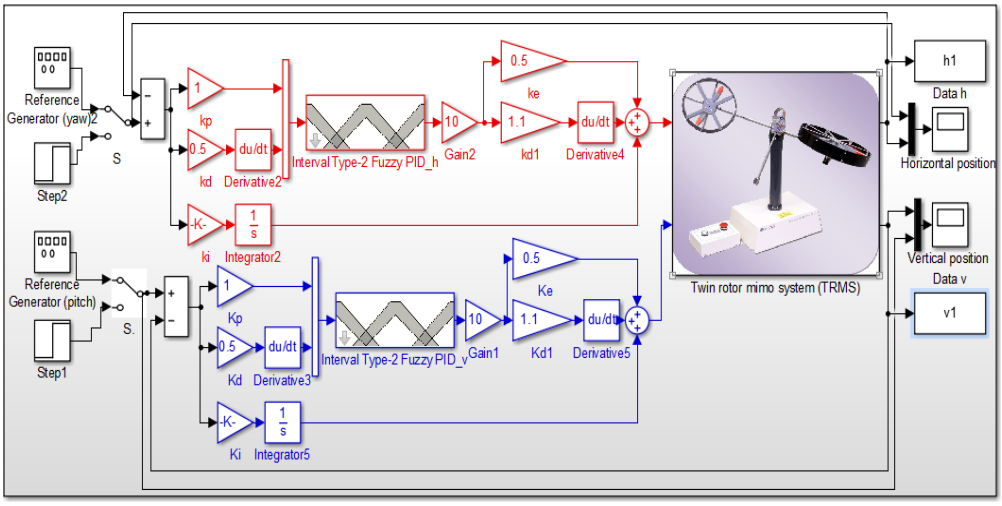

Figure 4.12. Block schema of the IT2FLC-PID controller in Matlab/Simulink

The following five fuzzy sets are chosen as: negative (N), negative medium (NM), zero (ZE), and positive medium (PM) and positive (P), they are used and summarized in Table 4.3.

Table 4.3 Fuzzy type-2 rules-base

de / e	VN	N	Z	P	VP
VN	N	N	N	N	NM
N	N	NM	Z	NM	Z
Z	NM	Z	Z	Z	PM
P	PM	PM	Z	PM	P
VP	PM	P	P	P	P

This MF's are same for input and output variables and characterized using triangular MF, as it can be seen in Figure 4.9 and Figure 4.8, the inference engine then infers the input fuzzy variable using the rule library and provides a suitable fuzzy set. And finally, a crisp output value is obtained from the defuzzifier. Fuzzy type-2 rules-base for the negative medium and positive medium respectively as shown in Figure 4.13. Figure 4.14 and Figure 4.15.

The following figures are the rules base representations:

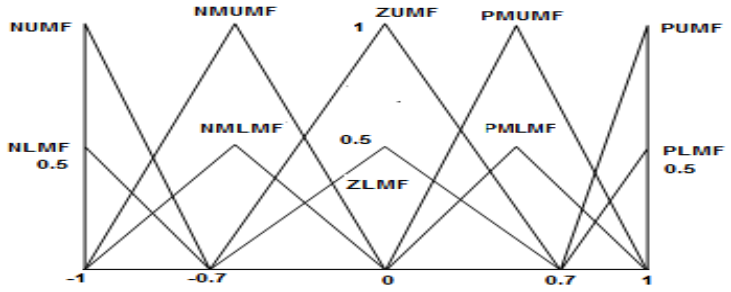

Figure 4.13. Error membership functions Type-2 fuzzy controller

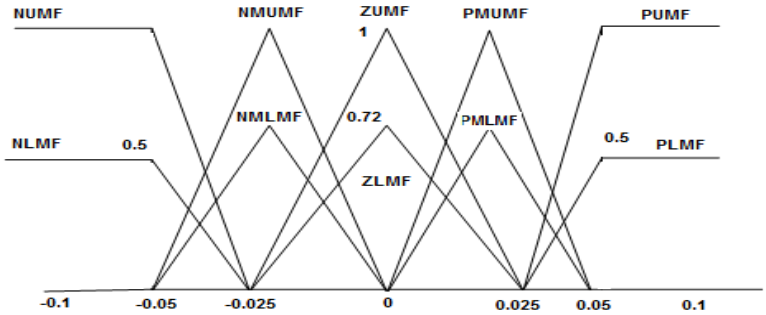

Figure 4.14. Error derivation membership functions Type-2 fuzzy controller

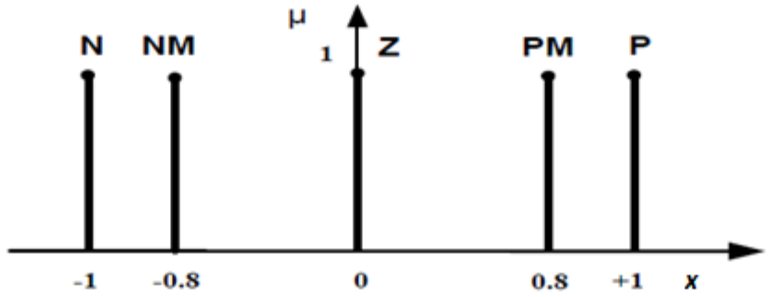

Figure 4.15. Output membership functions Type-2 fuzzy controller ($\mu = 1$)

4.4.1. Fuzzy Logic Toolbox Version

Generally the toolbox (MathWorks) of IT2FLC is used for understand the flow chart to design fuzzy logic controller, so they never uses to design practical controller. The IT2FLS Toolbox includes as shown in Figure 4.16 a series of program files some of them in to do its role for example (fuzzy2.m) for display editor of IT2FLC and its function is fuzzy2 (Kumbasar, 2014), so fuzzy2 is both a directory and a function, (defuzz2.m) for defuzzification, and so on. And also the toolkit supports the implementation of several types of fuzzy logic inference systems and has several aspects of its capabilities to allow the straightforward implementation of type-1 and interval type-2 fuzzy systems are:

The Mamdani and Takagi-Sugeno-Kang (TSK) Interval Type-2 Fuzzy Inference Models , and the design of Interval Type-2 membership functions and operators are implemented in the IT2FLS Toolbox (Interval Type-2 Fuzzy Logic Systems) reused from the Matlab® commercial Fuzzy Logic Toolbox as shown in Figure 4.16.

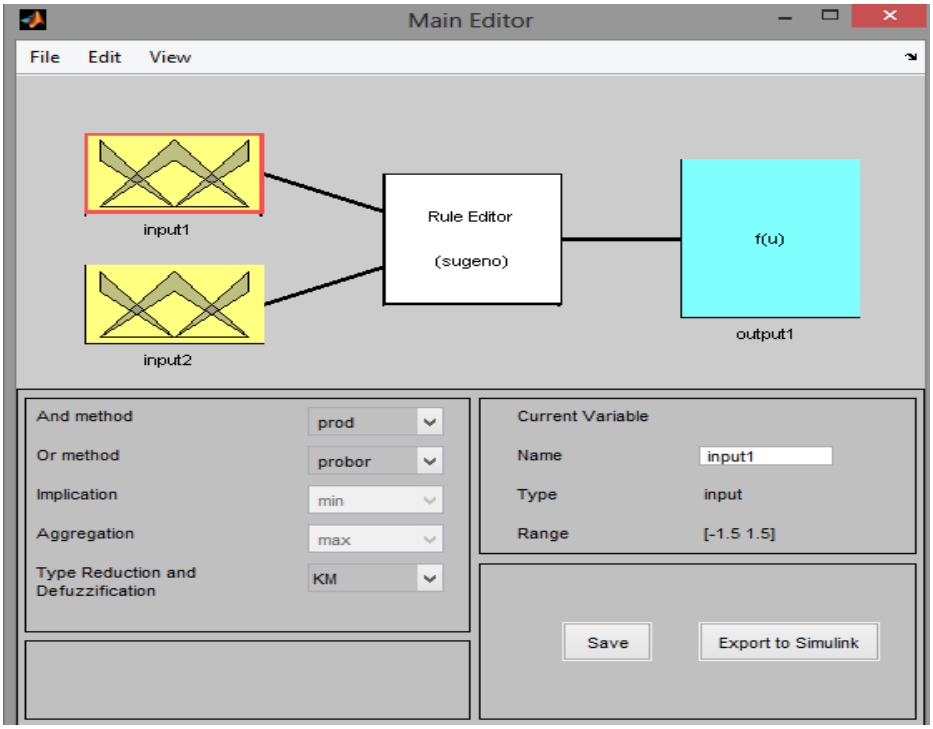

Figure 4.16. Type-2 Fuzzy Main editor toolbox

In this work singleton type-2 Mamdani method has been opted, and the AND method, OR method, implication, aggregation, Type-Reduction and defuzzifier are chosen to be min, max, min, max, center-of-sets and centroid, respectively. Also we have used a Gaussian membership functions.

4.5. Simulation results

Starting by the response of the system of the TRMS in the closed loop mode and the error calculation. Figure 4.16 and Figure 4.17 shown the TRMS's system closed loop for the vertical and the horizpntal plane respectively.

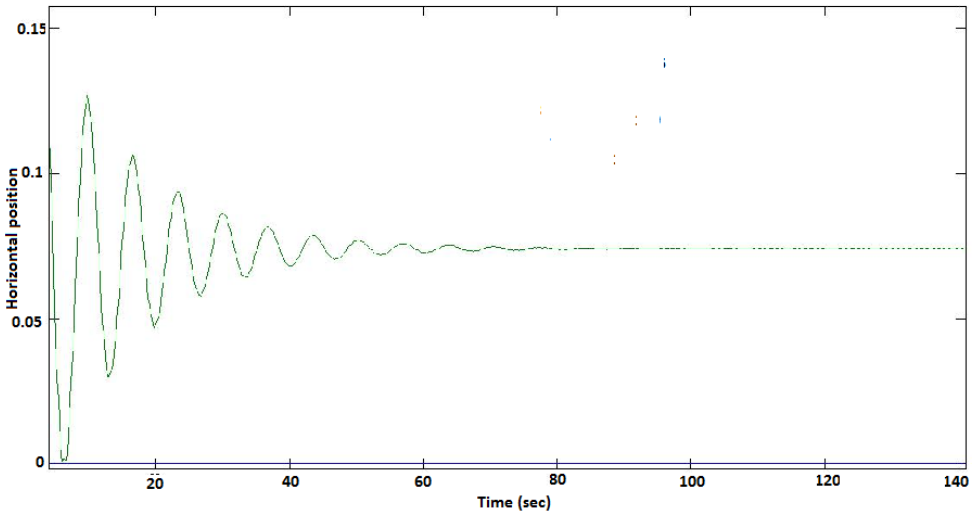

Figure 4.17. Horizontal position $\theta_h(t)$ of the Tail rotor, TRMS system in the closed loop

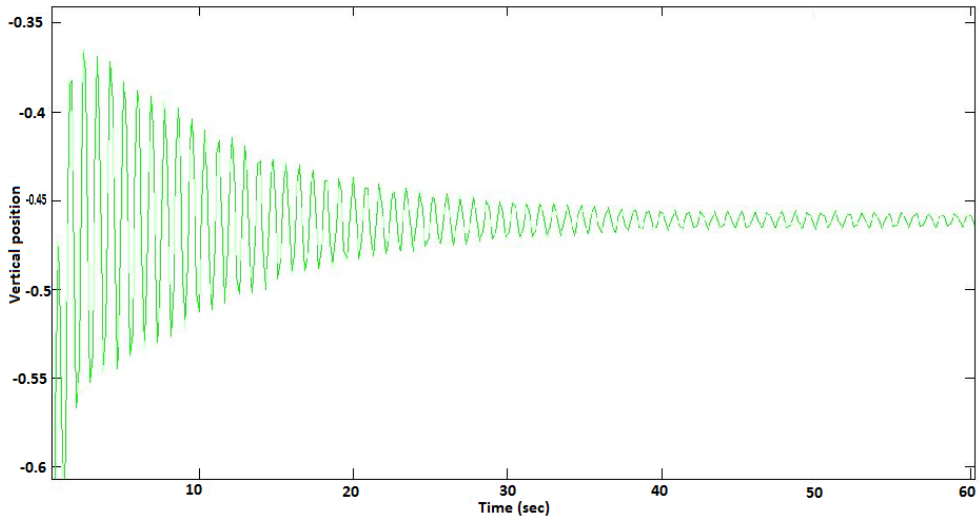

Figure 4.18. Vertical position $\theta_v(t)$ of the Main rotor, TRMS system in the closed loop

The signal outputs in horizontal direction show us behavior of the system. From that we can know our system function at certain range that correspond the inputs (red color) and will be stable after.

4.5.1. Tracking Performance

In this last section a TRMS model has been realized on Matlab/Simulink environment by using the above mathematical equations mentioned in the modeling part, the numerical parameters of the model were obtained from the company provider. The performance of the controllers have been examined using different performance indexes such as the integral of squared error (ISE), the integral of absolute error (IAE), the integral of time multiply squared error (ITSE) and the integral the multiply absolute error (ITAE). The overshoot response and the integral square of control input (ISCI) are used as well. The results are presented in Table 4.1 for the vertical plane (pitch motion) and Table 4.2 for the horizontal plane (yaw motion). Starting by the PID results.

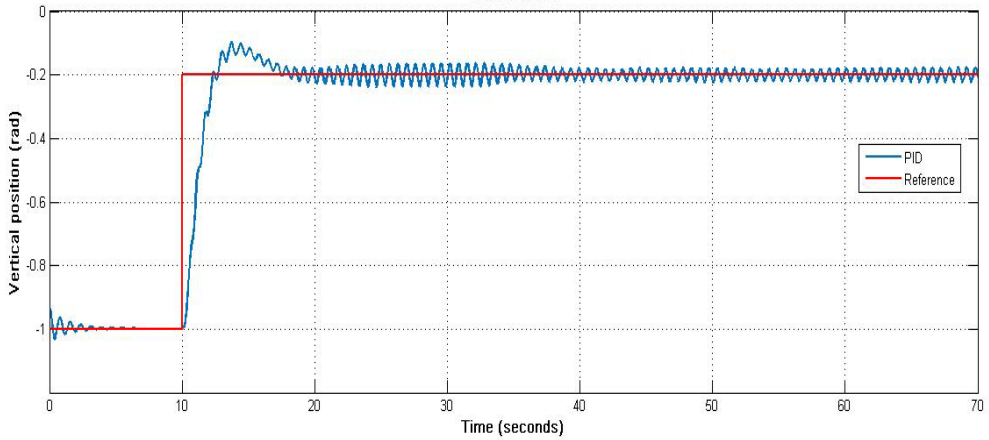

Figure 4.19. Step response of the vertical position $\theta_v(t)$ of the TRMS main rotor using PID controller

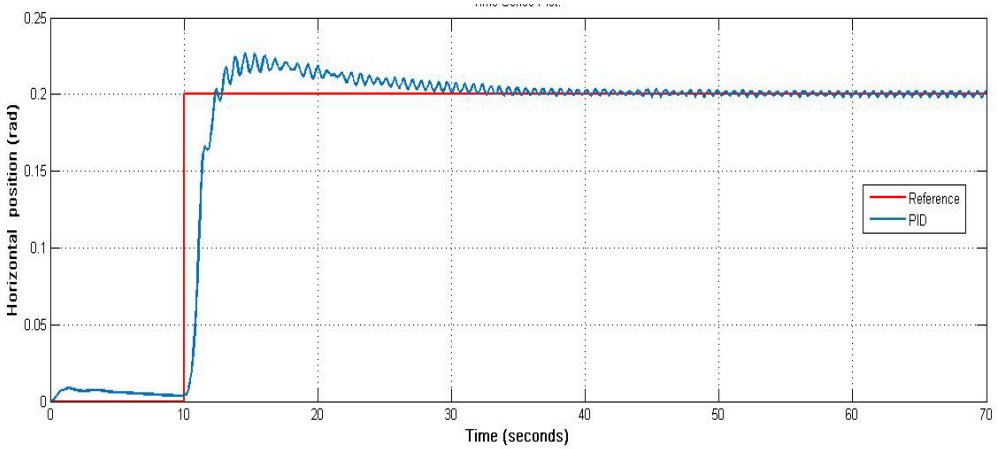

Figure 4.20. Step response of horizontal position $\theta_h(t)$ of the TRMS tail rotor using PID controller

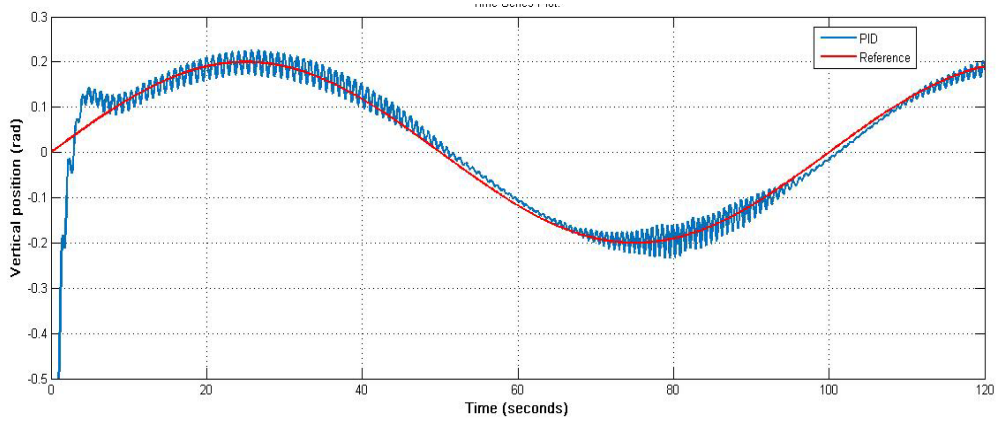

Figure 4.21. Response of vertical position $\theta_v(t)$ of the TRMS main rotor using PID controller tracking a sinusoidal trajectory (frequency of 0.20 Hz)

To examinate the performance of the three controllers, diffrent input sources were selected, staring by the step input as shown in figure 4.18 for the vertical plane under the PID controller and in Figure 4.19 for the horizontal plane. And a sinusoidale input source as shown in Figure 4.20 and 4.21 for the vertical and the horizontal plane respectively.

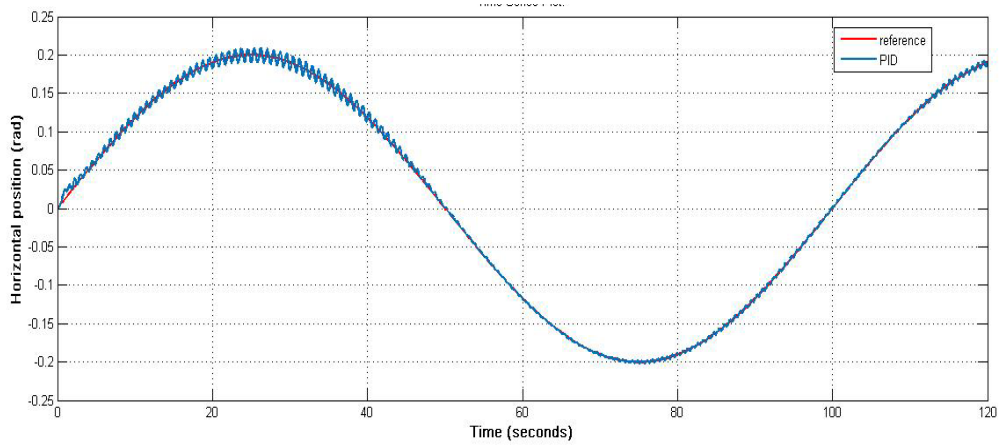

Figure 4.22. Response of horizontal position $\theta_h(t)$ of the TRMS tail rotor using PID controller tracking a sinusoidal trajectory (frequency of 0.20 Hz)

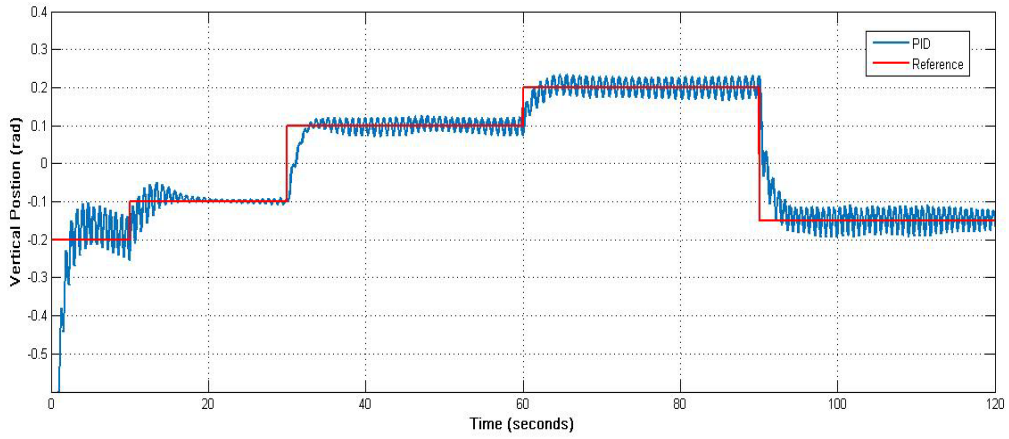

Figure 4.23. Response of vertical position $\theta_v(t)$ of the TRMS main rotor using PID controller tracking different set-points trajectory (frequency of 0.20 Hz)

The vertival position's reponse of the main motor to a square wave or different level trajectory in a frequency of 0.20 Hz, under the PID controller is shown in Figure 4.22 and in Figure 2.23 for the horizontal plane that is related to the motion in the tail motor.

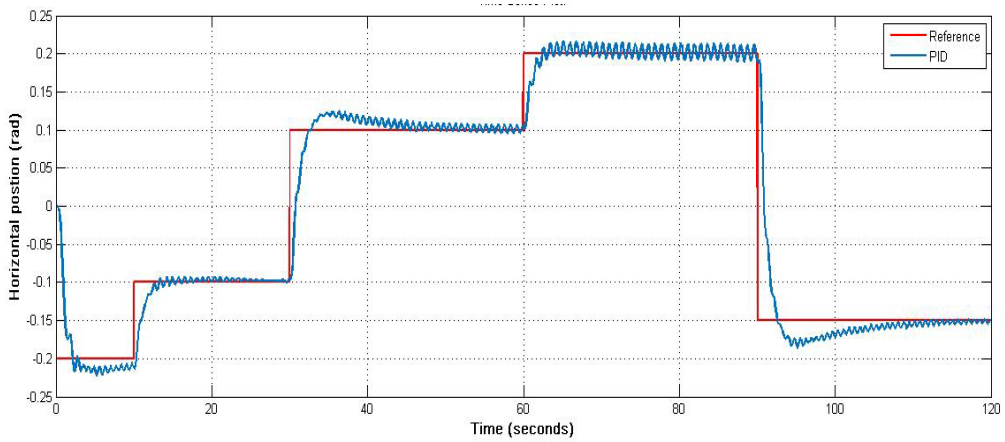

Figure 4.24. Response of horizontal position $\theta_h(t)$ of the TRMS tail rotor using PID controller tracking different set-points trajectory (frequency of 0.30 Hz)

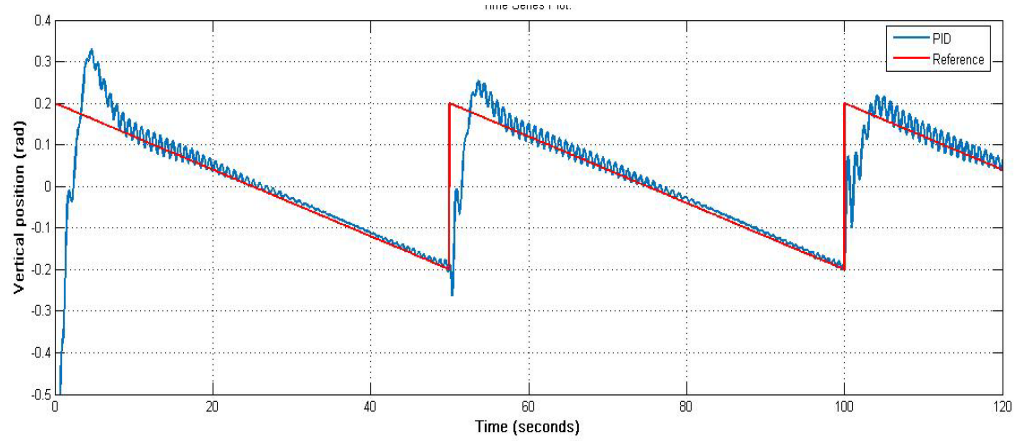

Figure 4.25. Response of vertical position $\theta_v(t)$ of the TRMS main rotor using PID controller tracking saw-tooth trajectory (frequency of 0.20 Hz)

The vertival position's reponse of the main motor to a sawtooth wave or different level trajectory in a frequency of 0.20 Hz, under the PID controller is shown in Figure 4.24 and in Figure 2.25 for the horizontal plane that is related to the motion in the tail motor.

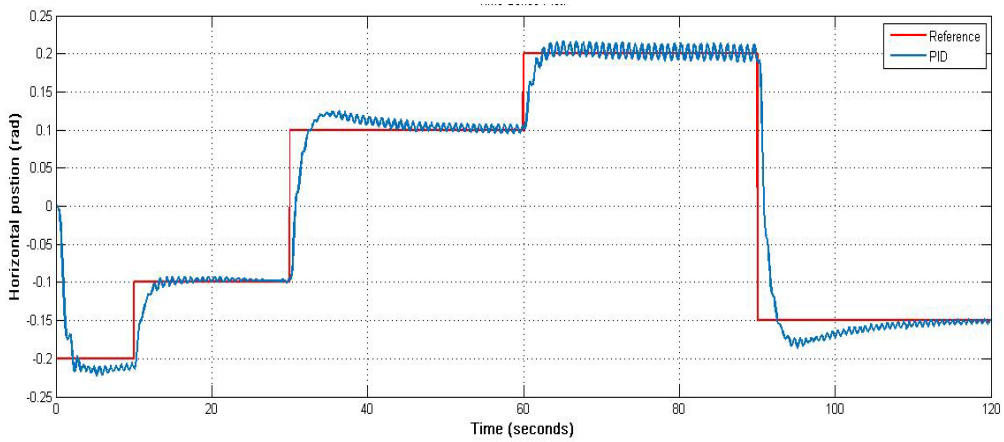

Figure 4.26. Response of vertical position $\theta_h(t)$ of the TRMS main rotor using PID controller tracking saw-tooth trajectory (frequency of 0.01 Hz)

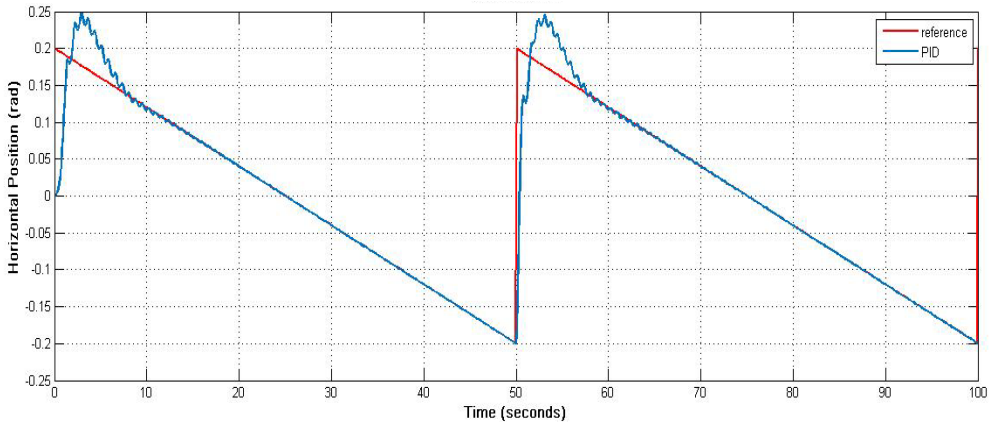

Figure 4.27. Response of horizontal position $\theta_h(t)$ of the TRMS tail rotor using PID controller tracking saw-tooth trajectory (frequency of 0.01 Hz)

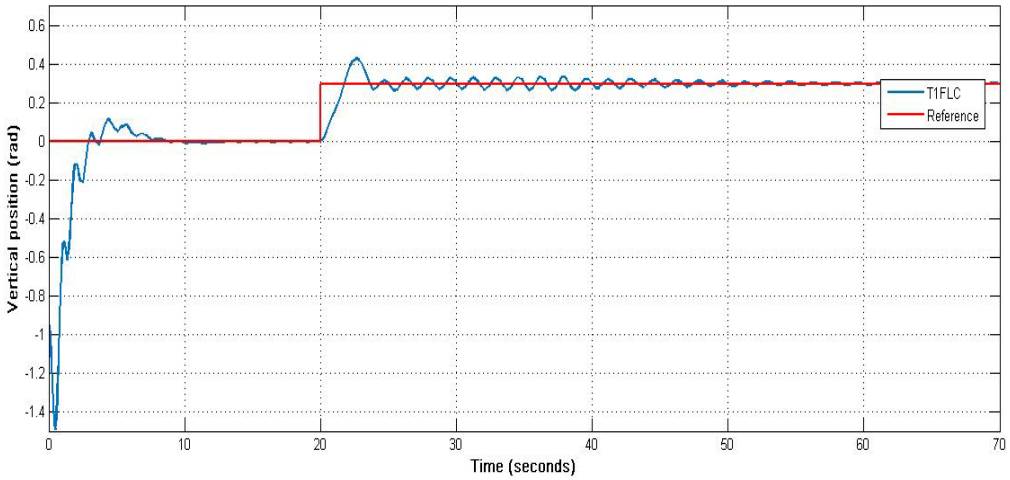

Figure 4.28. Step response of the vertical position $\theta_v(t)$ of the TRMS main rotor using Type 1 Fuzzy PID controller

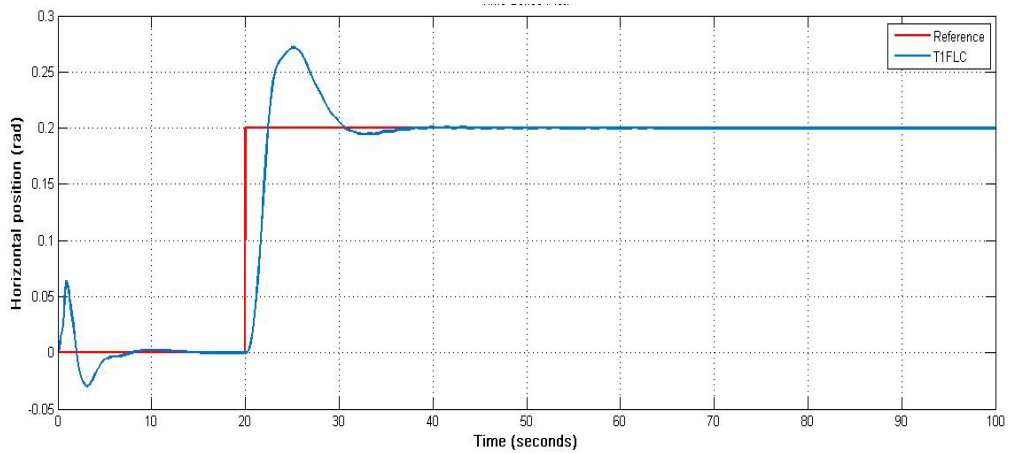

Figure 4.29. Step response of horizontal position $\theta_h(t)$ of the TRMS tail rotor using Type 1 Fuzzy PID controller

The vertival position's reponse of the main motor to a step wave under Fuzzy type 1 PID controller is shown in Figure 4.26 and in Figure 2.27 for the horizontal plane that is related to the motion in the tail motor.

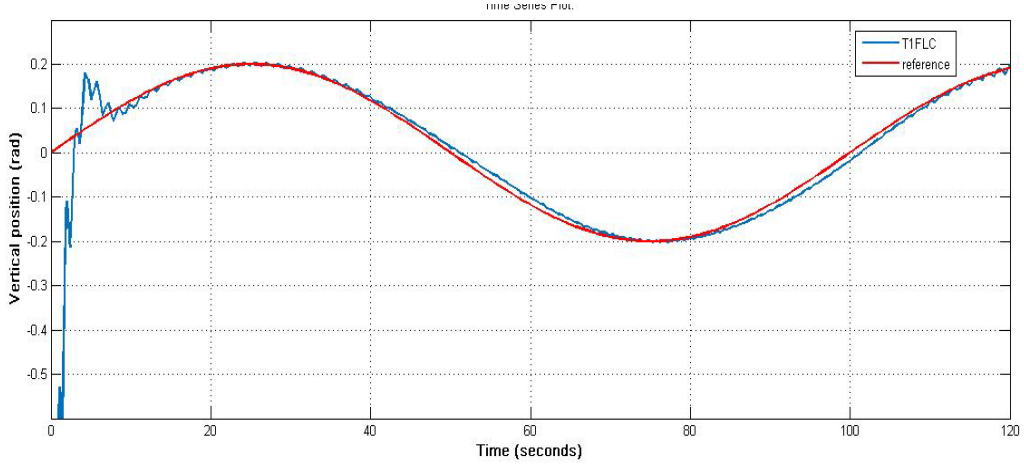

Figure 4.30. Response of vertical position $\theta_v(t)$ of the TRMS main rotor using Type 1 Fuzzy PID controller tracking a sinusoidal trajectory (frequencu of 0.20 Hz)

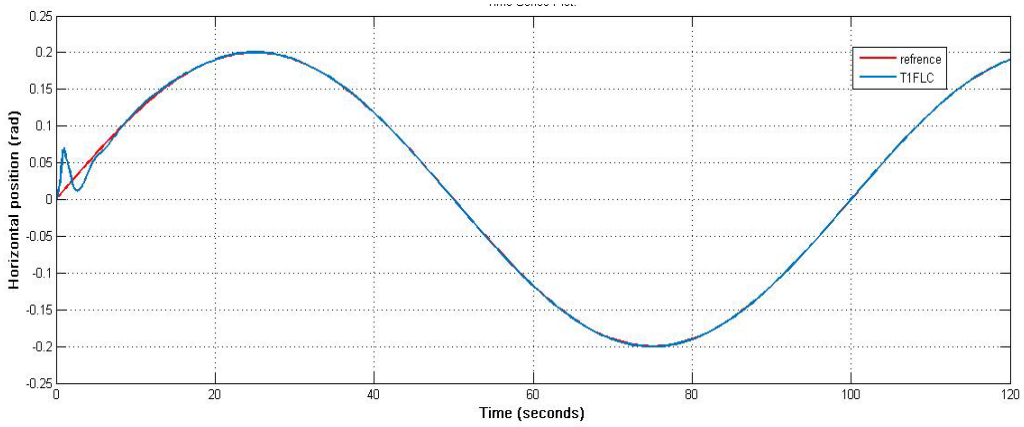

Figure 4.31. Response of horizontal position $\theta_h(t)$ of the TRMS tail rotor using Type 1 Fuzzy PID controller tracking a sinusoidal trajectory (frequency of 0.20 Hz)

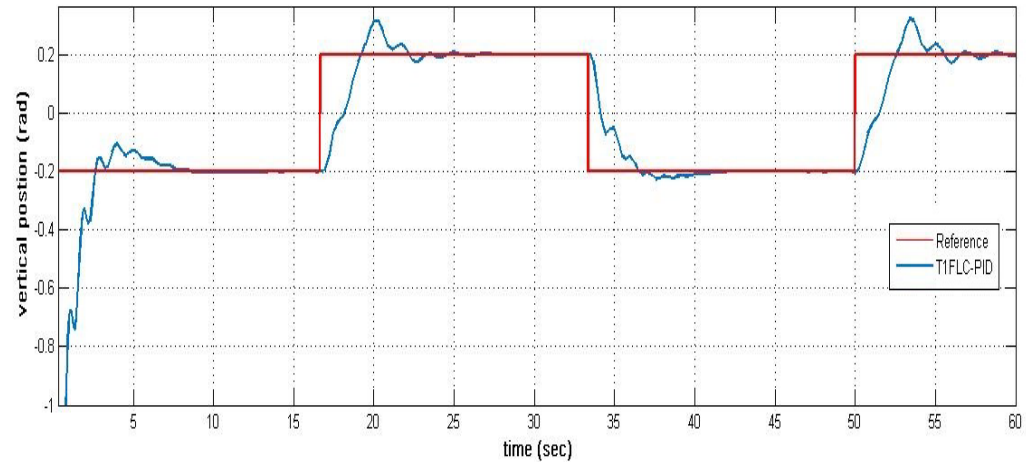

Figure 4.32. Response of vertical position $\theta_v(t)$ of the TRMS tail rotor using Type 1 Fuzzy PID controller tracking square trajectory (frequency of 0.30 Hz)

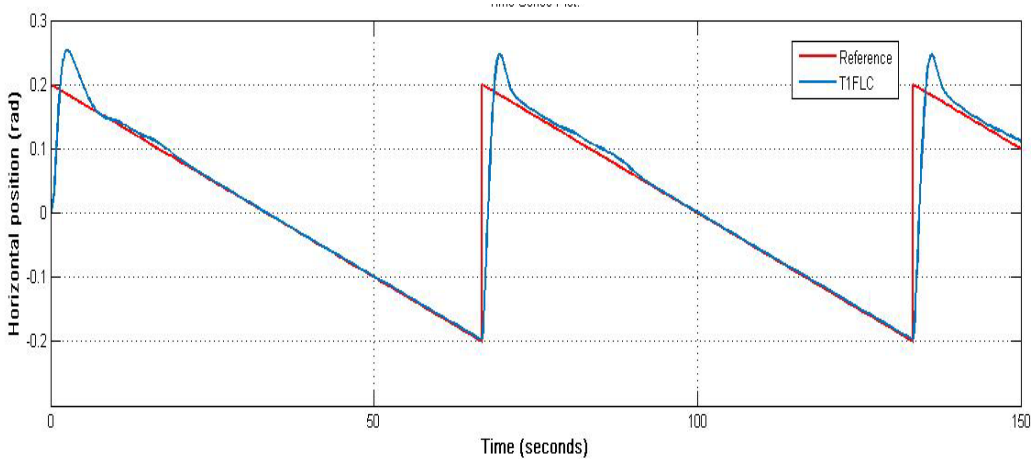

Figure 4.33. Response of horizontal position $\theta_h(t)$ of the TRMS tail rotor using Type 1 Fuzzy PID controller tracking saw-tooth trajectory (frequency of 0.30 Hz)

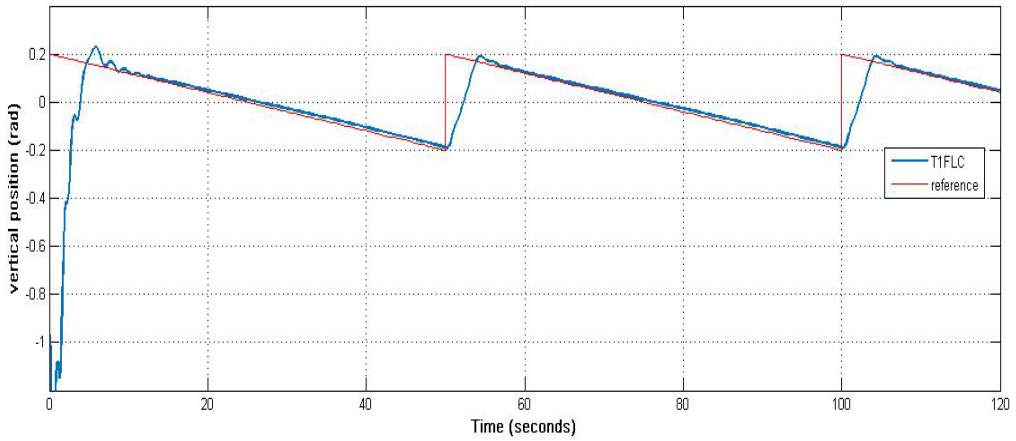

Figure 4.34. Response of vertical position $\theta_v(t)$ of the TRMS tail rotor using Type 1 Fuzzy PID controller tracking saw-tooth trajectory (frequency of 0.20 Hz)

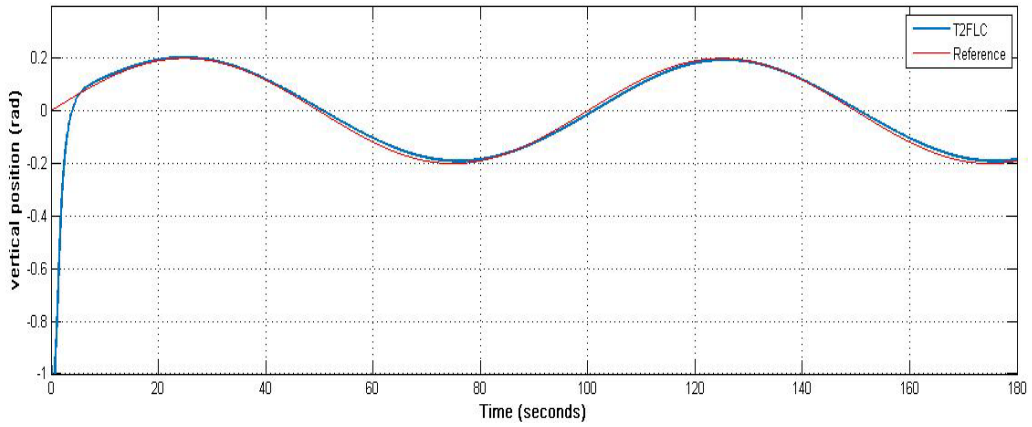

Figure 4.35. Response of vertical position $\theta_v(t)$ of the TRMS main rotor using Type 2 Fuzzy PID controller tracking a sinusoidal trajectory (frequency of .20 Hz)

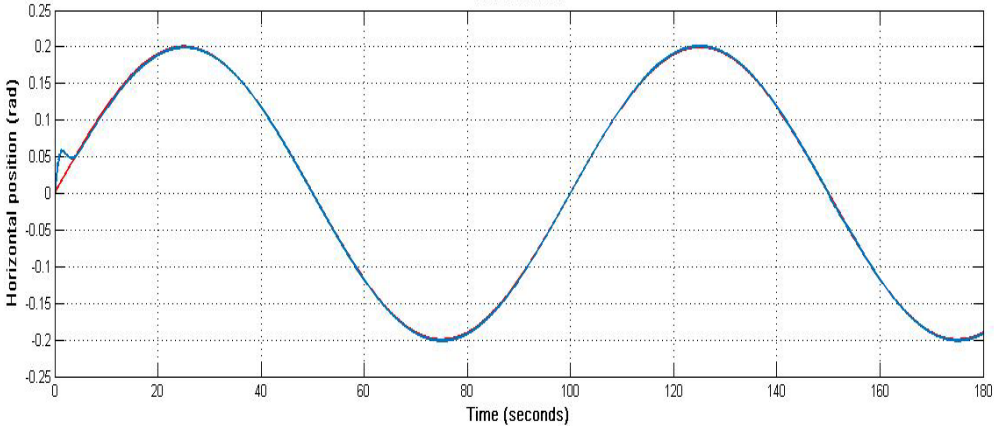

Figure 4.36. Response of horizontal position $\theta_h(t)$ of the TRMS main rotor using Type 2 Fuzzy PID controller tracking a sinusoidal trajectory (frequency of 0.20 Hz)

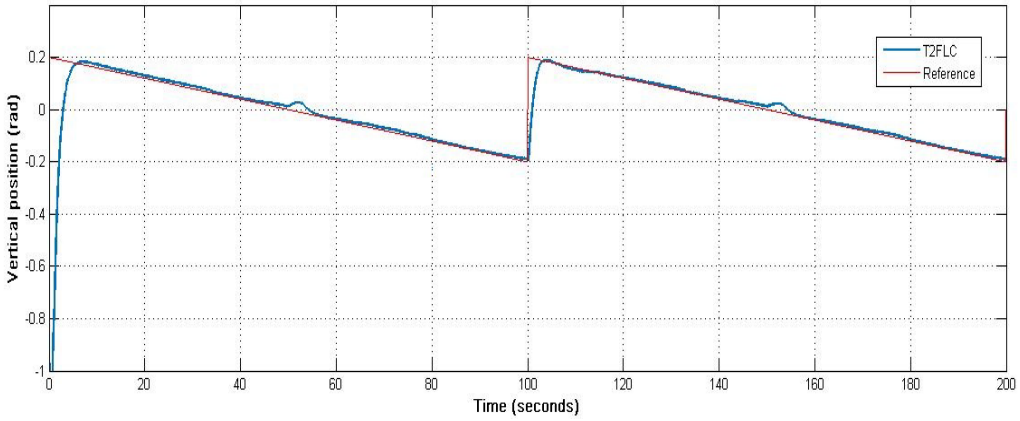

Figure 4.37. Response of vertical position $\theta_v(t)$ of the TRMS main rotor using Type 2 Fuzzy PID controller tracking a skew trajectory (frequency of 0.20 Hz)

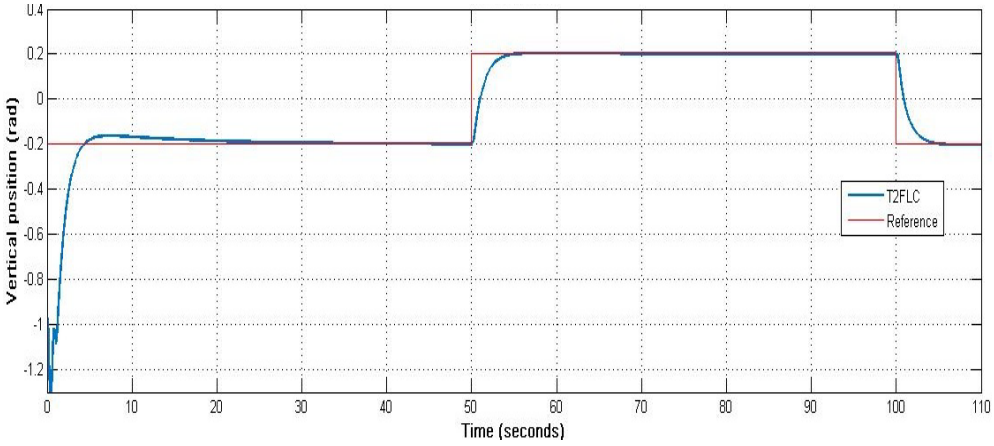

Figure 4.38. Response of vertical position $\theta_v(t)$ of the TRMS main rotor using Type 2 Fuzzy PID controller tracking square trajectory (frequency of 0.20 Hz)

4.5.2. Disturbance rejection performance

Later a sudden load disturbance is applied to test the performance responses of the controllers at the 80th second. The disturbance load is illustrated in Figure 4.38 to Figure 4.39 under the PID controller and in Figure 4.40 and Figure 4.41 under the Type 1 Fuzzy PID controller respectively and for the Type 2 Fyzzy PID the results to the applied disturbance is shown in Figure 4.43 and Figure 4.44. As can be seen from performance comparisons, the model-free PID control system yields favorable control performance superior to that of Fuzzy-PID control. Furthermore, the controllers are compared via several illustrations and numerical measures. In this sense, fuzzy-PID controller, which is highly sensitive to perturbations and uncertainties, has a drawback and it may cause performance degradation. In the meanwhile, applied on the same class of systems as described previously, the fuzzy-PID control has higher tracking errors, especially when disturbances arise.

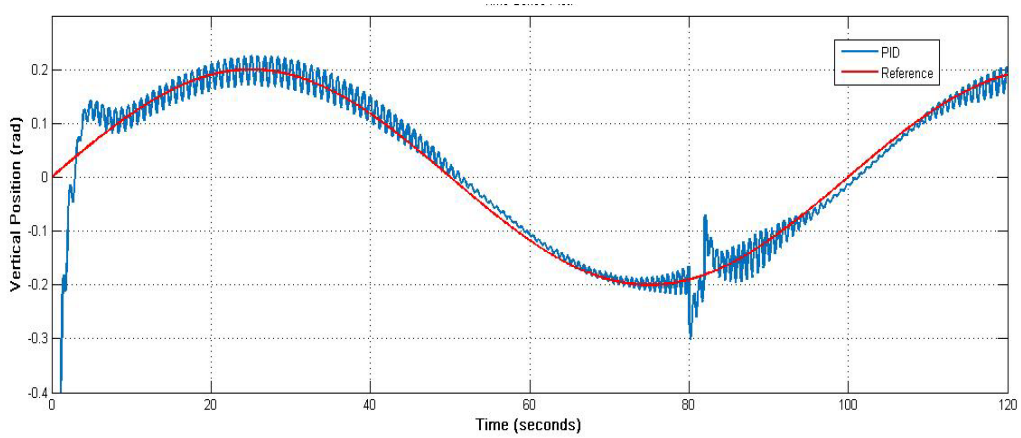

Figure 4.39. Response of horizontal $\theta_v(t)$ of the TRMS main rotor using PID controller tracking a sinusoidal trajectory (frequency 0.20 Hz) to load disturbance at the (80th sec)

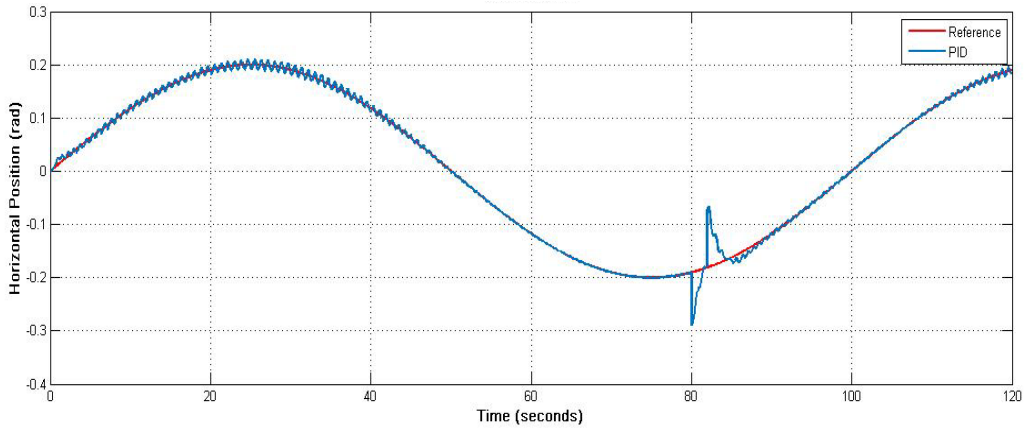

Figure 4.40. Response of horizontal position $\theta_h(t)$ of tail rotor using PID controller tracking a sinusoidal trajectory (frequency of 0.02 Hz) to load disturbance at the (80^{th} sec)

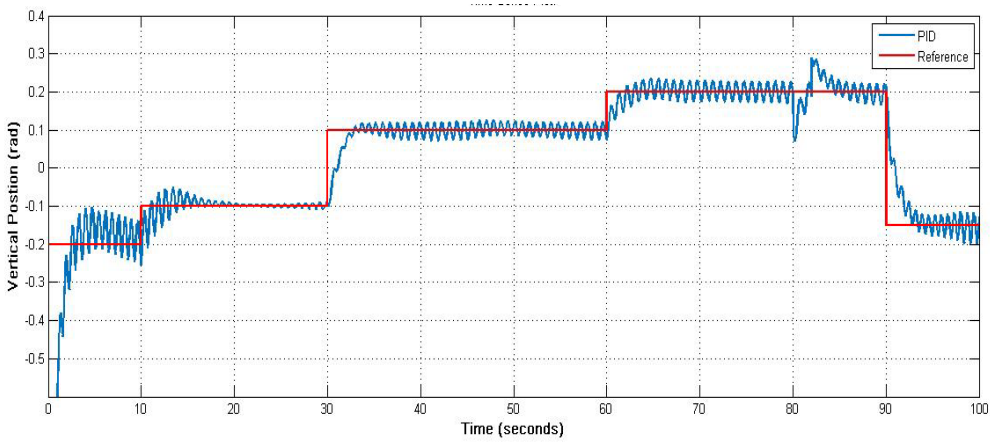

Figure 4.41. Response of vertical position $\theta_v(t)$ of the main rotor using PID controller tracking saw-tooth trajectory (frequency of 0.3 Hz) to load disturbance at the (80^{th} sec)

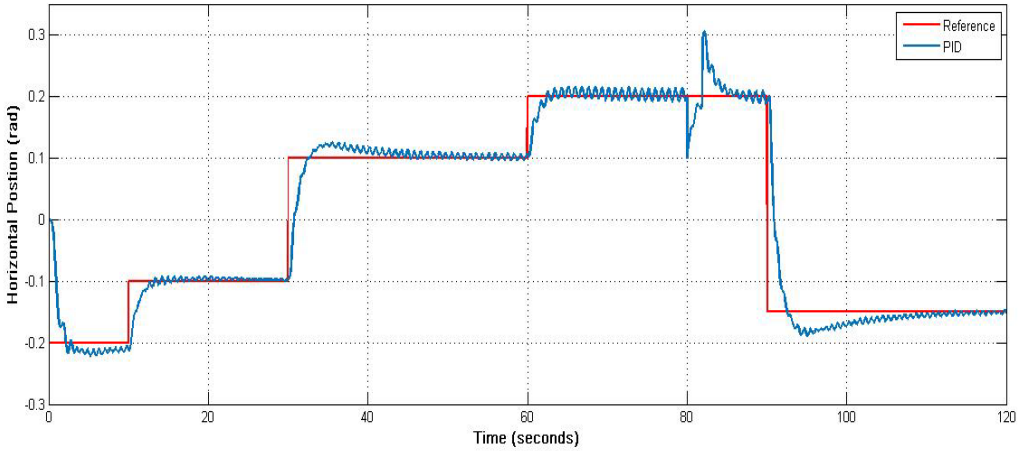

Figure 4.42. Response of horizontal position $\theta_h(t)$ of the tail rotor using PID controller tracking saw-tooth trajectory (frequency of 0.3 Hz) to load disturbance at the (80^{th} sec)

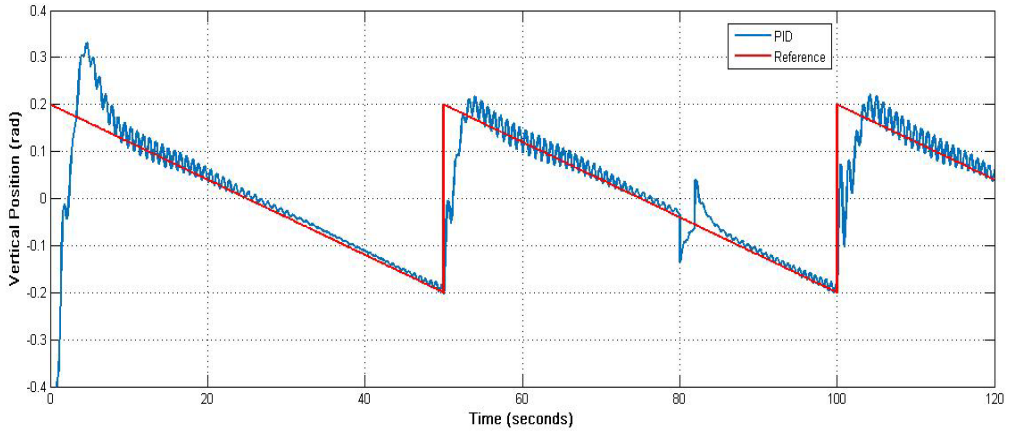

Figure 4.43. Response of vertical position $\theta_v(t)$ of the main rotor using PID controller tracking saw-tooth trajectory (frequency of 0.2 Hz) to load disturbance at the (80^{th} sec)

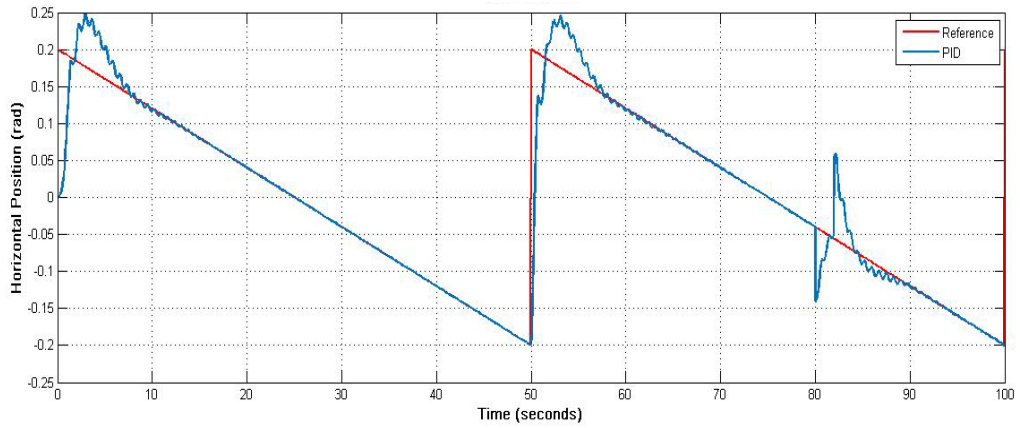

Figure 4.44. Response of horizontal position $\theta_h(t)$ of the tail rotor using PID controller tracking saw-tooth trajectory (frequency of 0.2 Hz) to load disturbance at the (80^{th} sec)

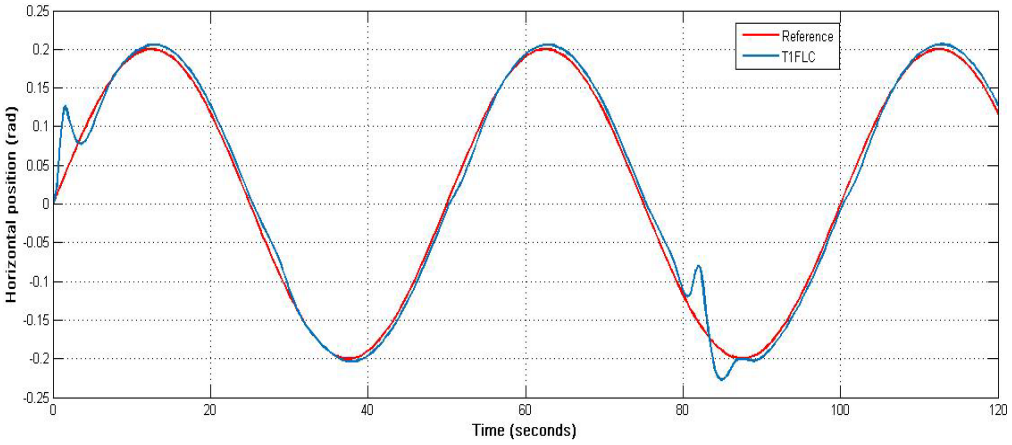

Figure 4.45. Response of horizontal position $\theta_h(t)$ of the tail rotor using Type 1 Fuzzy PID controller tracking sinusoidal trajectory (frequency of 0.25 Hz) to load disturbance at 80th sec

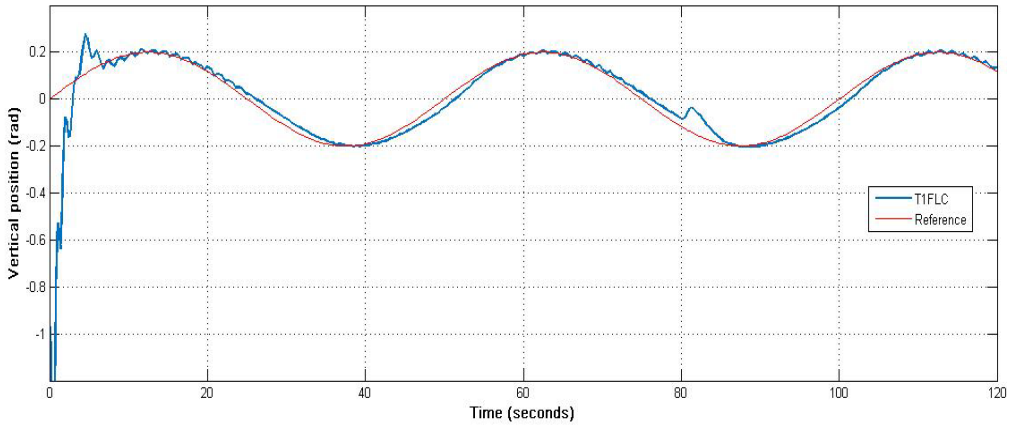

Figure 4.46. Response of vertical position $\theta_v(t)$ of the tail rotor using Type 1 Fuzzy PID controller tracking sinusoidal trajectory (frequency of 0.25 Hz) to load disturbance at the (80th sec)

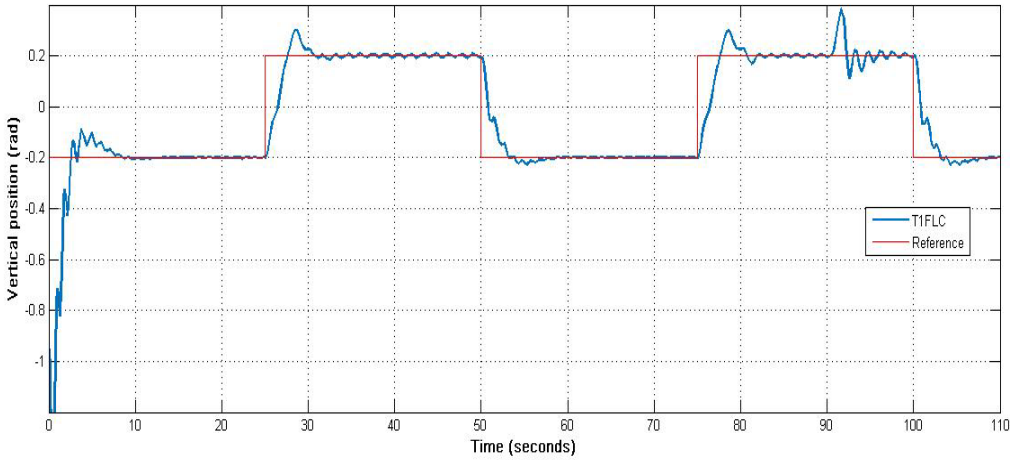

Figure 4.47. Response of vertical position $\theta_v(t)$ of the tail rotor using Type 2 Fuzzy PID controller tracking square trajectory (frequency of 0.25 Hz) to load disturbance at the (120th sec)

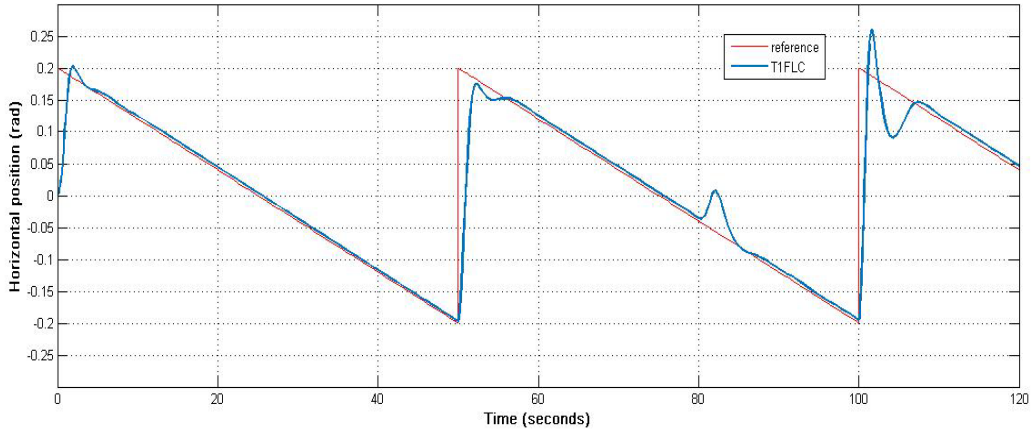

Figure 4.48. Response of horizontal position $\theta_h(t)$ of the tail rotor using Type 1 Fuzzy PID controller tracking saw-tooth trajectory (frequency of 0.2 Hz)) to load disturbance at the (120th sec)

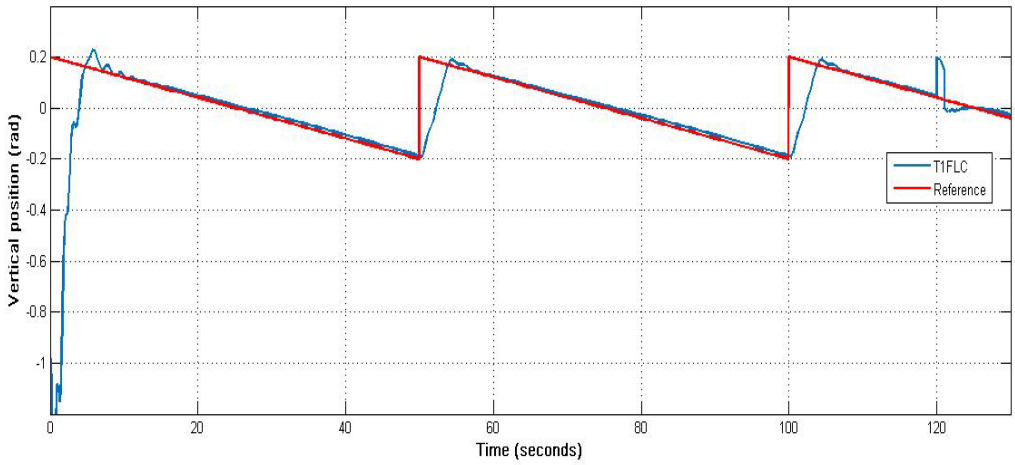

Figure 4.49. Response of vertical position $\theta_v(t)$ of the tail rotor using Type 1 Fuzzy PID controller tracking saw-tooth trajectory (frequency of 0.2 Hz) to load disturbance at the (120^{th} sec)

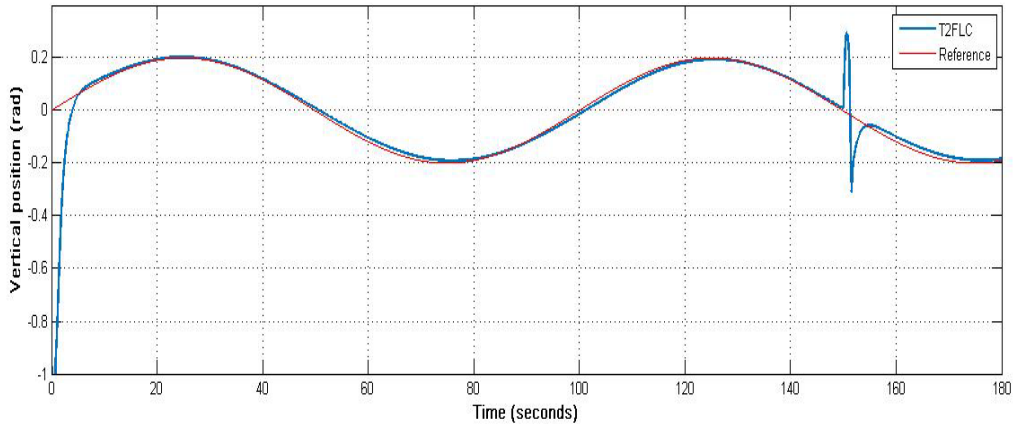

Figure 4.50. Response of vertical position $\theta_v(t)$ of the main rotor using Type 2 Fuzzy PID controller tracking a sinusoidal trajectory (frequency of 0.2 Hz) to load disturbance at the (130^{th} sec)

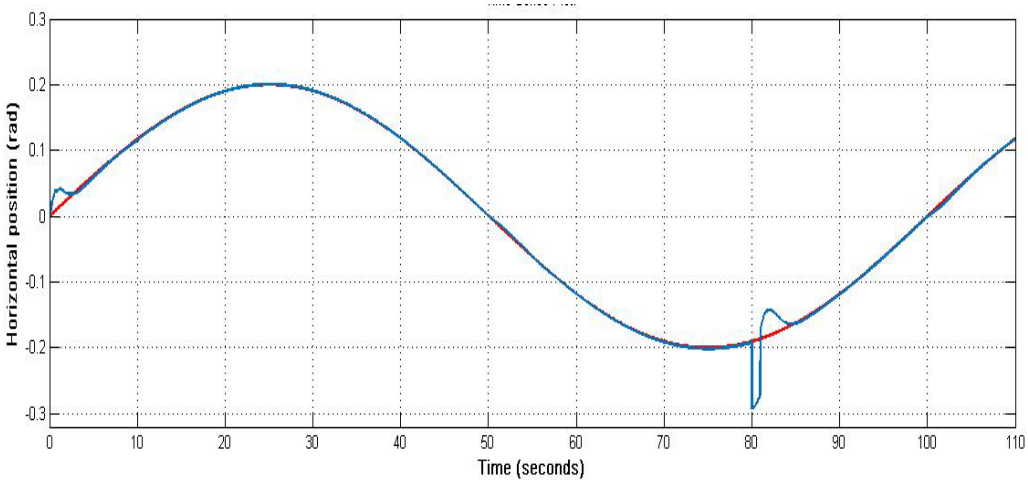

Figure 4.51. Response of horizontal position $\theta_h(t)$ of the main rotor using T2FLC controller tracking a sinusoidal trajectory (frequency of 0.2 Hz) to load disturbance at the (80th sec)

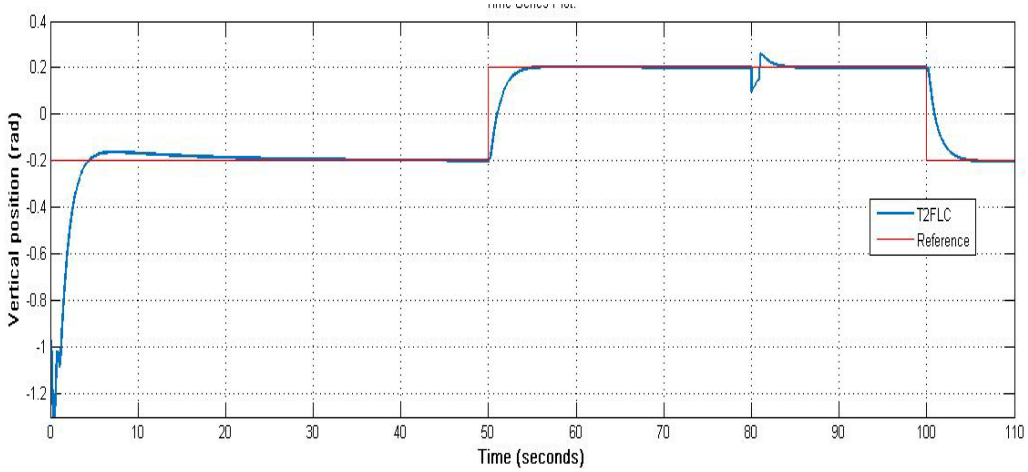

Figure 4.52. Response of the vertical position $\theta_v(t)$ of the main rotor using Type 2 Fuzzy PID controller tracking square trajectory (frequency of 0.2 Hz) to load disturbance at the (80th sec)

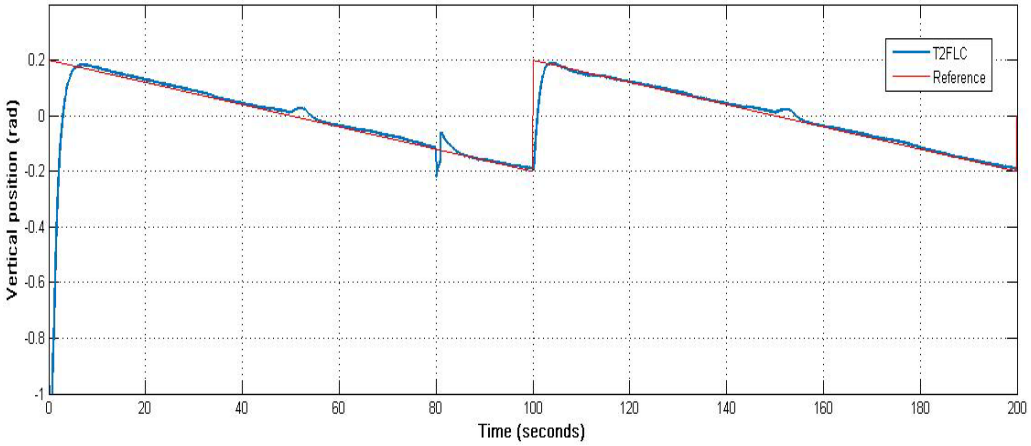

Figure 4.53. Response of vertical position $\theta_v(t)$ of the TRMS main rotor using Type 2 Fuzzy PID controller tracking a skew trajectory (frequency of 0.1 Hz) to load disturbance at the (80th sec)

Well. The results are presented in Table 4.4 for the vertical plane (pitch motion) and Table 4.5 for the horizontal plane (yaw motion).

Table 4.4. Performance indexes of the pitch motion

	IATE	IAE	ISE	ITSE	ISCI	Overshoot
PID	58.36	2.46	0.71	8.17	55.13	7%
T1FLC	41.34	2.42	1.01	7.66	52.32	3%
T2FLC	24.25	1.92	1.02	6.30	54.49	2%

Table 4.5. Performance indexes of the yaw motion

	IATE	IAE	ISE	ITSE	ISCI	Overshoot
PID	3.22	0.11	0.003	0.006	1.51	0.9%
T1FLC	2.70	0.13	0.003	0.008	0.79	3.1%
T2FLC	1.29	0.09	0.001	0.002	0.84	1.2%

DISCUSSION THE SIMULATIONS RESULTS

The simulation results of the TRMS attitude dynamics control are presented. The both of initial values of the pitch and yaw angles are taken 0 radians. The results obtained for the attitude stabilization of the TRMS are given in the Figure 4.20 and Figure 4.21 for the pitch and yaw angles respectively. It can be seen that, the Type-2 fuzzy logic controller ensures a good convergence, and the yaw angle time response is relatively quick compared to the pitch angle response for all the controllers . Also, as illustrated in Figure 4.37, the type-2 fuzzy logic controller provides a better performance than the type-1 fuzzy logic controller. Especially, the type-2 fuzzy logic controller presents fast step responses with small oscillations, as opposed to IT2FLC.

Figure 4.38 to Figure 4.44 shows the trajectory tracking accuracy of the proposed control low. In the case of the type-2 fuzzy controller, the actual angles pitch and yaw of the helicopter converge, without oscillation, to their desired values, especially when IT2FLC is used, While in the case of the type-1 fuzzy controller, oscillations with big amplitude are observed.

From all the obtained results, it can clearly be seen that, in the case of the type 2 fuzzy controller, all outputs converge accurately to their desired values. A poor performance is obtained in the case of the type-1 fuzzy logic controller. Thus, the type1- fuzzy logic controller cannot be used in mathematically ill-defined systems that may be subjected to structured and unstructured uncertainties

The goal of this chapter is to synthesize some proposed theories of system’s control in order to enslave the yaw and the pitch angles of the TRMS, basically with using the previous mentioned theories in the third chapter, we have taken the classical PID controller as a first application on the TRMS to compare its results later with FL controller’s one, but before this we had to choose whether to take a centralized application with a PID controller for the land for the cross-

coupling as well or to choose an independent PID controller for each rotor as an application strategy.

Secondly we get to control the TRMS through a FL controller application after, which it is not required a well knowing the mathematical model of the systems, therefore before starting applying these theories we had to obtain the values of the model parameters. And it is necessary to get some measurements. First, geometrical dimensions and moving masses of TRMS should be measured.

In this paper an off-line PID controller parameters are optimally designed by the ML algorithm then it has been verified through Simulink simulation as well as experimental work for Lab-scale twin rotor MIMO system. The process under study perceived as a challenging control engineering problem owing to its MIMO characteristics, high order non-linearity, significant cross coupling and inaccessibility of some of its states and outputs for measurements. LM based tuning methods have proved their excellence in giving better results by improving the steady state characteristics and performance indices. The proposed LM tuned controller shows better performance criteria comparable with Ziegler-Nichols tuned controller.

In this chapter the application of different controllers was evacuated as the PID controller, fuzzy type 1 and fuzzy type 2 . The first is largely used in the industrial field in reason of its simplicity and that allow us to control huge number of processes at the same, the fuzzy control do not require too much theoretical development but causes difficulties in the choosing of the parameters

5. CONCLUSION AND RECOMMENDATIONS

In this work, three different types of controllers have been presented each with its application for the TRMS stabilization, where this last is a laboratory process, has two inputs and two outputs that is characterized by its high nonlinearity, important cross coupling between its two axes, and total instability in open loop mode.

Our objective was firstly to synthesize some control theories, those insure the global stability of the system and the proper working under different conditions, and to implement them as well in a real system, but unfortunately the unpredicted conditions those we faced hadn't allow us to carry on to realize it, therefore it has been left as a future perspective. We have been focusing mainly on the simulations in Matlab platform. Through these simulations of the proposed controller's application, we were able to show and describe the advantages and disadvantages of each used controller. As a start, we have made an analytical modeling of the TRMS simulator mathematically which is quite difficult to model with precision due of the aerodynamics forces, to transfer after these found functions to Matlab. Later we have addressed the control theories where we had chosen the three following:

- PID controller
- Fuzzy type-1 logic controller
- Fuzzy type-2 logic controller

On which we had a detailed theoretical presentation of each controller, then we have moved to its synthesis, in order to wind up this chapter with some obtained simulation on the TRMS model. Where we have given the results of both stabilization and trajectory tracking.

5.1. Future work

The future work is target to be as an implementation of the TRMS model and a realization of the hardware schema both mechanical and electrical of the TRMS to get a real data that was measured only by experiments with TRMS equipment to know exactly the movements and control and to apply after the realized control algorithms in the lab, that gives a robustness and meaningful performance after the testing and validating of the control algorithms in the real TRMS system.

REFERENCES

Ahmad, A. J., Chipperfiled, Tokh,i M. O., 2001, Parametric modeling and dynamic characterization of a two-degree-of-freedom twin-rotor multi-input multi-output system, SAGE journal, Proceedings of the Institution of Mechanical Engineers, Part G: Journal of Aerospace Engineering vol. 215 no. 2 pp:63-78.

Ahmad, S. M., Chipperfield, A. J., and Tokhi, M. O., 2003, Dynamic Modelling and Linear Quadratic Gaussian Control of a Twin-rotor Multi-input Multi-output System, Proc. Instn Mech. Engrs Vol. 217 Part I, J. Systems and Control Engineering, pp: 203-227.

Ahmad, S. M., Chipperfield, A. J., Tokhi, M. O., 2000, Dynamic Modelling and Optimal Control of a Twin Rotor Mimo System, National Aerospace and Electronics Conference, IEEE, pp: 391-398.

Ahmad, U., Anjum, W., and Bukhari, S. M. A., 2013, H2 and H∞ Controller Design of Twin Rotor System, Intelligent Control and Automation Journal, 2013, 4, 55-62,.

Allouani, F.,Boukhetala, D., and Boudjema, F., 2012, "Particle swarm optimization based fuzzy sliding mode controller for the Twin Rotor MIMO system", IEEE Mediterranean Electrotechnical Conference, Yasmine Hammamet.

Andrew Ph., Ferat S., 2014, Optimal Control of a Twin Rotor MIMO System Using LQR with Integral Action, World Automation Congress (WAC) Conference, pp: 114 -119.

Astrom, K. J., Murray, R. M., 2010, 'Feedback Systems: An Introduction for Scientists and Engineers', Princeton University Press, pp: 408.

Aström, K. J., Wittenmark, B., 1973, On self-tuning regulators, Automatica Journal, vol. 9, Issue 2. pp: 185-199.

Bennett, S., 2001, "The past of PID controllers", Annual Reviews in Control, vol. 25, pp: 43-53.

Castillo, O., 2012, Type-2 Fuzzy Logic in Intelligent Control Applications, Studies in Fuzziness and Soft Computing, Vol. 272, Springer-Verlag,.

Cazarez-Castro, N. R., Aguilar, L. T., and Castillo, O., 2012, Designing Type-1 and Type-2 Fuzzy Logic Controllers via Fuzzy Lyapunov Synthesis for nonsmooth mechanical systems," Engineering Application of Artificial Intelligence, Vol. 25, pp: 971-979.

Celikyilmaz, A., Türksen, I. B., 2009, Modeling Uncertainty with Fuzzy Logic, Studies in Fuzziness and Soft Computing, Vol. 240, Springer.

Chalupa, P. , Přikryl, J., Novák, J., 2015, Modelling of Twin Rotor MIMO System, International Symposium on Intelligent Manufacturing and Automation 25th DAAAM, Procedia Engineering Journal Vol. 100, pp:249–258.

Chalupa, Přikryl, P. J., , Novák J., 2015, Modelling of Twin Rotor MIMO System, J. Procedia Engineering, Vol. 100, pp: 249–258.

Chaoui, H., Gueaieb, W., Biglarbegian, M., and Yagoub, M., 2013, Computationally Efficient Adaptive Type-2 Fuzzy Control of Flexible-Joint Manipulators," Robotics, pp: 66-91.

Dogan, F., 2015, Design, "Development and Control of a Twin Rotor System", Computer Applications in Engineering Education, Vol. 23, pp: 578–586.

Eker, I., Torin, Y., 2006, Fuzzy logic control to be conventional method, Energy Conversion and management, Energy Conversion and Management, Vol. 47, pp: 377-394.

El-Nagar, A. M., Bardini, M. El,, 2014, Derivation and stability analysis of the analytical structures of the interval type-2 fuzzy PID controller", Applied Soft Computing, Vol. 24, pp 704–716.

El-Telbany, M. E., 2007, Employing Particle Swarm Optimizer and Genetic Algorithms for Optimal Tuning of PID Controllers: A Comparative Study, International Conference on Computer Science and Engineering, Automatic Control and System Engineering Journal, Vol. 7, Issue 2, pp: 216-223.

El-Telbany, M. E., 2009, PID Controller Tuning Scheme For Twin Rotor Multi-Input Multi-Output System Based Particle Swarm Optimization Approach, Journal of Engineering Sciences, Assiut University, Vol. 37, No. 4, pp. 955-967.

Fayek, H.M., Elamvazuthi, I., Perumal ,N., and Venkatesh, B., 2014, A controller based on Optimal Type-2 fuzzy Logic: Systematic design, optimization and real-time implementation," ISA Transactions, pp: 1583–1591.

Federal A. (FAA), 2013, 'Helicopter Flying Handbook, Aviation Supplies & Academics, Incorporated, Skyhorse Publishing, Updated Edition edition, pages 194, ISBN-10: 162087492X, .

Furat, M., Eker, I., 2012, Experimental Evaluation of Sliding Mode Control Techniques. Çukurova University Journal of the Faculty of the Engineering and Architecture, Vol. 27, pp: 23-37.

Gilardi, G., Sharf, I., 2002, Literature survey of contact dynamics modeling, Mechanism and Machine Theory, Elsevier Journal, Vol. 37, Issue 10, pp :1021-1240.

Godoy, S. M., Friedhofer, M., 1997, An implementation methodology of a fuzzy based decision support algorithm, International Journal of Knowledge-Based Intelligent Engineering Systems,Vol.1 N. 4, pp. 267-275.

Hägglund, T.K., Åström, J., 2004, Revisiting the Ziegler- Nichols step response method for PID control, Journal of Process Control, Vol. 14, pp: 635-650.

Hagras, H., 2004, "A Hierarchical Type-2 Fuzzy Logic Control Architecture for Autonomous Mobile Robots", IEEE Transactions on Fuzzy Systems, Vol. 12, pp: 524-539.

Huang, L., 2011, An approach for robust control of a twin-rotor multiple input multiple output TRMS system, IEEE International Conference on Robotics and Automation (ICRA), Pp: 4423- 4428.

Huang, Y. J., Wu, H. W., 2013, PID-based fuzzy sliding mode control for twin rotor multi-input multi-output systems, TENCON Spring Conference, IEEE, pp: 204-207.

Islam, B. U., Ahmed, N., Bhatli, D. L., Khan, S., 2003, Controller Design Using Fuzzy Logic for a Twin Rotor MIMO System, IEEE Multi Topic Conference, INMIC 2003. 7th International, pp: 264-268.

Islam, B. UI, Ahmed, N., Bhatli, D. L., and Khan, Sh., 2003, Controller Design Using Fuzzy Logic for a Twin Rotor MIMO System, Multi Topic Conference, INMIC. 7th International, pp: 264-268.

Jahed, M., Mohammad, F., 2013, Robust adaptive fuzzy control of twin rotor MIMO system, Methodologies And Application Soft Computing , Vol. 7, Issue 10, pp:1847-1860.

Juang, W.K. Liu, R.W. Lin, 2011, Hybrid Intelligent Controller for a Twin Rotor MIMO System and Its Hardware Implementation, ISA Trans, Vol. 50, pp: 609–619.

Kim, H., and Song, J., 2013, Low-cost Robot Arm with 3-DOF Counterbalance Mechanism, IEEE International Conference on Robotics and Automation (ICRA), Karlsruhe, Germany, pp: 4183- 4188.

Knudsen, M., Jensen, J., 1995, Estimation of nonlinear dc-motor models using a sensitivity approach, proceedings of the 3rd European Control Conference, ECC'95, pp:319- 325.

Kumbasar, T., 2015, Robust Stability Analysis and Systematic Design of Single Input Interval Type-2 Fuzzy Logic Controllers", IEEE Transactions on Fuzzy Systems, Vol pp, pp:1.

Kumbasar, T., Dodurka , M. F., Yesil, and Sakallı, E., A., 2014, The Simplest Interval Type-2 Fuzzy PID Controller Structural Analysis, IEEE International Conference on Fuzzy Systems, pp: 626-633.

Kumbasar, T., Eksin, I., Guzelkaya , M., and Yesil, E., 2012 , Type-2 fuzzy model based controller design for neutralization processes," ISA Transactions, Vol. 51, pp: 277–287.

Lendek, Z., Babuska, R., and Schutter , B. De, 2010, Stability bounds for fuzzy estimation and control Part I: State estimation, Proceedings of the 2010 IEEE International Conference on Automation, Quality and Testing, Robotics (AQTR 2010), pp: A-S1-3-3023.

Liu, Ch., Chen, L., Ting, Ch., Hwang, J., Wu, Sh., 2011, Improved Twin Rotor MIMO System Tracking and Transient Response Using Fuzzy Control Technology, Journal of Aeronautics, Astronautics and Aviation, Series A, Vol.43, No.1 pp.037-044.

Liu, Ch.Sh., Chen, L.R., Ting , Ch.Sh., Hwang, J. Ch., and Sh, L. Wu., 2011, Improvement Twin Rotor MIMO System Tracking and Transient Response Using Fuzzy Control Technology, Journal of Aeronautics and Aviation, Vol. 43, pp: 037–044.

Mahmoud, M. S., Yuanqing, X., 2012, 'Applied Control Systems Design', Springer Science & Business Media, Technology & Engineering, pp: 560.

Martinez, R., Castillo, ., O., Aguilar, L.T. , and Rodriguez, A. , 2009, Evolutionary Optimization of Type-2 Fuzzy Logic Systems Applied to Linear Plants, Studies in Fuzziness and Soft Computing, pp:11-18.

Meon, M.., Mohamed, T., Ramli, M., Mohamed, M., and Manan, N., 2012, "Review and current study on new approach using PID Active Force Control (PIDAFC) of twin rotor multi input multi output system (TRMS), in 2012 IEEE Symposium on Humanities, Science and Engineering Research, Kuala Lumpur .

Mohamed, T. L. T., and Ishak, K. M. A. K., 2012, Intelligent Hybrid Active Force Control in Identification of a Nonlinear MIMO System, Research and Development (SCOReD), pp: 114-119.

Mondal S., Mahanta, Ch., 2011, Second Order Sliding Mode Controller for Twin Rotor MIMO System, India Conference (INDICON), Annual IEEE, pp: 1-5.

Nghia, N. H., 2007, Modeling Simulation and Calibration of Twin Rotor MIMO System, Master's thesis Erasmus Mundus, pp:101.

Patel, A. A. ,Pithadiya, P. M., Kannad, H. V., 2009, Control of Twin Rotor MIMO System (TRMS) using PID Controller, International Journal of Advance Engineering and Research Development IJAERD, e-ISSN: 2348 – 4470.

Patel, A. A., Pithadiya , P. M., and Kannad, H. V., 2015 Control of Twin Rotor MIMO System (TRMS) using PID Controller," J. IJAERD, National Conference on Emerging Trends in Computer & Electrical Engineering.

Phillips, A., Ferat S., 2004, Optimal Control of a Twin Rotor MIMO System Using LQR with Integral Action, IEEE, World Automation Congress (WAC), pp: 114-119.

Rahideh, A. and Shaheed, M. H., 2007, Mathematical dynamic modeling of a twin-rotor multiple input–multiple output system, Systems and Control Engineering Journal.

Rahideh, A., B., Shaheeda, M.H., Huijbertsa, H. J. C., 2008, Dynamic modeling of a TRMS using analytical and empirical approaches, Control Engineering Practice, Elsevier Journal, Vol. 16, Issue 4, pp :241–259.

Rahideh, A., Shaheed, M. H., 2007, Mathematical dynamic modelling of a twin-rotor multiple input–multiple output system, Journal of Systems and Control Engineering, pp: 89-101.

Rahideha, A. B., Bajodahc, A.H. , and Shaheedb M.H. , 2012, Real time adaptive nonlinear model inversion control of a twin rotor MIMO system using neural networks, Engineering Applications of Artificial Intelligence, Elsevier Journal, Vol. 25, Issue 6, pp: 1289–1297.

Rahideha, A., M.H. Shaheeda, and H.J.C. Huijberts, 2008, Dynamic Modelling of a TRMS Using Analytical and Empirical pproaches, Journal of Control Engineering Practice, Vol. 16, pp: 241–259,.

Raymond, S., Serway, A., Jewett John W., 2004, Physics for Scientists and Engineers (with Physics NOW and InfoTrac), David Harris, 6th edition, pp: 253:1382 ISBN 0-534-40949-0.

Salas, H., Castañeda, De León-Morales, J. , 2013, Attitude observer-based robust control for a twin rotor system, Kybernetika Journal.

Shih, Ch., Chen, M., Wang, J., 2008, Mathematical Model And Set-Point Stabilizing Controller Design Of A Twin Rotor MIMO System, Asian Journal of Control, vol. 10, No. 1, pp. 107-114.

Stanislaw, H. Z., 2003 , “System and Control”, Oxford University Press, pp: 781.

Taskin, A., Kumbasar, T., 2015, An Open Source Matlab/Simulink Toolbox for Interval Type-2 Fuzzy Logic Systems, IEEE Symposium Series on Computational Intelligence.

Toha, S. F., Tokhi, M. O., 2009, Real-coded Genetic Algorithm for Parametric Modelling of a TRMS, Evolutionary Computation, proceedings of the 3rd European Control Conference CEC '09. IEEE Congress, pp: 2022 -2028.

Twin Rotor MIMO System Getting Started 33-007-1M5, Feedback Instruments Ltd,

Wang, W., Lee, T., and Huang, H., 2002, Evolutionary Design of PID Controller for Twin Rotor Multi-Input Multi-Output System, Proceedings of the 4th World Congress on Intelligent Control and Automation, IEEE, Vol. 2, pp: 913-917.

Wen, P., Li,Y., 2011, Twin Rotor System Modeling, De-coupling and Optimal Control Proceedings of the IEEE International Conference on Mechatronics and Automation, Beijing, China, pp: 1839 -1842.

Wen, P., T.W. Lu, 2008, Decoupling control of a twin rotor mimo system using robust deadbeat control technique," IET Control Theory & Applications, Vol. 2, pp: 999-1007.

Witczak, M., 2014 , 'Fault Diagnosis and Fault-Tolerant Control Strategies for Non-Linear Systems', Analytical and Soft Computing Approaches, Lecture Notes in Electrical Engineering Vol. 266, Springer International Publishing Switzerland, pp:239.

Zadeh, L. A., 1965, Fuzzy sets, Information and Control, vol. 8, pp: 338-353.

BIBLIOGRAPHY

I hold an Engineer’s degree in Electrical Electronics Engineering from the Faculty of technology at M’sila University,Algeria. and I am currently an Msc student in Electrical Electronics Engineering department at the University of Cukurova, faculty of Engineering and Architecture , in Adana, Turkey

APPENDIX

APPENDIX 1. Physical parameters

The following are the results of measurements for a given laboratory set-up. All are related to the system stability. Representing the masses weights of each part of the TRMS also the lengths between each mass and the center of gravity in TRMS .

$m_m = 0.0145\ [kg]$ $\quad$ $l_m = 0.24\ [m]$

$m_{mr} = 0.228\ [kg]$ $\quad$ $l_t = 0.25\ [m]$

$m_{ms} = 0.225\ [kg]$ $\quad$ $l_b = 0.26\ [m]$

$m_t = 0.0155\ [kg]$ $\quad$ $l_{cb} = 0.13\ [m]$

$m_{tr} = 0.206\ [kg]$ $\quad$ $r_{ms} = 0.155\ [m]$

$m_{ts} = 0.165\ [kg]$ $\quad$ $r_{ts} = 0.10\ [m]$

$m_b = 0.022\ [kg]$ $\quad$ $m_{cb} = 0.068\ [kg]$

The returning torque from gravity forces is given by:

$$M_g(t) = gm_t \frac{l_t \cos\theta_v(t)}{2} + gm_{tr} l_t \cos\theta_v(t) + gm_{ts} l_t \cos\theta_v(t) - gm_m \frac{l_m \cos\theta_v(t)}{2} - \ldots$$
$$- gm_{mr} l_m \cos\theta_v(t) - gm_{ms} l_m \cos\theta_v - gm_b \frac{l_b \sin\theta_v(t)}{2} - gm_{cb} l_{cb} \sin\theta_v(t)$$

The measured values of the eight terms in the equation above are shown below:

$$gm_t \frac{l_t \cos\theta_v(t)}{2} = 0.0019375 \cos\theta_v(t) \quad \text{[Nm]}$$

$$gm_{tr} l_t \cos\theta_v(t) = 0.0515 \cos\theta_v(t) \quad \text{[Nm]}$$

$$gm_{ts}l_t \cos\theta_v(t) = 0.04125\cos\theta_v(t) \quad \text{[Nm]}$$

$$gm_m \frac{l_m \cos\theta_v(t)}{2} = -0.001711\cos\theta_v(t) \quad \text{[Nm]}$$

$$gm_{mr}l_m \cos\theta_v(t) = -0.053808\cos\theta_v(t) \quad \text{[Nm]}$$

$$gm_{ms}l_m \cos\theta_v = -0.0531\cos\theta_v \quad \text{[Nm]}$$

$$gm_b \frac{l_b \sin\theta_v(t)}{2} = -0.00286\sin\theta_v(t) \quad \text{[Nm]}$$

$$gm_{cb}l_{cb} \sin\theta_v(t) = -0.00884\sin\theta_v(t) \quad \text{[Nm]}$$

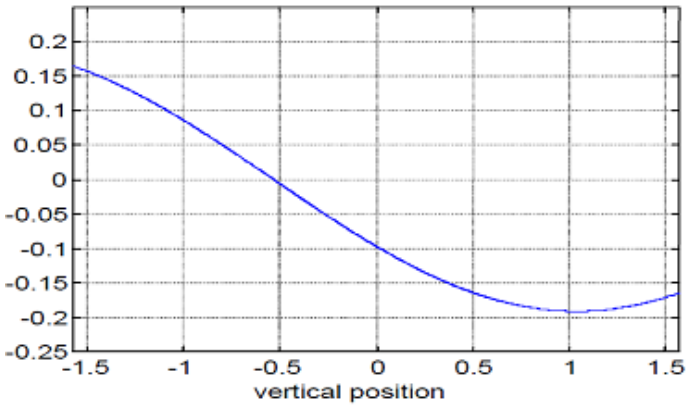

Figure 1. Returning moment of gravity forces M_g

Figure 4.1 shown the variation of the moment regarding the variation in ages of rotation The total measured values of the eight terms giving:

$$M_g(t) = 9.81\left(-0.0139315\cos\theta_v(t) + 0.0117016065\sin\theta_v(t)\right) \quad \text{[Nm]}$$

The moment of centrifugal forces is:

$$M_c(t) = -\omega_h^2(t)\{Al_m + Bl_t - Cl_c\}\sin\theta_v(t)\cos\theta_v(t)$$

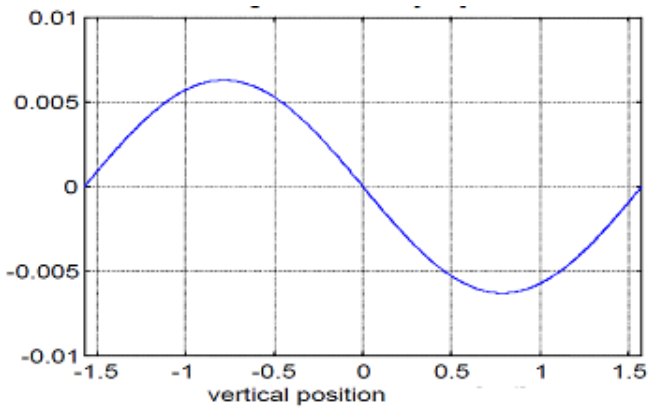

Figure 2. Centrifugal moment for ω=1 [*rad/s*]

$$M_c(t) = -0.05038268\omega_h^2(t)\sin\theta_v(t)\cos\theta_v(t)$$

Figure 8.2 shows the variation in moment of inertia at the horizontal plan depending to the position of its axis.

Using the above measurements the moment of inertia about the horizontal axis can be calculated as:

$$J_v = \sum_{i=1}^{8} J_{vi}$$

The terms of the sum are calculated from elementary physics laws

$$J_{mr} = m_{mr}l_m^2 = 0.013132 \quad [\mathrm{kg.m^2}]$$

$$J_m = m_m l\frac{l_m^2}{3} = 0.000278 \quad [\mathrm{kg.m^2}]$$

$$J_{tr} = m_{tr}l_t^2 = 0.012875 \quad [\mathrm{kg.m^2}]$$

$$J_t = m_t \frac{l_t^2}{3} = 0.000322 \quad [\mathrm{kg.m^2}]$$

$$J_{cb} = m_{cb} l_{cb}^2 = 0.001149 \quad [\mathrm{kg.m^2}]$$

$$J_b = m_b \frac{l_b^2}{3} = 0.000495 \quad [\mathrm{kg.m^2}]$$

$$J_{ms} = \frac{m_{ms}}{2} r_{ms}^2 + m_{ms} l_m^2 = 0.015622 \quad [\mathrm{kg.m^2}]$$

$$J_{ts} = \frac{m_{ts}}{2} r_{ts}^2 + m_{ts} l_t^2 = 0.011962 \quad [\mathrm{kg.m^2}]$$

All are giving:

$J_v = 0.055846 \quad [\mathrm{kg.m^2}]$

The calculated moment of inertia in the horizontal axis is:

$$J_h = \sum_{i=1}^{8} J_{hi}$$

where the terms of the sum are:

$$J_{h1}(t) = \frac{m_m}{3}\left(l_m \cos\theta_v(t)\right)^2 = 0.0002784\left(\cos\theta_v(t)\right)^2 \quad [\mathrm{kg.m^2}]$$

$$J_{h5}(t) = m_{mr}\left(l_m \cos\theta_v(t)\right)^2 = 0.013132\left(\cos\theta_v(t)\right)^2 \quad [\mathrm{kg.m^2}]$$

$$J_{h2}(t) = \frac{m_t}{3}\left(l_t \cos\theta_v(t)\right)^2 = 0.0003229\left(\cos\theta_v(t)\right)^2 \quad [\mathrm{kg.m^2}]$$

$$J_{h4}(t) = m_{tr}\left(l_t \cos\theta_v(t)\right)^2 = 0.012875\left(\cos\theta_v(t)\right)^2 \quad [\mathrm{kg.m^2}]$$

$$J_{h3}(t) = \frac{m_b}{3}\left(l_b \sin\theta_v(t)\right)^2 = 0.0004595\left(\sin\theta_v(t)\right)^2 \quad [\mathrm{kg.m^2}]$$

$$J_{h6}(t) = m_{cb}\left(l_{cb}\sin\theta_v(t)\right)^2 = 0.0011492\left(\sin\theta_v(t)\right)^2 \quad [\text{kg}.\text{m}^2]$$

$$J_{h7}(t) = \frac{m_{ts}}{2}r_{ts}^2 + m_{ts}\left(l_t\cos\theta_v(t)\right)^2 = 0.000825 \; + \; 0.010312\left(\cos\theta_v(t)\right)^2 \quad [\text{kg}.\text{m}^2]$$

$$J_{h8}(t) = \frac{m_{ms}}{2}r_{ms}^2 + m_{ms}\left(l_m\cos\theta_v(t)\right)^2 = 0.00540 \; + \; 0.0129611\left(\cos\theta_v(t)\right)^2 \quad [\text{kg}.\text{m}^2]$$

The total moment of inertia is given as following:

$$J_h(t) = 0.04901\cos^2\theta_v(t) + 0.0016065\sin^2\theta_v(t) + 0.0063306 \quad [\text{kg}.\text{m}^2]$$

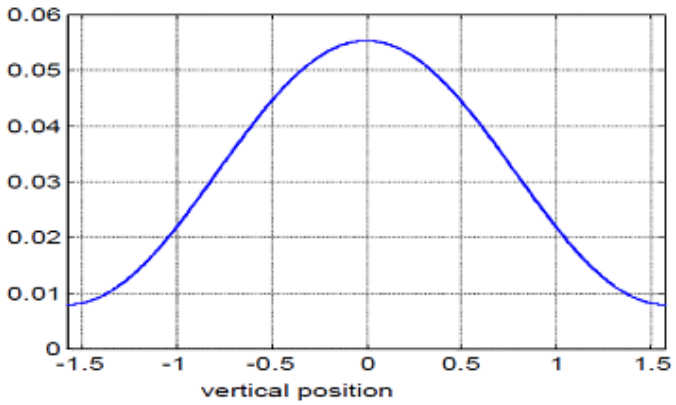

Figure 3. Moment of inertia J_h

Figure 4.3 shows the variation in moment of inertia at the horizontal plan depending to the position of its axis.

$$J_{tr} = \frac{1}{12}m_{tr}\left(l_{wl}{}^2 + l_{tl}{}^2\right)$$

$$J_{mr} = \frac{1}{12}m_{mr}\left(l_{mw}{}^2 + l_{ml}{}^2\right)$$